# Xe-100 Licensing Topical Report Mechanistic Source Term Approach

| | | |
|---|---|---|
| **Document ID Number** | **:** | **000632** |
| **Configuration Classification** | **:** | **XE00-R-R1ZZ-RDZZ-L** |
| **Revision** | **:** | **2** |
| **Security Classification** | **:** | **Non Proprietary** |
| **Status** | **:** | **Approved** |
| **Date Created** | **:** | **8-May-2024** |
| **Project** | **:** | **XE-100** |

**E-SIGNATURES**

**Document Approval Signees**

| Action | Designation | Name | Signature | Date |
|---|---|---|---|---|
| **Preparer** | Principal Consultant | Juan Cajigas | Maintained in Teamcenter | May 8, 2024 |
| **Reviewer** | Manager, Nuclear Software Engineering | Milan Hanus | Maintained in Teamcenter | May 8, 2024 |
| **Reviewer** | Licensing Project Manager | Jessica Maddocks | Maintained in Teamcenter | May 8, 2024 |
| **Approver** | Director, Licensing | Stephen Vaughn | Maintained in Teamcenter | May 8, 2024 |

## SYNOPSIS

One of the principal advantages of high-temperature gas-cooled reactors (HTGRs), such as the Xe-100, is their high degree of passive safety. The fuel, which does not significantly degrade during the slow transients characteristic of HTGRs, is located at the center of a series of barriers to radionuclide transport that constitute a robust functional containment. Therefore, the radionuclide source terms and associated radiological consequences from design basis accidents (DBAs) are expected to be relatively low.

X Energy, LLC (X-energy) has developed models to mechanistically simulate the transport of radionuclides that constitute the source term from their birth in the fuel to their potential release to, and transport in, the environment.

This licensing topical report describes the functional containment and mechanistic source term methodology used in Xe-100 design and safety analysis and the plans to verify and validate the computer code that model these physical phenomena. Additional information from these activities will be provided, as required, in future revisions to this licensing topical report and/or in the design and licensing bases submitted for site or design-specific licensing applications under 10 CFR 50, 10 CFR 52, or future 10 CFR 53.

## Configuration Control/Document Change History

### Document Change History

| Rev. | Date | Preparer | Page/Section Revised | Description |
|---|---|---|---|---|
| **1** | 29-Apr-2021 | P. Loza | NA | Initial issue |
| **2** | 08-May-2024 | J. Cajigas | All | Complete rewrite. This revision replaced XSTERM Software Verification and Validation (V&V) details with a high level overview of the XSTERM V&V plans. This report now describes the theory and models associated with the mechanistic source term approach. |

# Table of Contents

## Appendices

# List of Tables



# List of Figures

## Abbreviations/Acronyms

| Short Form | Phrase |
|---|---|
| **ACRS** | Advisory Committee on Reactor Safeguards |
| **AGR** | Advanced Gas Reactor |
| **ANS** | American Nuclear Society |
| **ASME** | American Society of Mechanical Engineers |
| **AST** | Alternative Source Term |
| **ATR** | Advanced Test Reactor |
| **BDBE** | Beyond Design Basis Event |
| **CFR** | Code of Federal Regulations |
| **CR** | Control Room |
| **CORRM** | Core Corrosion Calculations Model |
| **DBA** | Design Basis Accident |
| **DLOFC** | Depressurized Loss of Forced Circulation |
| **DUSTM** | Dust Production Rate Calculations Model |
| **EAB** | Exclusion Area Boundary |
| **EFPY** | Effective Full Power Years |
| **EM** | Evaluation Model |
| **EMDAP** | Evaluation Model Development and Assessment Process |
| **EPA** | Environmental Protection Agency |
| **FHS** | Fuel Handling System |
| **FOM** | Figures of Merit |
| **FP** | Fission Products |
| **FPM** | TRISO-coated particle Failure Probability Model |
| **GASM** | Steady-State Gaseous Fission Products Transport Calculations Model |
| **HFR** | High Flux Reactor |
| **HM** | Heavy Metal |
| **HPB** | Helium Pressure Boundary |
| **HPBM** | HPB Radionuclide Transport, Deposition and Lift-off Calculations Model |
| **HTGR** | High Temperature Gas Reactor |
| **IAEA** | International Atomic Energy Agency |
| **INET** | Institute of Nuclear and New Energy Technology |
| **INL** | Idaho National Laboratories |
| **IPyC** | Inner Pyrolytic Carbon |

| Short Form | Phrase |
|---|---|
| **KFA** | Institute for Safety Research and Reactor Technology Research Centre Jülich Gmbh |
| **KSIM** | 2D Point Kinetics Core Simulation Model |
| **LBE** | Licensing Basis Event |
| **LLPF** | Lifting-Line Platform Facility |
| **LMP** | Licensing Modernization Project |
| **LPZ** | Low Population Zone |
| **LTR** | Licensing Topical Report |
| **LWR** | Light Water Reactor |
| **MST** | Mechanistic Source Term |
| **NEI** | Nuclear Energy Institute |
| **NRC** | U.S. Nuclear Regulatory Commission |
| **OPyC** | Outer Pyrolytic Carbon |
| **PAG** | Protective Action Guide |
| **PIRT** | Phenomena Identification and Ranking Tables |
| **PLOFC** | Pressurized Loss of Forced Circulation |
| **PRA** | Probabilistic Risk Assessment |
| **PSAR** | Preliminary Safety Analysis Report |
| **RB** | Reactor Building |
| **R/B** | Release Over Birth Ratio |
| **RCS** | Reactivity Control System |
| **RG** | Regulatory Guide |
| **RN** | Radionuclide |
| **RPV** | Reactor Pressure Vessel |
| **RSS** | Reserve Shutdown System |
| **SDS** | Software Design Specification |
| **SG** | Steam Generator |
| **SGTR** | Steam Generator Tube Rupture |
| **SiC** | Silicon Carbide |
| **SOLM** | Solids Fission Products Transport Calculations Model |
| **SSCs** | Structures, Systems, and Components |
| **SRM** | Staff Requirements Memorandum |
| **SRP** | Standard Review Plan |
| **SRS** | Software Requirements Specification |
| **STM** | Software Theory Manual |

| Short Form | Phrase |
|---|---|
| **THM** | Thermodynamics Calculation Model |
| **TRISO** | Triple Coated Isotropic Particle |
| **TRITM** | Tritium Production and Transport Model |
| **TSAM** | Transient and Safety Analysis Methodology |
| **UCO** | Uranium Oxycarbide, a Heterogeneous Mixture of $UO_2$ and UC2 |
| **V&V** | Verification and Validation |
| **VSOP** | Very Superior Old Programs |
| **X-Energy** | X Energy, LLC |

# 1. Introduction

X Energy, LLC (X-energy) has developed models to mechanistically simulate the transport of radionuclides that constitute the source term from their birth in the fuel to their potential release and transport in the environment. This topical report addresses the physical phenomena that lead to such releases.

## 1.1 Purpose

One of the principal advantages of the high-temperature gas-cooled reactor (HTGR) is its high degree of passive safety. The Xe-100 reactor employs TRIstructural-ISOtropic (TRISO) fuel that does not significantly degrade during gradually progressing transients due to the core's low power density and high heat capacity, Reference [1]. Therefore, the reactor source terms, or quantities, timing, physical/chemical forms, and thermal energy of radionuclides released to the environment during licensing basis events (LBEs), Reference [2], are expected to be low. The Xe-100 HTGR source terms are:

- LBE-specific
- Determined mechanistically using models of fission product/radionuclide generation and transport that account for the reactor's inherent and passive design features and the performance of fission product release barriers that constitute the functional containment
- Inclusive of the quantities, timing, physical and chemical forms, and thermal energy of the release
- Different from light water reactor (LWR) source terms that have traditionally been based on severe core damage event(s)

The Xe-100 reactor technology employs a radionuclide functional containment consisting of a series of barriers to radionuclide transport. These barriers include the layers of the TRISO fuel, the reactor core graphite and other carbonaceous materials, the helium pressure boundary (HPB), and the reactor building (RB). Together, these barriers effectively retain radionuclides such that a traditional containment building is not necessary to meet regulatory dose requirements at the exclusion area boundary (EAB).

## 1.2 Scope

X-energy has developed models to simulate radionuclide transport phenomena and estimate source terms for the Xe-100. These integrated models, each treating a particular transport barrier or group of related transport phenomena, mechanistically simulate the transport of radionuclides that constitute the source term from its birth in the fuel to its potential release and transport in the environment.

The mechanistic source term (MST) methodology and theory discussion in this report is preceded by a description of the Xe-100 design that summarizes the Xe-100 functional containment approach. The detailed theory associated with each independent model used in the development of the MST is described and expanded in Appendices. The report also describes the verification and validation (V&V) plans for the Evaluation Model (EM) used to calculate mechanistic source terms and doses based on these source term models.

## 1.3 Interfacing Documents

This Licensing Topical Report (LTR) is one of several reports covering key regulatory issues submitted to the U.S. Nuclear Regulatory Commission (NRC) staff as part of Xe-100 pre-application process. The X-energy mechanistic source term methodology is part of the overall approach to implement of a risk-informed and performance-based design and licensing basis as described in Nuclear Energy Institute (NEI) 18-04, Reference [3] and endorsed and clarified by NRC Regulatory Guide (RG) 1.233, Reference [4]. This LTR interfaces with the following documents:

- Probabilistic Risk Assessment (PRA) efforts, Reference [5], being conducted using the standard American Society of Mechanical Engineers (ASME)/American Nuclear Society (ANS) RA-S-1.4-2021 Probabilistic Risk Assessment Standard for Advanced Non-Light Water Reactor Nuclear Power Plants [54] as endorsed by RG 1.247.
- LBE identification and selection, Structures, Systems, and Components (SSCs) safety classification, and the evaluation of defense-in-depth adequacy methodology described in NEI 18-04 as implemented by X-energy, described in LTR XE00-R-R1ZZ-RDZZ-L-000687 “Risk-Informed Performance-Based Licensing Basis Approach for the Xe-100 Reactor” , Reference [6]
- An integrated approach to analyzing LBEs through the development of evaluation models and implementation of various codes and analysis techniques as described in the “Xe-100 Licensing Topical Report: Transient and Safety Analysis Methodology,” Reference [7]. This MST LTR describes the MST models used in the calculations performed by the XSTERM computer code, see Section 4.2, a code developed as an Evaluation Model for the quantification of Xe-100 source terms and dose calculations. The XSTERM code V&V plans are addressed in Section 6 of this LTR.
- The principal design criteria (PDC) for the X-energy Xe-100 pebble-bed, high-temperature gas-cooled reactor (HTGR), Xe-100 Principal Design Criteria Licensing Topical Report, Reference [8]
- The “Xe-100 Licensing Topical Report TRISO-X Pebble Fuel Qualification Methodology”, Revision 3, Reference [52] provides the technical foundation for the fuel qualification approach as well as the planned fuel fabrication, irradiation, safety testing activities, and approach to qualify the reference fuel (UCO TRISO-coated particles).
- A generic set of dispersion factors has been developed to provide generally conservative values as part of the standard Xe-100 technology development process. The “Xe-100 Licensing Topical Report Atmospheric Dispersion and Dose Calculation Methodology,” Reference [14], is discussed further in Section 5.3 of this report.

## 1.4 Document Layout

This Section is followed by an overview of applicable regulatory requirements, Section 2.

An overview of the Xe-100 plant design and key design features is presented in Section 3.

Section 4 describes the Xe-100 mechanistic source term approach and includes an outline of the series of transport processes that occur from the birth of radionuclides to their potential release to the environment (i.e., functional containment.).

Section 5 documents the theory associated with each independent Xe-100 MST model and expanded in Appendices as required.

Section 6 of the report describes the plans for the Verification and Validation efforts of the MST Evaluation Models.

Conclusions are documented in Section 7 followed by References in Section 8.

## 1.5 Outcome Objectives

X-energy is requesting the NRC review and approval of the MST models described in Section 4.1, Section 5, and Appendices A through H of this LTR as an appropriate means to evaluate radionuclide transport phenomena and estimate mechanistic source terms.

# 2. Overview of Regulatory Requirements and Guidance

## 2.1 10 CFR Regulatory Requirements

The Xe-100 mechanistic source term methodology supports the Xe-100 safety analyses required to comply with the appropriate sections of:

- 10 CFR 50.34(a) (Construction Permits)
- 10 CFR 50.34(b) (Operating Licenses)
- 10 CFR 52.17(a)(1)(ix) (Early Site Permits)
- 10 CFR 52.47(a)(2)(iv) (Design Certifications)
- 10 CFR 52.79(a)(1)(vi) (Combined Licenses)
- 10 CFR 52.137(a)(2)(iv) (Design Approvals)
- 10 CFR 52.157(d) (Manufacturing Licenses)
- 10 CFR 100 (Reactor Site Criteria)

## 2.2 Regulatory Guidance

### 2.2.1 NUREG-2246

NUREG-2246 [9] provides a fuel qualification framework for advanced reactor designs, including power and non-power reactors, to support regulatory findings that nuclear fuel is qualified for use. This NUREG discusses the fission product retention functions of the nuclear fuel. Specifically, Section 3.2, G2-Safety Criteria, addresses the role of the fuel in the protection against the release of radionuclides. X-energy plans on submitting Revision 4 of the "Xe-100 Licensing Topical Report TRISO-X Pebble Fuel Qualification Methodology", which will meet the requirements of this NUREG.

## 2.3 Regulatory Guides

The following regulatory guidance relates to NRC's review and development of LWR source terms and has been examined for potential applicability to mechanistic source terms for the HTGR.

### 2.3.1 Regulatory Guide 1.233

Regulatory Guide 1.233 [4] provides guidance on using a technology-inclusive, risk-informed, and performance-based methodology to inform the licensing basis and content of applications for non-light-water reactors (non-LWRs).

An evaluation of events, plant features and programs, and related uncertainties must address the state of knowledge related to the behavior of reactor systems, fuel, and the way in which radionuclides may move within and be released from a facility. The established methods for addressing radiological source terms for LWRs have limited applicability to non-LWR designs, and more mechanistic approaches have been proposed. The NRC can validate analytical tools and computer codes by comparing results to information available from operating experience and experiments. In SRM-SECY-93-092 [18] the Commission approved the NRC staff's recommendation that source terms for non-LWRs be based upon a mechanistic analysis and that the acceptability of the applicant's analysis will rely on the staff's assurance that the following conditions are met:

- The performance of the reactor and fuel under normal and off-normal conditions is sufficiently well understood to permit a mechanistic analysis. Sufficient data should exist on the reactor and fuel performance through the research, development, and testing programs to provide adequate confidence in the mechanistic approach.
- The transport of fission products can be adequately modeled for all barriers and pathways to the environs, including the specific consideration of containment design. The calculations should be as realistic as possible so that the values and limitations of any mechanism or barrier are not obscured.
- The events considered in the analyses to develop the set of source terms for each design are selected to bound severe accidents and design-dependent uncertainties.
- The design-specific source terms for each accident category would constitute one component for evaluating the acceptability of the design.

The above conditions remain valid for the assessment of mechanistic source terms used to estimate radiological consequences within the analyses of event sequences as described in [NEI 18-04] [3].

Although NEI 18-04 does not address the topic in detail, the development of mechanistic source terms for designs and specific event families is an element of an integrated, risk-informed, performance-based approach to designing and licensing non-LWRs. The NRC staff expects applications or related reports to describe the mechanistic source terms, including the retention of radionuclides by barriers and the transport of radionuclides for all barriers and pathways to the environs. Where applicable, a facility may have multiple mechanistic source terms and specific event sequences to address various systems that contain significant inventories of radioactive material.

### 2.3.2 Regulatory Guide 1.253

This RG 1.253 [38] endorses the methodology described in NEI 21-07 [10], with clarifications and additions, where applicable, as one acceptable process for use in developing certain portions of the SAR for an application for a non-LWR construction permit or operating license.

The guidance indicates source term information should cover all radioactive material inventories and include the type, quantity, and timing of the release of radioactive material from the facility during LBEs. Analysis methodologies, assumptions, bases, and justifications associated with transport of radioactive material from its point of origin to the accessible environment should be included. For a Licensing Modernization Project (LMP)-based safety analysis, the use of a mechanistic source term, consistent with the advanced non-LWR PRA standard definition should be included.

## 2.4 Staff Requirements Memoranda (SRM) and SECY Paper Precedents

The NRC has released several Commission SECY papers and Staff Requirements Memoranda (SRM) relevant to development and use of a mechanistic source term.

### 2.4.1 SECY-93-092 (1993)

In SECY-93-092, “Issues Pertaining to the Advanced Reactor (PRISM, MHTGR, and Process Inherent Ultimately Safe [PIUS]) and CANDU 3 Designs and Their Relationship to Current Regulatory Requirements,” [18] the staff addressed the source term issue for the PRISM, Modular HTGR, PIUS, and

the CANDU-3 reactor designs and recommended to the Commission that mechanistic source terms be allowed provided that the:

- Reactor and fuel performance under normal and off-normal operating conditions is sufficiently well understood to permit a mechanistic analysis. Sufficient data should exist on the reactor and fuel performance through the research, development, and testing programs to provide the adequate confidence in the mechanistic approach.
- Transport of fission products can be adequately modelled for all barriers and pathways to the environs, including specific consideration of containment design. The calculations should be as realistic as possible so that the values and limitations of any mechanism or barrier are not obscured.
- Events considered in the analyses to develop the set of source terms for each design are selected to bound severe accidents and design-dependent uncertainties.

In a July 30, 1993, Staff Requirements Memorandum (SRM), SECY-93-092 SRM [18], the Commission approved the staff's recommendations including its agreement with the ACRS.

### 2.4.2 SECY-97-171 (1997)

There were further regulatory developments between 1993 and 2002 that add to the source term discussion. Although these developments were LWR focused, their regulatory adoption led to NRC's current licensing framework in which mechanistic source terms are used. In SECY-97-171 [41], "Consideration of Severe Accident Risk in NRC Regulatory Decisions," the staff noted:

"During the past 30 years substantial additional information on fission product releases has been developed based on significant severe accident research. As a result of this research, a revised accident source term has been developed for regulatory applications for future LWRs in NUREG-1465 [45], "Accident Source Terms for Light-Water Nuclear Power Plants".

### 2.4.3 SECY-02-0139 (2002)

SECY-02-0139, "Plan for Resolving Policy Issues Related to Licensing Non-Light Water Reactor Designs," [53] identified seven reactor licensing policy issues. Issue 5 related to licensing source terms by stating that:

"…future plants, particularly non-LWRs, propose not to use a predetermined source term for assessing the effectiveness of plant mitigation features or site suitability, but rather to use plant specific accident source terms corresponding to each of the AOOs and DBEs defined for the plant. Such an approach puts a burden on the applicant and staff to understand the fission product release characteristics and uncertainties associated with a variety of accident scenarios."

### 2.4.4 SECY-03-0047 (2003)

SECY-03-0047, "Policy Issues Related to Licensing Non-Light Water Reactor Designs," [46] offered staff recommendations on the policy issues discussed in SECY-02-0139. Issue 5 postulated, "Under what conditions, if any, should scenario-specific accident source terms be used for licensing decisions?" The NRC staff recommended the following action to the Commission:

- "Retain the Commission's guidance contained in the July 30, 1993, SECY-93-092 SRM [18] that allows the use of scenario specific source terms, provided there is sufficient understanding and assurance of plant and fuel performance and deterministic engineering judgment is used to bound uncertainties."
- "This recommendation will allow credit to be given for the unique aspects of plant design (i.e., performance based). Furthermore, this approach is consistent with prior Commission and ACRS views. However, this approach is also dependent upon understanding fuel and fission product behavior under a wide range of scenarios and on ensuring fuel and plant performance is maintained over the life of the plant."

This recommendation acknowledged unique performance aspects of possible plant designs and provided for a probabilistic event identification approach to be considered. Sufficient understanding of plant and fuel performance and deterministic engineering judgment would be used to bound uncertainties.

In SECY-03-0047 SRM [47] dated June 26, 2003, the Commission approved the NRC staff recommendation cited in Issue 5 of SECY-03-047 [46], thereby endorsing consideration of mechanistic scenario-specific source terms for non-LWR licensing decisions.

### 2.4.5 SECY-05-0006 (2005)

SECY-05-0006, "Second Status Paper on the Staff's Proposed Regulatory Structure for New Plant Licensing and Update on Policy Issues Related to New Plant Licensing," [48] which has not yet been approved by the Commission, provides additional information regarding NRC staff thinking on scenario specific source terms. It discussed how the staff intends to incorporate, among other topics, the use of scenario-specific source terms into the proposed regulatory structure for new plant licensing. This paper was written in response to the SECY-03-0047 SRM [47].

### 2.4.6 SECY-18-0096 (2018)

SECY-18-0096 "Functional Containment Performance Criteria for Non-Light-Water-Reactors" [17] sought Commission approval of a methodology for establishing functional containment performance criteria for non-LWR plants. The SECY-18-0096 background notes that the primary safety function of any nuclear reactor is limiting the release of RN. This was historically addressed using the defence in depth philosophy with multiple defence layers and allowable component leakage rates, but non-LWRs are designed differently. This required a new mindset with definition of a functional containment providing the equivalent RN release protection.

The discussion first describes the proposed methodology developed by the staff to be used by non-LWR designers to define functional containment performance criteria in a manner that is technology inclusive, risk informed, and performance based. Enclosure 2 of SECY-18-0096 describes in more detail how the proposed methodology defines logical performance criteria for specific design features that have a role in limiting RN release, and requests Commission approval of this methodology.

For the next steps, pending Commission approval, the staff committed to incorporate the proposed methodology for functional containment performance criteria in ongoing activities, including RG 1.233, RG 1.232, and continue interactions with specific designers. The Commission's vote and subsequent approval of the methodology was issued in a Staff Requirements Memorandum in December 2018.

Since SECY-18-0096 was issued, the effective incorporation of these performance criteria has occurred through the development of the frequency-consequence curve and defence-in-depth adequacy evaluation guidance in NEI 18-04 [3].

## 2.5 Additional Guidance

### 2.5.1 Sandia National Laboratory Report

Sandia National Laboratories report, SAND2020-6730 “Mechanistic Source Term Considerations for Advanced Non-LWRs” [49], addresses considerations that must be accounted for in the development of a mechanistic source term to the environment. Radionuclide release scenarios based on a more realistic representation of the system from the unique physics and characteristics of the system are necessary for the licensing of non-LWR reactors.

The Licensing Modernization Project (LMP), coordinated by the Nuclear Energy Institute in NEI 18-04 [3], is a guideline for a technology-inclusive, risk-informed, performance-based approach for the selection of event scenarios, safety systems and correlating risk-informed treatment of the system. It is endorsed and clarified by NRC Regulatory Guide 1.233 [4].

### 2.5.2 Idaho National Laboratory Report

Idaho National Laboratory paper INL/EXT-10-17997, Rev. 0, "Mechanistic Source Terms White Paper," [2] summarizes the event specific mechanistic approach that the NGNP Project is taking in developing radiological source terms for licensing basis events. The source terms developed with this approach, and radionuclide inventories determined elsewhere in the facility during source term analysis, can also be used for other purposes such as equipment environmental qualification, control room habitability analyses, and assessments of severe accident risks in environmental impact statements. The mechanistic approach to source term development is required to establish the technical basis and credit the appropriate radionuclide retention capabilities of each of the multiple barriers to radionuclide transport to the environment consistent with the plant design approach.

Table 1 summarizes the NGNP plant radionuclide classifications and key behavior characteristics outside of the fuel kernel.

***Table 1: Classes of Radionuclides of Interest for an HTGR Design Based on the NGNP Plant***

| Radionuclide Class | Key Nuclide | Form in Fuel | Principal In-Core Behaviour | Principal Ex-Core Behaviour |
|---|---|---|---|---|
| Tritium | H-3 | Element (gas) | Permeates intact SiC; sorbs on core graphite | Permeates through heat exchangers |
| Noble gases | Xe-133 | Element (gas) | Retained by PyC/SiC | Removed by helium purification system |
| Halogens | I-131 | Element (gas) | Retained by PyC/SiC | Deposits on colder metals |
| Alkali metals | Cs-137 | Oxide-element | Retained by SiC; some matrix/graphite retention | Deposits on metals/dust |
| Tellurium group | Te-132 | Complex | Retained by PyC/SiC | Deposits on metals/dust |
| Alkaline earths | Sr-90 | Oxide-carbide | High matrix/graphite retention | Deposits on metals/dust |
| Noble metals | Ag-110m | Element | Permeates intact SiC | Deposits on metals |
| Lanthanides | La-140 | Oxide | High matrix/graphite retention | Deposits on metals/dust |
| Actinides | Pu-239 | Oxide-carbide | Quantitative matrix/graphite retention | Retained in core |

## 2.6 EPA Regulations

The most limiting top-level RN control requirement impacting fuel performance, fission product release, and the mechanistic source term is to meet the Environmental Protection Agency (EPA) Protective Action Guides (PAGs) at the Exclusion Area Boundary (EAB). Specifically, this requirement states that "During design basis accidents, offsite doses at the site Exclusion Area Boundary (EAB) shall be less than those specified in the PAG Manual: Protective Action Guides and Planning Guidance for Radiological Incidents [50] for sheltering and evacuation."

The EPA developed the PAGs to help state and local authorities make radiation protection decisions during nuclear power plant emergencies with the potential to produce significant public exposures [50]. The PAGs suggest precautions that state and local authorities can take during an emergency to keep the public from receiving an amount of radiation that might be detrimental to their health. The PAGs provide guidance during the early, intermediate, and late phases of the exposure incident.

For a Nuclear Power Plant, the PAG phase of concern is the early phase described as: "The beginning of a radiological incident for which immediate decisions for effective use of protective actions are required and must therefore be based primarily on the status of the radiological incident and the prognosis for worsening conditions. When available, predictions of radiological conditions in the environment based on the condition of the source or actual environmental measurements may be used. Protective actions based on the PAGs may be preceded by precautionary actions during the period. This phase may last from hours to days."

Use of the PAG limits in plant siting is addressed in Section 3.2 of NEI 18-04 [3].

## 2.7 Additional Guidance

### 2.7.1 ANS-53.1

The American Nuclear Society standard, “Nuclear Safety Criteria and Safety Design Process for Modular Helium-Cooled Reactor Plants”, Reference [51], specifies that event-specific source terms might include contributions from circulating activity, liftoff of plateout and dust, and release from fuel during events. Physical mechanisms that can reduce the source term prior to release to the environment, including retention within reactor graphite, deposition on primary circuit components, retention within other plant systems, deposition on equipment and structure surfaces within plant buildings, chemical interaction with reactor and building environment constituents, and radioactive decay may be considered. All radionuclide source-term calculations must use qualified models of the source term reduction processes. The standard cites NRC Regulatory Guide 1.203 [55] as one approach for qualifying methods. The Xe-100 MST approach is consistent with both RG 1.203 and ANS-53.1 as applicable.

# 3. Overview of the Xe-100 Plant Design

The Xe-100 reactor is depicted in Figure 1 and its characteristics, including dimensions, thermal power, and major operating conditions provided in Table 2, Reference [11] . The active core volume is filled with approximately 224,000 graphite fuel spheres, or pebbles, to form the pebble bed. Each pebble contains approximately 19,000 LEU UCO TRISO particles contained in a graphitic matrix. The fuel particles consist of a fissionable ceramic fuel kernel surrounded by three ceramic coating layers designed for the retention of fission products. Fissions within the coated particles produce nuclear heat conducted to the pebble's surface. Two circulators mounted on top of the steam generator (SG) vessel transport the He coolant through the pebble bed, transferring heat from the pebbles to the SG.

During normal operations, the maximum fuel core temperature is limited to less than 1000°C, which is significantly lower than many earlier HTGR designs, Reference [12]. The core excess reactivity is limited by on-line refueling as fuel can be loaded and unloaded as desired during full power operation. The Xe 100 has an overall negative temperature coefficient of reactivity due to Doppler broadening of the uranium kernel content and the fuel pebble's and reflector's graphite. This ensures stability of operations and negative reactivity insertion during core heat-up events. This inherent reactivity feedback is one of the fuel safety functions credited during transient safety analysis and allows the Xe-100 to achieve a safe shutdown condition in certain LBEs, Reference [13].

Shutdown margin and reactivity control is provided by two banks of control rods inserted into the graphite side reflector. One control rod bank, the Reactivity Control System (RCS), is used in normal operation and can achieve hot shutdown if inserted. The second control rod bank, the Reserve Shutdown System (RSS), designed as a diverse reactivity control function, is inserted by the safety-related Reactor Protection System (RPS) and used to establish long-term cold shutdown conditions. The relatively small core diameter allows safe shutdown by inserting the control rods into the side reflectors without the need of in-core control rods, Reference [13].

The Xe-100 TRISO fuel particles consist of a uranium dicarbide (UCO) fuel microsphere ("kernel") coated with multiple layers of pyrocarbon and silicon carbide (SiC) as shown in Figure 2. Using UCO for the Xe-100 design allows the use of the ongoing Advanced Gas Reactor (AGR) Fuel Development and Qualification Program data at Idaho National Laboratory and Oak Ridge National Laboratory, see Section 6. The different coating layers, consisting of the buffer, inner pyrolytic carbon (IPyC), SiC, and outer pyrolytic carbon (OPyC) layers are collectively referred to as a TRISO coating. The coating system constitutes a miniature multi-shell pressure vessel that provides retention of the fission products generated by fissioning of the nuclear material in the kernel. A substantial fraction of the fission products is retained inside the kernel itself. The performance of these coatings supports the functional containment approach for evaluating the Xe-100 design and safety analyses.

As shown in Figure 2, the four coating layers of the TRISO-coated particles have specialized purposes but in composite constitute a high-integrity pressure vessel for retaining fission products. The functions of the low-density buffer layer are 1) to provide a reservoir for fission gases (Noble gases and Halogens classes) released from the fuel kernel, 2) to attenuate fission recoils, and 3) to accommodate kernel swelling under irradiation. The main functions of the high-density IPyC coating are to provide a smooth regular substrate for the adhesion of a high integrity SiC coating and to prevent chlorine (Cl-2) and hydrogen chloride (HCl) from reacting with the fuel kernel during the SiC deposition process; hence, a major benefit of the IPyC coating is realized during fuel fabrication. The IPyC coating, which is intimately

bonded to the SiC coating, also helps to maintain the SiC coating in compression, as the former shrinks under irradiation, while the latter is dimensionally stable.

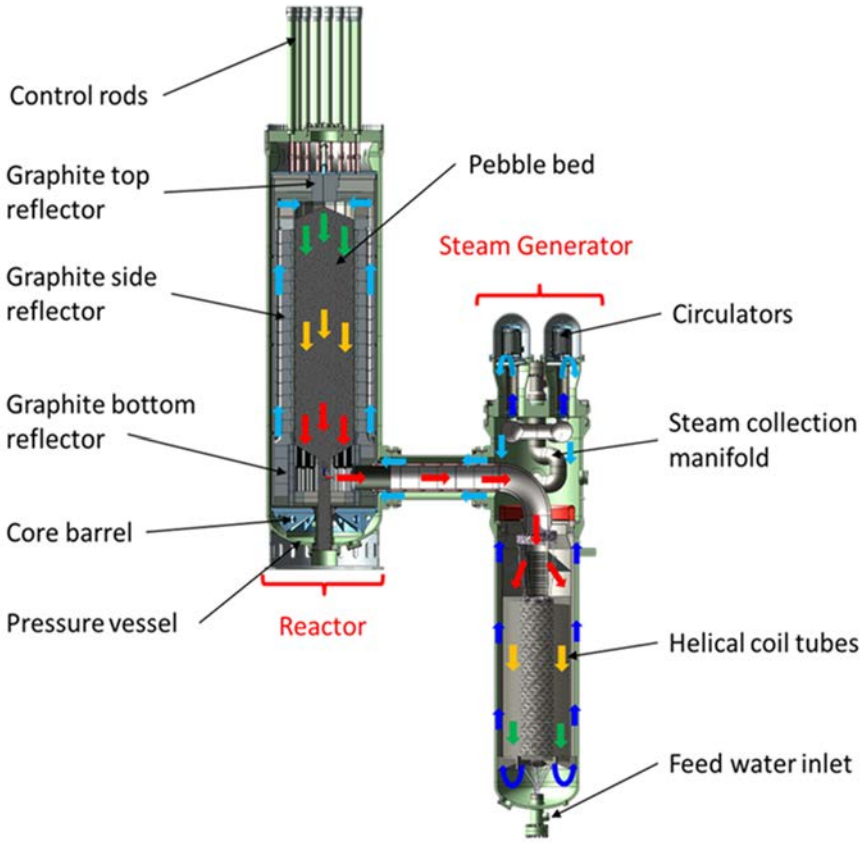


***Figure 1: Xe-100 Primary Coolant Circuit***

***Table 2: Xe-100 Reactor Main Characteristics***

| | | | |
|---|---|---|---|
| **Thermal Power** | **200 MWt** | **Helium flow rate (excluding bypass)** | **[[ ]]P** |
| **Core Volume** | [[ ]]P | **Helium pressure** | 7 Mpa |
| **Core Average Power Density** | [[ ]]P | **Pebble packing fraction** | [[ ]]P |
| **Height (Flattened Pebble Bed)** | [[ ]]P | **Particle packing fraction** | [[ ]]P |
| **Diameter of Pebble Bed** | [[ ]]P | **Burnup** | 168 GWd/MTU |
| **Average Pebble Passes through the Core** | 6 | **Enrichment** | 15.5% |
| **Heavy Metal Loading per Pebble** | [[ ]]P | **Moderation ration (C/U)** | [[ ]]P |
| **TRISO-Coated Particles per Pebble** | ~19,000 | **U-235 per pebble** | [[ ]]P |
| **Gas Inlet Temperature** | [[ ]]P | **Daily pebble charge** | [[ ]]P |
| **Gas Outlet Temperature** | [[ ]]P | **Average fuel residence time** | [[ ]]P |

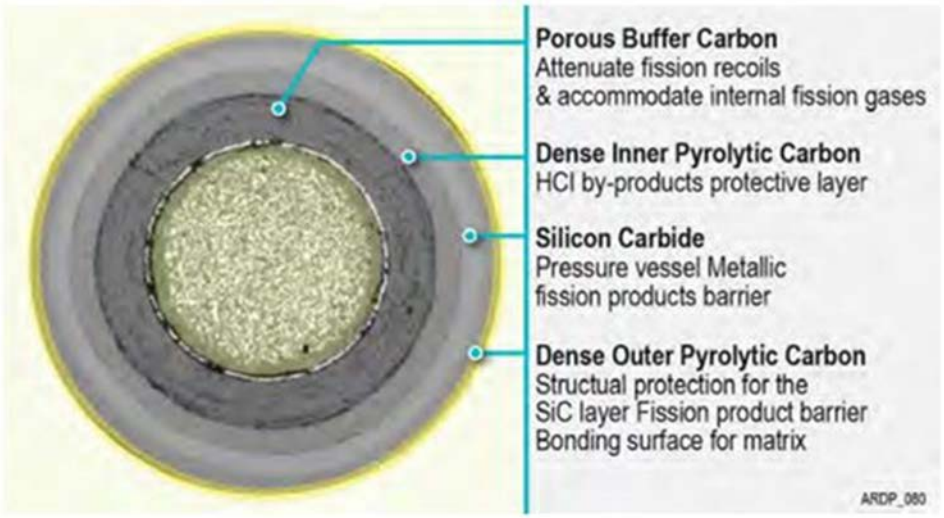


***Figure 2: TRISO Fuel Particle Configuration and Coating Functions***

## 3.1 Design Background

To facilitate NRC review and approval of this report, key Xe-100 design features are provided in this section. These features are not expected to change during the reactor's design development and provide the basis to support the safety review. Should fundamental changes occur to these key design features or revised regulations be promulgated that affect the Xe-100 MST methodology, such changes will be reconciled and addressed in future license application submittals.

## 3.2 Key Design Features of the Xe-100

In contrast to LWRs, modular HTGRs such as the Xe-100 use a functional containment approach fundamental to their licensing strategy. The functional containment is a collection of multiple independent radionuclide release barriers. Taken as a group, these barriers ensure that radionuclides are mostly retained in the fuel and that regulatory requirements and facility design goals for release of radionuclides are met at the Exclusion Area Boundary (EAB) across a broad spectrum of LBEs. As shown in Figure 3, these five release barriers are (See Reference [16]):

a. Fuel particle kernel (UCO, a heterogeneous mixture of UO2 and UCx)

b. SiC and PyC coatings applied to the fuel kernel

c. Fuel matrix and fuel free zone of the fuel pebble

d. Reactor HPB

e. Reactor building

The most important consideration in predicting the radionuclide release rates from a HTGR core is to predict the in-service performance of the TRISO-coated fuel particles. TRISO fuel is an integrated system of multiple barriers to radionuclide release. The kernel, two PyC layers, SiC layer, and fuel pebble matrix all act together to retain fission products through different physical processes. For example, the dense TRISO coating layers (PyC and SiC) are gas-tight and act as diffusion barriers. The kernel retains many metallic (Alkali metals, Tellurium group, Alkaline earths, and Lanthanide classes) fission products and some fraction of the fission gases (Noble gases and Halogens classes). The pebble fuel matrix provides some retention of metallic fission products (e.g., retention of cesium (Alkali Metals class) by a factor of 10 and strontium (Alkaline Earths class) by a factor of more than 100 but is essentially non-retentive for the gaseous fission products (e.g., iodine and noble gases).

# 4. Mechanistic Source Term Approach

As part of X-energy's Xe-100 safety analysis process, a comprehensive set of mechanistic source term analysis models have been developed for the quantification of the Xe-100 source terms and dose calculations. The approach and mechanisms used in these models is summarized below.

## 4.1 Mechanistic Source Term Approach for the Xe-100 Reactor

As addressed in Section 3.2, the Xe-100 functional containment is a collection of multiple independent radionuclide (RN) release barriers depicted in Figure 3. The various RN transport phenomena in the core, primary circuit and reactor building available for modelling when predicting source terms are also shown.

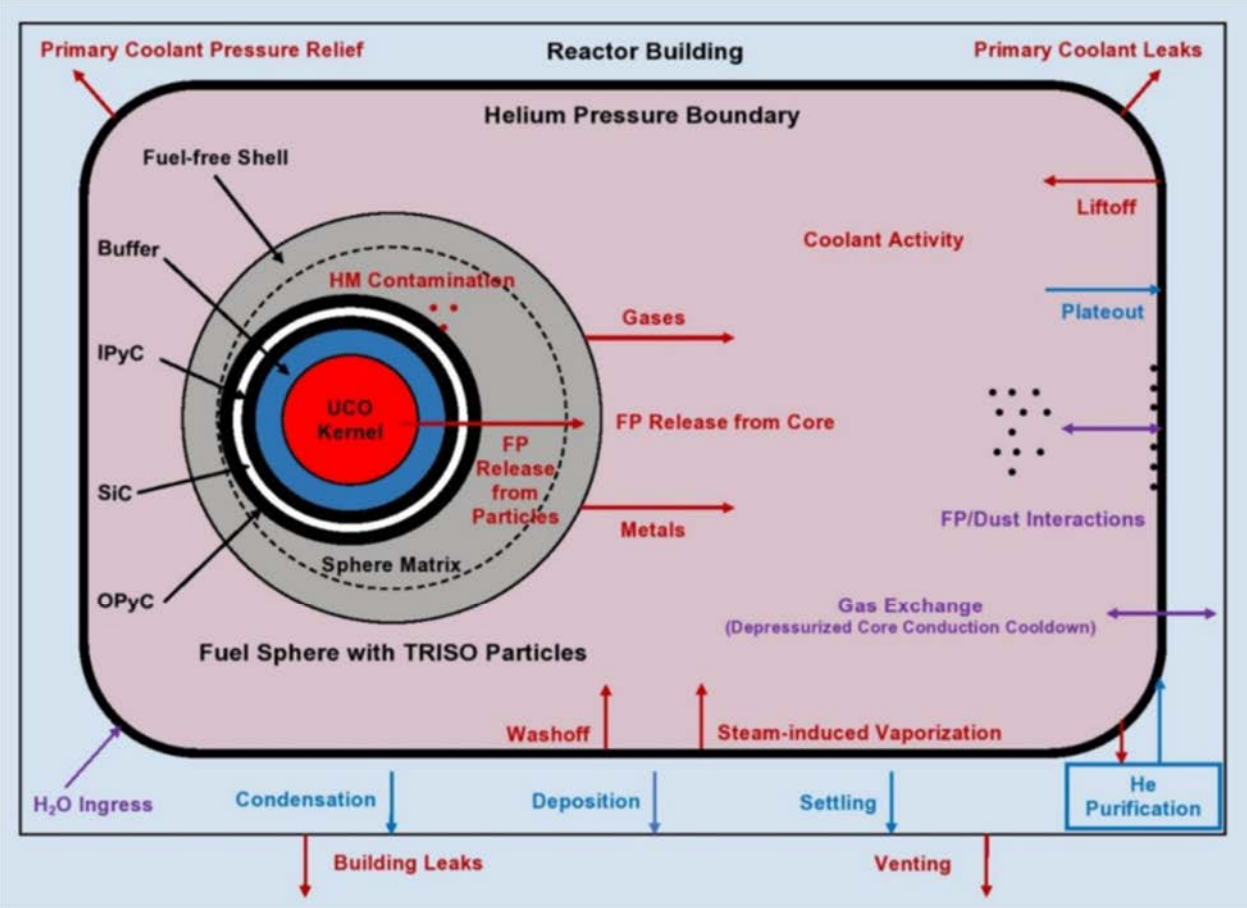


***Figure 3: Pebble Bed HTGR Radionuclide Retention System***

These RN transport phenomena include:

- Radionuclide Transport and Retention in the TRISO Fuel Particle Kernels
- Radionuclide Transport and Retention in the Silicon Carbide and Pyro-Carbon Coatings of the TRISO Fuel Particles
- Radionuclide Transport and Retention in the Fuel Matrix of Pebble Fuel Element
- Radionuclide Transport in the Primary Circuit Helium Pressure Boundary (HPB)
- Radionuclide Transport in the Reactor Building

Each of these barriers contributes to limit the release of radionuclides to the environment. The contribution of each of the barriers in limiting radionuclides releases to the environment is calculated for each licensing basis event. The barrier performance is design, licensing basis event, and radionuclide species' dependent. The phenomena that determine RN transport and release from licensing basis events are schematically shown in Figure 3.

Collectively, the fuel constitutes the first three release barriers. Typically, the fuel particles retain the bulk of the fission products even during Beyond Design Basis Events (BDBEs). In a Xe-100 reactor, failure of one of the fuel barriers (e.g., a broken pebble, failure of TRISO-coated particles) does not have an impact on any of the neighboring radionuclide barriers.

The release fraction from the particles is calculated accounting for the as-manufactured fuel reliability (e.g., the allowable heavy-metal contamination and coating defects), fuel failure during irradiation, incremental fuel failure under LBE conditions, and diffusion of fission products through the intact particle coatings under LBE conditions. These factors are calculated on a LBE-specific basis, as a function of fuel burnup, maximum operating temperature, maximum post-LBE temperature and, where applicable, air and/or moisture contamination in the reactor helium coolant, (e.g., from of a steam generator tube rupture). See Reference [17] for Non-LWR functional containment regulatory guidance. Further radionuclide retention is accomplished via plateout on the HPB component surfaces. Although additional radionuclide deposition and holdup can be obtained in the Reactor Building, these dose reduction mechanisms are conservatively not credited.

The MST methodology documented in this LTR interfaces with the Xe-100 Transient and Safety Analysis Methodology (TSAM) LTR, Reference [7], to complete the documentation of LBE dose determinations. The TSAM LTR interfaces with the MST LTR as follows:

a. Documents the identification and application of LBE analytical codes with descriptions of the Xe-100 LBE system transient evaluation models. This includes references to MST related analytical code qualification LTRs if available. (EMDAP Elements 1 & 4)

b. Identifies explicitly modeled SSCs (including I&C) as well as outline SR SSCs credited explicitly for DBAs

c. Includes TSAM Phenomena Identification & Ranking Tables (PIRT) and associated Figures of Merit (FOM) as well as implementation of the Evaluation Model Development and Assessment Process (EMDAP) for all referenced codes and Evaluation Models (EM). (EMDAP Elements 1 & 4)

d. Describes LBE specific safety evaluation methodologies and approach, in particular:

- As part of the safety analysis of the Xe-100, it is necessary to calculate the radiological dose to the public following LBEs. Radiological dose analyses require the equilibrium inventory of radionuclides (RN) in the reactor core and helium pressure boundary (HPB). The Xe-100 steady state isotopic inventory and calculations are addressed.
- During short duration LBE's, increases in particle and pebble temperatures may result in thermal-induced diffusion of radionuclides off the pebbles. These events are analyzed with a thermal hydraulics code to determine the fuel temperature increase history. Calculation of these RN inventory increases do not require an event specific MST core heat-up analysis provided conservative dose estimates are developed from MST based calculations at different postulated fuel temperatures. The event driven inventory is then added to the equilibrium inventory to determine the radiological dose consequence of the LBE.

## 4.2 XSTERM

As part of X-energy's radiological code development process, a comprehensive software code, XSTERM, has been developed for the quantification of the Xe-100 source terms and dose calculations.

The code includes subroutines for:

- Thermal hydraulic modeling and transient analysis (e.g., reactor physics and thermal hydraulic simulations)
- Radionuclide production, decay, transmutation and transport in the fuel spheres
- Radionuclide retention, transport and release from fuel pebbles into the helium coolant
- Transport and distribution of radionuclides, including dust effects, within the HPB
- Transport of radionuclides into the reactor building and the environment
- Point-source to point-receptor dose calculations

The XSTERM code subroutines operate in an integrated fashion to evaluate the source term and subsequent dose consequences of Xe-100 LBE evaluation models. Each code subroutine module has specific modeling requirements as detailed in Section 5. Applications of XSTERM include dose consequence calculations for LBEs identified by probabilistic risk assessment to develop the frequency-consequence curves specified in NEI 18-04, Reference [3] and calculating the source term and dose consequences of deterministically evaluated DBAs.

The underlying methodology and theory upon which the XSTERM subroutines are based is addressed in Section 5 and described in detail in Appendices A-H as required. These models may be revised to improve accuracy and performance, but the as documented base theory is not expected to change.

# 5. Mechanistic Source Term Models

The functional containment, Section 3.2 and Figure 3, is a collection of multiple independent radionuclide release barriers. These barriers ensure that radionuclides are mostly retained in the fuel and EAB dose regulatory limits are met across a broad spectrum of LBEs. The Xe-100 MST models associated with these release barriers are described in this Section. The computational relationships between these MST models are summarized in Appendix H, Figure H-1.

## 5.1 Xe-100 MST Models

### 5.1.1 TRISO Particle Failure Probability Model

#### 5.1.1.1 Overview of Particle Failure Probability Calculations(FPM)

The TRISO-coated particle failure probability model (FPM) calculates the TRISO-coated particle failure probabilities during normal and LBE conditions. Particle failure probabilities are calculated for failure mechanisms including vessel failure (i.e., Silicon Carbide (SiC) layer failure due to internal gas pressure in the particle), kernel migration (amoeba), fission product corrosion, thermal decomposition, IPyC cracking and manufacturing defects.

##### 5.1.1.1.1 Xe-100 Fission Product Retention

Irradiation experiments have shown that most of all fission products are contained within the coated particles and thus the coated particles are seen as the first barrier that protects the public from offsite fission product releases. Many of these fission products have short half-lives and thus are of a lesser concern for radiation protection. Certain radionuclides form stable oxide compounds in the kernel of the fuel particles which, in general, eliminates or reduces their mobility. However, a small amount of the radioactive gases, including iodine (I) isotopes, as well as volatile metals such cesium (Cs) and silver (Ag) can escape from the coated particles into the fuel elements and may enter the primary circulating helium, Reference [11].

##### 5.1.1.1.2 Particle Failure Mechanisms

Radionuclide releases from the TRISO-coated particles can occur through several mechanisms. These mechanisms range from manufacturing defects to temperature and irradiation-induced damage.

During the manufacturing process, a small fraction of the TRISO-coated particles can experience defects, References [11] and [17]. In addition, there can be some uranium contamination in the particle layers as well as in the pebble graphite matrix. These as-manufactured defects are potential sources of fission product release into the circulating helium and could plateout in the HPB. Under LBE conditions, abnormally high temperatures may cause a small fraction of the TRISO-coated particles to fail and release fission products.

In general, sources of fission product release can be divided in three groups, including heavy metal (HM) contamination, failed, and intact particles:

- Uranium and Thorium Contamination in the Fuel Constituent Materials:

  This contamination is usually present in both the graphite matrix and the OPyC layer. Fission products created by fission of this contamination need only to diffuse through the OPyC and the matrix material and desorb into the helium before being released. Modern fuel specifications restrict this HM contamination to a small fraction (approximately $10^{-5}$ is typical, Reference [20])

- Defective and Failed Coated Particles:

  A small fraction of the as-manufactured TRISO-coated fuel particles can contain various types of defects. In addition, during both steady-state irradiation and LBE conditions, a small fraction of the standard coated fuel particles may fail. In the event of failed particles, it is assumed that fission products do not migrate through the layers but rather are released directly from the fuel kernel to the matrix material.

- Intact TRISO-Coated Particles:

  In fully intact TRISO-coated particles, fission products must migrate through all the layers before they are released to the graphite matrix. Diffusion coefficients of gaseous fission products are extremely small, Reference [15]. Therefore, the transport rates of gaseous fission products and release fractions from intact coated particles are significantly smaller than defective or failed particles. Some metallic fission products have considerable mobility and their release is accounted in intact TRISO coated particles.

Particle failure fractions , fractional releases from contamination, and graphite attenuation factors can vary in space and time. Particles with a failed SiC coating but with intact inner and/or outer pyrocarbon coatings are also accounted.

#### 5.1.1.1.2.1 In-Service Particle Service Mechanisms

The following failure mechanisms have been identified as capable of causing functional degradation and/or through-coating failure of the TRISO-coating system under irradiation and/or during LBEs (References [15], [21], and [22]).

- Pressure vessel failure of standard (“intact”) particles (i.e., particles without manufacturing defects)
- Pressure vessel failure of particles with defective or missing coatings
- Irradiation-induced failure of the OPyC coating
- Failure of the SiC coating caused by kernel migration in the presence of a temperature gradient
- Failure of the SiC coating caused by chemical attack of fission products
- Failure of the SiC coating caused by CO corrosion
- Failure of the SiC coating resulting from thermal decomposition

These fuel failure mechanisms are limited through a combination of fuel kernel choice and design of the TRISO coating system, fuel pebble, and reactor core and associated operating envelope. Phenomenological performance models, based on first principles and correlated with experimental data, have been developed to model each of these failure mechanisms (e.g., References [22] and [23]).

A full discussion of the particle failure probability calculations methodology and theory is included in Appendix A.

### 5.1.2 Solids Fission Products Transport Calculations Model (SOLM)

#### 5.1.2.1 Overview of Solids Fission Products Transport Calculations

A radionuclide diffusion model is used for calculating the production, decay, transmutation, transport, and leakage of gaseous and solid fission products from fuel pebbles into the helium pressure boundary under steady-state and LBE conditions. The model is normally used for pebble calculations for fuel paths through the core and couples with the thermodynamics model to update the pebble's temperature distribution. TRISO-coated particle failure probabilities are integrated from the particle's failure probabilities model. Inventories and the distribution of fission products in the HPB are provided by the HPB model. Thus, in an integrated calculation, the solids fission transport, thermodynamics, particle failure probabilities, and the inventory/distribution of fission products in the HPB are calculated.

The fission product releases from the pebbles are calculated for a 2D core configuration containing the fission product history at each point in the core. A fission product distribution library is generated for all particle and pebble radial zones in all the core regions accounting for fuel movement in a multi-pass fueling regime.

The solids fission product transport calculation model performs the following functions:

- Integrates the fuel particle and element materials data
- Models the fuel pebbles and particles in a fine mesh (20 radial zones for spheres, 50 radial zones for particles)
- Calculates the production of metallic fission products in the fine meshes, accounting for direct fission, decay, transmutation, and activation sources
- Calculates removal by means of decay and neutron capture
- Models transport and release of fission products from particles and fuel elements by means of diffusion calculations using time-dependent diffusion equations with temperature-dependent effective diffusion coefficients
- Accounts for the effects on isotope transport and retention from as-manufactured particle defects, contamination, and particle failure fractions calculated by the particle failure probability model
- Calculates isotope concentrations in the fuel elements and particle meshes in all core nodes
- Creates the core isotopic library concentration distributions used as the initial condition for transient calculations, selects and calculates isotope reaction chains used in source, decay, and removal calculations
- Models irradiation and safety (annealing) experiments for both spherical and compact geometries
- Can be used in Monte Carlo uncertainty calculations

The gaseous and solid fission product densities in the TRISO particles and graphite matrix are calculated in this model. The transport and release behavior of these radionuclides are strongly dependent on the fuel temperature. A diffusion transport model is applied to calculate the radionuclide distribution in the TRISO-coated particles and fuel pebbles, and the leakage rates from the fuel surfaces into the helium pressure boundary (HPB).

This model can also simulate gaseous and halogen radionuclide releases during temperature transients. The model receives input data such as fuel temperature, burnup, and fluence levels from the thermodynamics model (THM) and failed particle fractions from the particle failure probability model (FPM). During steady state irradiations, release over birth ratios (R/B) are estimated by dividing the rate of releases by the generation rate for the isotopes of interest. In addition, during temperature transients and annealing experiment's simulations, fractional isotopic releases are estimated by dividing the transient or annealing release by the initial sample inventory.

The SOLM can be used for TRISO fuel experiments as well as full-core analysis of the Xe-100 reactor. The Xe-100 reactor design fuel is uranium oxycarbide (UCO), however, historic experiments used uranium dioxide (UO2) fuel. In addition, many experiments, including the Advanced Gas Reactor (AGR) experiments, were performed using fuel compacts instead of fuel spheres. The solids fission transport model can be used to calculate releases from the following:

- TRISO fuel particles with UCO
- Graphite fuel spheres for High Temperature Gas Reactors (HTGRs) and fuel experiments
- Graphite fuel compacts for fuel experiments
- Pebble-bed HTGRs with multi-pass fuel management schemes

A full discussion of the solids fission products calculation methodology and theory is contained in Appendix C.

### 5.1.3 Thermodynamics Calculation Model (THM)

#### 5.1.3.1 Overview of Thermodynamics Calculation Model

A thermodynamics methodology has been developed to calculate detailed temperature distributions in fuel pebbles, TRISO-coated fuel particles, and all the core components such as reflectors, barrel, and reactor pressure vessel (RPV) during normal and LBE conditions. Component temperature profiles are required to calculate parameters such as fuel failure fractions and diffusion coefficients. This model is used in calculations for the long-term portion of LBEs where use of detailed thermal hydraulic codes is not practical.

The models calculate detailed temperature profiles in the appropriate model geometry of TRISO-coated particles, fuel elements, core, and other reactor components, using multi-pass pebble power profile, helium temperature and core mass flow rate imported from the neutronics design code Very Superior Old Programs (VSOP).

Detailed fuel element and TRISO-coated particle temperatures are needed to perform fuel failure probability calculations and radionuclide transport calculations. Fuel failure models and diffusion coefficients in radionuclide transport calculations strongly depend on TRISO-coated particle and fuel element graphite matrix temperatures, respectively. Because the neutronics design code VSOP does not calculate temperatures at this level of detail, the thermodynamics model performs detailed temperature calculations for the entire core using boundary conditions.

A full discussion of the thermodynamics methodology and theory is contained in Appendix B.

### 5.1.4 Steady-State Gaseous Fission Products Transport Calculations Model (GASM)

#### 5.1.4.1 Overview of Steady-State Gaseous Fission Products Transport Calculations

This model performs steady-state calculations of gaseous fractional R/B ratio of fission products release from TRISO-coated fuel particles and pebbles (spheres) into the primary circuit coolant gas.

The calculations consider gaseous fission product releases from manufactured heavy metal (HM) contamination, particles coating failure during normal operation, and incremental particle coating failure during core heat-up. Two different gaseous fission product transport models are implemented, the Röllig and Richards models. Both models are applicable for gaseous fission product release from fuel pebbles under irradiation and in the absence of oxidants.

##### 5.1.4.1.1 Sources of Fuel Fission Products Release

A large inventory of radioactive fission and activation products are accumulated in the HTGR TRISO fuel. Many of these radioactive fission products have short half-lives and others form stable oxide compounds in the kernel section of the fuel particles which generally tends to reduce their mobility. However, some of the radioactive gases, including iodine isotopes, as well as volatile metals such as cesium (Cs) and silver (Ag) might escape from the fuel elements and enter the primary coolant circuit.

As addressed in Section 5.1.1, FPM, during the manufacturing process, a small fraction of the TRISO-coated particles will contain various defects. In addition, there will be some uranium contamination in the particle layers as well as in the pebble's graphite matrix. These as-manufactured defects are potential sources of fission products release into the coolant gas. Under LBE conditions, abnormally high temperatures may cause a small fraction of the TRISO-coated particles to fail and release fission products. Condensable radionuclides released from the core can plateout in the cooler regions of the primary coolant circuit causing a radiation hazard to operating personnel and, if released from the primary coolant circuit, a potential release to the public.

In general, sources of fission product release can be divided in three groups, including heavy metal (HM) contamination, failed, and intact particles.

The two dominant sources of fission product release from the fuel are "as manufactured" heavy metal (HM) contamination and particles whose coatings fail in service. The latter source can be subdivided into: (1) coating failure during normal operation and (2) incremental coating failure during core heatup.

The observed failure mechanisms for TRISO fuel can be categorized as either structural/mechanical or thermochemical in nature. Failure mechanisms in both categories can be affected by the release of excess oxygen during fission and subsequent formation of carbon monoxide.

##### 5.1.4.1.2 Gaseous Fission Product Flow Patterns

The flow pattern of the rare gas atoms from failed and contaminated particles to the fuel pebble surface and into the coolant is shown in Figure 4 and Figure 5.

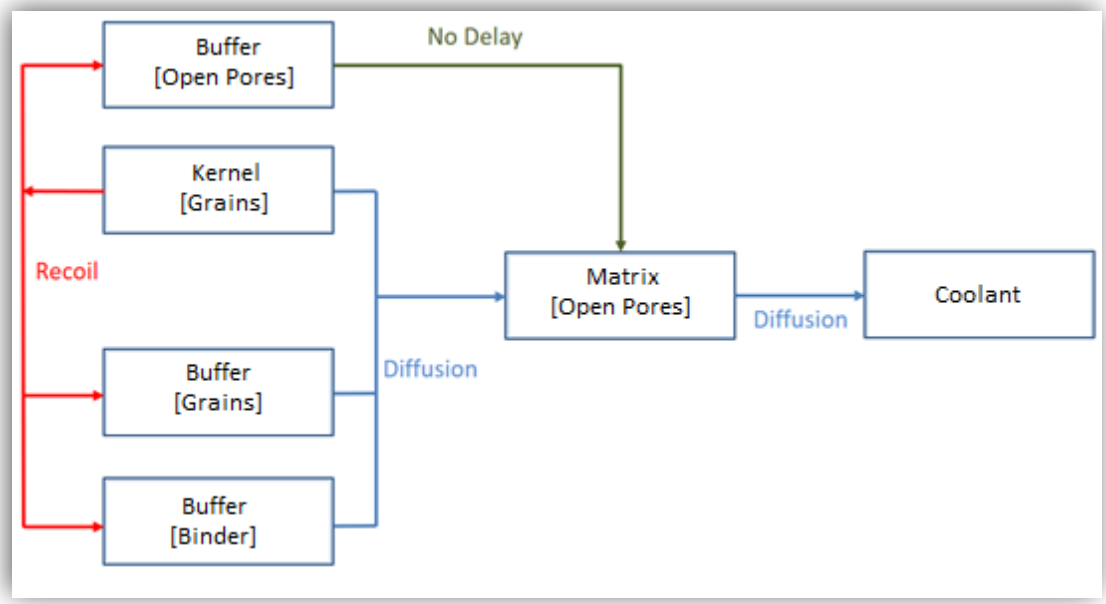


***Figure 4: Defective and Failed Particle Gas Transport Model***

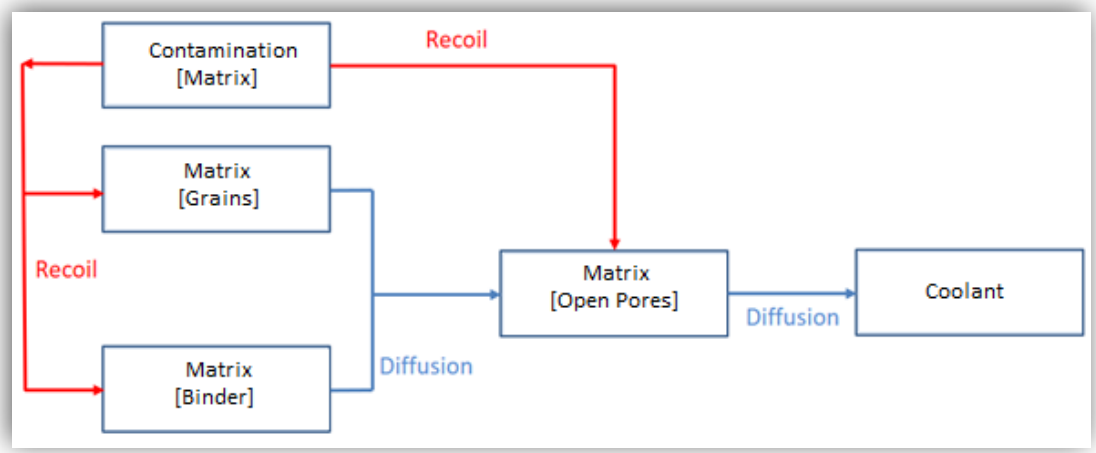


***Figure 5: Matrix Heavy Metal Contamination Gas Transport Model***

Due to the relatively short half-lives of the gas isotopes, the transport from the fuel kernel through intact coatings can be neglected. Therefore, the fuel contamination of the outer PyC coating controls the gas release from intact particles. This release occurs via two principal mechanisms: direct recoil and diffusion. Gas atoms and their pre-cursors diffuse from the recoil sites within the fuel matrix material into the open porosity of the fuel element. The atoms reach the element surface and the coolant by gas-phase transport through the porous medium.

For particles with defective coatings, Figure 4, most of the gas release initiates from the kernel. After leaving the grains of the kernel by volume diffusion, the fission products migrate along the grain boundaries and/or the interconnected porosity to the kernel surface. The atoms from the fission sites near the kernel surface are released by diffusion from surface grains and by fission recoil into the surrounding buffer layer. After release from the kernel, the gases permeate through the coating defects and release via the interconnected porosity of the matrix material. It has been demonstrated experimentally that failed coatings mostly retain fission gases as long as the coatings are constrained by the matrix, Reference [15], Section 3.3.2.

The shortest release route corresponds to the rare gases generated by the fuel contamination in the matrix material, Figure 5. The fission products are recoiled from the contamination into the different matrix components where they are released by volume diffusion, followed by gas phase transport to the fuel element surface.

A full discussion of the steady-state gaseous fission products transport calculation methodology and theory is contained in Appendix D.

### 5.1.5 Dust Production Rate Calculations Model (DUSTM)

#### 5.1.5.1 Overview of Dust Production Rate Calculations Model

This model calculates graphite and metallic dust production rates for the Xe-100. A dust production model is required as radionuclides produced in the core can be transported with the dust in the helium coolant throughout the helium pressure boundary (HPB). Dust is produced from mechanical wear such as the pebble-to-pebble and pebble-to-reflector interactions in the core, pebble-to-pipe interactions in the fuel handling system (FHS), and control rod-to-reflector interactions in the reactivity control system (RCS). Mechanical wear is the only mechanism accounted as a major source of dust.

The calculations include a model calibration based on operating pebble bed reactors data. For this purpose, a dust production model constant is calculated for the German Arbeitsgemeinschaft Versuchs Reaktor (AVR) reactor configuration and operating conditions. The dust model constant was then systematically varied until the total dust production in the AVR matched the best estimated value of graphite production for a given effective full power years (EFPY). The resultant calibration model constant is assumed reactor independent and applied to the Xe-100 configuration.

A full discussion of the dust production calculation methodology and theory is contained in Appendix E.

### 5.1.6 HPB Radionuclide Transport, Deposition and Lift-off Calculations Model (HPBM)

#### 5.1.6.1 Overview of the HPB Radionuclide Deposition and Lift-off Calculations Model

The HPB is the fourth radionuclide release barrier represented in Figure 3. The HPB Deposition/Lift-off model (HPBM) is used to calculate the amount and distribution of radionuclides within the HPB under steady-state and LBE conditions. The calculations include a mass balance of the helium pressure boundary including the reactor core, and model the time-dependent transport, activation, plateout, and re-entrainment through all HPB components. The radionuclide distributions calculated by this module are used for plant design as well as provide the initial boundary conditions for source term calculations if there is a breach in the HPB.

The calculations consider radionuclide transport within the HPB by means of helium flow either as atomic species or as dust particles, as well as pebble movement through the core and the fuel handling system (FHS). The module incorporates mechanisms such as (1) sorption or attachment of condensable radionuclides to dust particles; (2) the deposit ("plateout") of dust particles and condensable radionuclides on the structural components and pebbles; (3) the movement of plated-out radionuclides and dust particles on the fuel pebbles in the core and fuel handling system; and (4) the re-entrainment ("liftoff") of radionuclides and dust particles.

The model utilizes reactor parameters that influence the radionuclide and dust behavior throughout the HPB such as: neutron flux, activation cross-sections, radioactive decay constants, dust production rates, radionuclide release rates, dust impurity levels, dust filter efficiencies, dust particle size distributions, HPB layout and dimensions, thermal–hydraulic parameters and material properties, such as sorption isotherms. The model is integrated with the DUSTM model addressed in Section 5.1.5. The governing equations contain the rate of deposition and re-entrainment coefficients expressed as correlations. These correlations contain calibrated parameters derived empirically from the Arbeitgemeinschaft Versuchsreaktor (AVR) experimental data, Reference [34].

A full discussion of the HPB radionuclide deposition/lift-off methodology and theory is contained in Appendix F.

### 5.1.7 Core Corrosion Calculations Model (CORRM)

#### 5.1.7.1 Overview of the Core Corrossion Calculations Model

The Core Corrosion Calculations Model (CORRM) is used to simulate the mass transport and chemical reaction aspects of the core corrosion phenomena encountered during water or air ingress into the core of the Xe-100.

While the primary helium coolant of a modular HTGR is chemically inert, trace quantities of oxidants can be introduced into the primary circuit during normal operation and more significant quantities of water or air can be introduced into the reactor vessel during some LBEs with a spectrum of consequence. In particular, water and oxygen can react with the fuel pebbles and the structural graphite components and potentially compromise the structural integrity of these components and, in the case of the fuel pebbles, result in additional Fission Products (FP) releases from the core. Plant features eliminate or mitigate these corrosion related impacts to meet design requirements.

The interactions of oxidants with core materials are generally described as heterogeneous gas-solid reactions. Heterogeneous gas-solid reactions have been extensively investigated both experimentally and theoretically due to their prominent role in industrial chemical synthesis, particularly with solid metal catalysts. As a result, there is a large literature compilation emphasizing the various types of gas-solid reactions which provide comprehensive relevant data associated with the interactions of water and air with HTGR core materials. A full discussion of the Core Corrosion Calculations Model methodology and theory is contained in Appendix G.

### 5.1.8 Tritium Production and Transport Model (TRITM)

The TRITM model is used to calculate the overall tritium (T, H 3, 1H3) mass balance in the Xe-100. The model's mass balance calculations account for the production and transport of tritium in the core, as well as permeation into the secondary steam system. Tritium is produced in a HTGR by various nuclear

reactions. Given its high mobility, especially at high temperatures, some tritium will permeate through the steam-generator tubes into the secondary steam.

Sources of tritium production have been identified, primarily from early surveillance programs at operating HTGRs. They include ternary fission, neutron activation of He-3 in the primary helium coolant, neutron activation of lithium impurities in the fuel-element matrix and core graphite, and neutron capture reactions in boron used in control materials. Tritium chemisorbs on irradiated nuclear graphite at elevated temperatures. Consequently, a large fraction of the tritium entering the primary helium coolant will be absorbed on the huge mass of graphite in the core. However, a large fraction of this stored tritium can be rapidly released back into the coolant if water is introduced into the primary circuit which causes the tritium to desorb from the fuel-element matrix and core structural graphite. Tritium can permeate through the steam-generator tubes and process piping in a co-generation plant and contaminate the process steam. Surface films will play a dominant role in establishing the in-reactor, tritium permeation rates. Oxide films can reduce H 3 permeability by orders of magnitude; however, normal plant operating transients (e.g., startup/shutdown, etc.) may compromise film integrity and result in increased H 3 permeation rates.

Although there is a large international data base of integral H-3 transport data, primarily from operating HTGRs, there are still important gaps in the H-3 material property data base (e.g., the H-3 sorptivity on irradiated fuel-element matrix, including the effects of coolant impurities). The Xe-100 TRITM model is under development.

### 5.1.9 2D Point Kinetics Core Simulation Model (KSIM)

#### 5.1.9.1 Overview of the 2-D Point Kinetics Simulation Model

The reactor Kinetics Core Simulation Model (KSIM) uses a 2D axisymmetric geometry model to simulate the transient behavior of the Xe-100 core. The discretization consists of 13 radial zones (five for the fueled core zone and eight for reactor structure), each divided into 30 axial nodes. This model is used to initialize the simulation's steady state and the SGTR event, see Appendix B, Figure B-1.

The model is initialized via steady state transport boundary conditions obtained from the neutronics code VSOP and performs transient simulations from this initial steady state. A point kinetics approach is applied to each cell individually, using that cell's nuclear data (cross sections, isotopic concentrations, etc.) and the geometric buckling from the current flux solution (to compute leakage terms). The model can reshape the flux profile between timesteps using a diffusion kernel approach. Two implicit methods for time stepping are used, the first order accurate backwards Euler method and a second order accurate backwards differentiation (BDF2).

Six delayed neutron groups are calculated for each of the 150 core nodes, based upon delayed neutron data and densities of U-235, U-238, Pu-239, Pu-240 and Pu-241 in each node. Fission yield and half-life data provided in Reference [26] is listed in Table 3.

A one-group, cross-section weighted neutron flux is mapped from VSOP. Temperature dependent reactivity feedback (which plays an essential role in reactor control and safety) is modeled. See Section 5.1.3 for a discussion on temperature computations.

The Reactivity Control System (RCS) and Reserve Shutdown System (RSS) consist of control rods outside of the fueled core region, within the channels of the neutron reflectors. Movements of these rods are simulated in the kinetic solver via a modification of neutronic boundary terms (albedo).

The production and decay of notable neutron poisons Xe-135 and Sm-149, which play an important role in short term (hours) power transients such as load following, is simulated. To facilitate the Xe-135 accounting, the precursor I-135 production and decay is tracked within the model. Similarly, the Sm-149 precursor Pm-149 is also tracked.

The model implements a simulated turbine control, affecting the heat removal rate from the helium cooling gas by the steam generator heat exchanger. In principle, the reactor power will follow the turbine power through the temperature reactivity feedback mechanisms.

***Table 3: Delayed Neutron Yield & Half-Life Data [26]***

| $^{235}U$: $\nu_d = 0.01668 \pm 0.0070\ n/f$ | | | $^{238}U$: $\nu_d = 0.0460 \pm 0.0025\ n/f$ | | |
|---|---|---|---|---|---|
| **Group** | $T_{1/2}$ | **Relative Yield** | **Group** | $T_{1/2}$ | **Relative Yield** |
| 1 | 54.51 | 0.038 ± 0.004 | 1 | 52.38 | 0.013 |
| 2 | 21.84 | 0.213 ± 0.007 | 2 | 21.58 | 0.137 |
| 3 | 6.00 | 0.188 ± 0.024 | 3 | 5.00 | 0.162 |
| 4 | 2.23 | 0.407 ± 0.010 | 4 | 1.93 | 0.388 |
| 5 | 0.496 | 0.128 ± 0.012 | 5 | 0.493 | 0.225 |
| 6 | 0.179 | 0.026 ± 0.004 | 6 | 0.172 | 0.075 |
| $^{239}Pu$: $\nu_d = 0.00645 \pm 0.00040\ n/f$ | | | $^{240}Pu$: $\nu_d = 0.0090 \pm 0.0009\ n/f$ | | |
| **Group** | $T_{1/2}$ | **Relative Yield** | **Group** | $T_{1/2}$ | **Relative Yield** |
| 1 | 53.75 | 0.038 | 1 | 53.56 | 0.028 |
| 2 | 22.29 | 0.280 | 2 | 22.14 | 0.273 |
| 3 | 5.19 | 0.216 | 3 | 5.14 | 0.192 |
| 4 | 2.09 | 0.328 | 4 | 2.08 | 0.350 |
| 5 | 0.549 | 0.103 | 5 | 0.511 | 0.128 |
| 6 | 0.216 | 0.035 | 6 | 0.172 | 0.029 |

| $^{241}Pu$: $\nu_d = 0.0157 \pm 0.0015\ n/f$ | | |
|---|---|---|
| **Group** | $T_{1/2}$ | **Relative Yield** |
| 1 | 54.0 | 0.010 |
| 2 | 23.2 | 0.229 |
| 3 | 5.6 | 0.173 |
| 4 | 1.97 | 0.390 |
| 5 | 0.43 | 0.182 |
| 6 | 0.2 | 0.016 |

## 5.2 Radionuclide Transport in the Reactor Building

The Reactor Building is the fifth radionuclide release barrier identified in Figure 3. The current Xe-100 safety analysis does not credit decay (holdup) or deposition in the RB. Releases from the RB are assumed to discharge at ground level without credit for stack elevation or filters. See Section 5.3.

## 5.3 Atmospheric Dispersion and Dose Calculations

An atmospheric dispersion and dose calculation model is used to generate the associated doses from DBAs. The model calculates LBE doses to the plant EAB as well as to the Control Room (CR) location. Dose dispersion factors are calculated based on user inputs or from dispersion factors calculated elsewhere and input by the analyst. Offsite doses are calculated based on a Gaussian plume model.

A list of isotopes significant to dose calculations is included in Table 4. Key radionuclides are selected based on the combination of their fission yield, their transport and release properties, and their

radiological hazard level. The radiologically most relevant radioisotopes monitored during LBE simulation include the long-lived strontium (Sr-90), silver (Ag-110m), cesium (Cs-134, Cs-137), europium (Eu-152, Eu-154, Eu-155) and krypton (Kr-85) activation and fission products, and the short-lived iodine (I-131) and xenon (Xe-133) fission products. Isotopes of the same chemical group are assumed to have similar transport and retention attributes.

A generic set of dispersion factors has been developed to provide generally conservative values as part of the standard Xe-100 technology development process. This methodology is described in Section 5.1 of the "Xe-100 Licensing Topical Report Atmospheric Dispersion and Dose Calculation Methodology," Reference [14], and ensures that conservative accident doses are calculated for most locations within the continental United States. This allows X-energy to evaluate the Xe-100 LBEs in a manner similar to other reactor technologies that consider a range of prospective project sites defined by a parameter envelope. These conservative dispersion factors are calculated for a generic site using applicable regulatory guidance and the theory and site field data presented in Reference [25]. Site-specific evaluations will be conducted to either 1) affirm the Xe-100 analysis results using these generic dispersion factors are conservatively bounding, or 2) provide site-specific analysis results using dispersion factors developed during site characterization. It is expected that site-specific EAB atmospheric dispersion factor calculations will use the latest regulatory guidance, including RG 1.249 for use of the ARCON code, Reference [24].

For further details, see the "Xe-100 Licensing Topical Report Atmospheric Dispersion and Dose Calculation Methodology," Reference [14].

***Table 4: Isotopes used in Dose Calculations***

| Isotope | File Order No. |
|---|---|
| I-131 | 1 |
| I-132 | 2 |
| I-133 | 3 |
| I-134 | 4 |
| I-135 | 5 |
| Kr-83m | 6 |
| Kr-85 | 7 |
| Kr-85m | 8 |
| Kr-87 | 9 |
| Kr-88 | 10 |
| Kr-89 | 11 |
| Xe-131m | 12 |
| Xe-133 | 13 |
| Xe-133m | 14 |
| Xe-135 | 15 |
| Xe-135m | 16 |
| Xe-137 | 17 |
| Xe-138 | 18 |
| Cs-137 | 19 |
| Cs-134 | 20 |
| Ag-110m | 21 |
| Sr-90 | 22 |
| Eu-152 | 23 |
| Eu-154 | 24 |
| Eu-155 | 25 |
| Te-132 | 26 |
| La-140 | 27 |

# 6. MST Models V&V Plans

X-energy Procedure QAP-3.10, "Software V&V for Design & Safety Analysis Procedure" [44] defines the process to ensure that Software used for design, analysis and supporting activities that impact safety of the Xe-100 program is verified and validated in a planned and systematic manner. The procedure defines Verification as the process to demonstrate that the Software implements the required theoretical and mathematical basis in a correct and error free manner that is consistent with the Software Design Specification (SDS). The procedure defines Validation as the process to assess the fitness-for-purpose of the Software and quantifies the accuracy of key parameters calculated by the Software. QAP-3.10 notes that in the context of NQA-1, Validation is referred to as Acceptance Testing.

The X-energy code XSTERM is being used in the Xe-100 safety analysis. This Section of this LTR documents the V&V Plans developed to ensure that the XSTERM code is verified and validated in accordance with the requirements of QAP-3.10.

## 6.1 V&V Scope

The XSTERM code has been developed by X-energy over several years and is currently maintained in accordance with the X-energy Quality Assurance Program Description (QAPD) [19]. The code V&V effort is underway to ensure the Software is fully qualified to support the final safety analysis. The scope of these V&V efforts is documented in this Section.

### 6.1.1 V&V Efforts

The XSTERM Software is being verified to demonstrate that the code implements the required theoretical and mathematical basis in a correct and error free manner consistent with the Software Design Specification (SDS). The code will undergo line-by-line verification to ensure proper implementation of each code segment's intent. Segments which implement mathematical models specified within the theory manual(s) will be compared against the relevant equation(s) and methods. Upon completion of initial unit and integration testing, automated testing frameworks will be leveraged to aid in verification of future revisions.

The remainder of this section summarizes current validation plans for XSTERM. These validation plans are phased to ensure that XSTERM is validated in a prioritized, systematic, and approved manner.

XSTERM was developed to facilitate the mechanistic source term calculations for the Xe-100 reactor under normal and off-normal operating conditions. Some of the LBEs considered for XSTERM validation include, but are not limited to:

- Large steam pipe failure
- Pressurized Loss of Forced Circulation (PLOFC) – circulator trip
- Control Rod Withdrawal
- Depressurized Loss of Forced Circulation (DLOFC)
- Steam Generator Tube Rupture
- Seismic Event

Key output parameters were selected based on their impact to dose assessments. The Phenomena Identification and Ranking Table (PIRT) for the Xe-100 safety analysis is documented in Table 28 of

Reference [27]. The phenomena modeled by XSTERM as shown in the validation plans were extracted from an earlier version of Reference [27] but the impact of the revised PIRT on the validation plans is minimal. Execution of the plans will ensure adequate coverage of the high and medium ranked phenomena. The relevant phenomena, figures of merit (FOMs) and key output parameters for each validation phase are identified in the sections below. Where applicable, results will be compared against additional analytical solutions and/or external calculations.

#### 6.1.1.1 Activity Release and Transport (Phase 1)

The XSTERM V&V Phase 1 plans address the validation of the release fractions for different isotopes and transport of radioactive isotopes inside the Helium Pressure Boundary (HPB).

The phenomena in Reference [27] to be validated include:

- Hydrodynamic conditions for dust suspension (fluid structural interactions) (DLOFC-5)
- (De)absorption of fission products on dust (DU-2)
- Sorptivity graphite (FPRT-11)
- H-3 generation and circulating coolant inventory (FPRT-19)
- Surface roughness (FPRT-23)
- Fission Product (FP) diffusivity, sorptivity on nongraphite surfaces (FPRT-25)
- Aerosol/dust deposition (FPRT-26)
- Resuspension (FPRT-28)
- Transport out of the reactor circuit during normal operation (tritium permeation, refueling) (FPT-1)
- Transport out of the reactor circuit due to pressure boundary breach, liftoff, venting, desorption, dust, aerosols (FPT-2)
- Decay heat (transient) (GLOFC-18)
- Ag-110m release and plateout (NOC-22)
- FP plateout and dust distribution under normal operation (NOC-24)
- Various TRISO phenomena such as fuel element gas phase diffusion (TRI-7) and kernel burnup (TRI-10) in accordance with Table 27 of Reference [27]

The following FOMs are proposed (where experimental results are available): (1) retained activity in the pebbles, (2) fractional release (R/B) of fission products from intact and failed kernels, (3) failure fraction of TRISO particles, (4) gas borne activity in the HPB and (5) deposited activity on the HPB surfaces.

The FOMs identified above focus on the release fraction and transport of significant nuclides inside the HPB. The relevant parameters will be validated for the LBE scenarios identified in Section 6.1.1. Fission products release from the fuel is the result of concurrent thermally driven processes and therefore isolation of individual phenomena in tests is difficult. The selected validation approach is to use a variety of experiments at different temperatures in inert or oxidizing environments. Additionally, comparison between XSTERM simulations and a mature, relevant code may be used exclusively when experimental data is not available.

As of the date of the release of this LTR, the Phase 1 validation activities are in progress. XSTERM is being validated against experimental information obtained during irradiations in the Advanced Test Reactor (ATR) at Idaho National Laboratories (INL) [28] and [29] and in the High Flux Reactor (HFR) in

Petten, the Netherlands [30]. In particular, fuel compacts and pebbles from the AGR-1, AGR-2, HFR-K3 and HFR-K6 irradiations were also subjected to furnace annealing tests. The irradiation and annealing facilities are described in the References [31], [32], and [33]. The last phase of the experiments included disassembly of the fuel elements to investigate TRISO failure mechanisms and fission product transport. The experimental design (irradiation followed by annealing) mimics the conditions that would be experienced during normal operation of the Xe-100 (irradiation) followed by an LBE (annealing). The experimental annealing times are long, making them relevant to long-term LBE scenarios, such as the Depressurized Loss of Forced Circulation (DLOFC) event.

Phase 1 will also include validation using high temperature annealing safety tests (T > 1800°C) from the pebble test performed at the Research Centre Jülich (i.e., Kernforchungsanlage (KFA)), and the loose TRISO particles test performed at General Atomics in San Diego, CA.

Phase 1 also includes simulation of some of the Vampyr I and Vampyr II isotope plateout experiments conducted in the AVR HTGR in Germany [34] to facilitate comparison of XSTERM to MELCOR.

#### 6.1.1.2 Pebble Bed and Reactor Structures Temperature and Power Changes (Phase 2)

The Phase 2 V&V Plan addresses the validation of reactor temperature and transient power predictions by XSTERM. This covers the TRISO particle and pebble temperature distribution calculations during normal operation and transient simulations with only neutron flux changes during transient simulations. The validation of additional phenomena related to reactor physics and thermal hydraulics is addressed by other codes used in the design and analysis of the Xe-100 reactor.

The phenomena in Reference [27] to be validated include:

- Decay heat distribution vs time (DLOFC-2)
- Heatup accident fuel performance modeling (DLOFC-4)
- Core thermal conductivity (effective) (GLOFC-1)
- Decay heat (transient) (GLOFC-18)
- Core specific heat function (GLOFC-2)
- Vessel emissivity (GLOFC-3)
- Vessel to RCCS effective view factors (GLOFC-5)
- Reactor vessel cavity air circulation and heat transfer (GLOFC-6)
- Core barrel emissivity (GLOFC-9)
- Thermal conduction (HT1)
- Convective heat transfer (HT2-A)
- Radiative heat transfer (HT3)
- Core coolant bypass flow (NOC-1)
- Effective fuel element thermal conductivity (NOC-14)
- Core flow distribution, flow in active core (NOC-2)
- Burn-in behavior (NOC-25)
- Coolant properties - viscosity and friction effects (NOC-8)
- Coolant heat transfer (correlations and flow regimes) (NOC-9)
- Fuel-temperature-change induced reactivity (PH1)

- Device-movement induced reactivity (PH3)
- Kinetics effects (PH4)
- Reactivity changes due to graphite temperature and configuration changes (PH6)
- Reactivity changes due to changes in fuel composition due to irradiation and decay (PH7)
- Various TRISO phenomena such as fuel element temperature difference (TRI-4) and buffer layer temperature gradient (TRI-22) in accordance with Table 27 of Reference [27]

The following figures of merit are proposed (where experimental results are available): (1) TRISO particle and pebble temperature, (2) core temperature, (3) reflector temperature, (4) reactor vessel temperature and (5) transient reactor power.

The FOMs identified above focus on reactor power calculations and temperature distributions in individual pebbles, the pebble bed core, core reflectors, and the core pressure vessel. The relevant parameters will be the focus of the validation activities for the LBE scenarios identified in Section 6.1.1. As addressed in Phase 1, reactor power and temperature distributions are the result of concurrent thermally driven processes, therefore, isolation of individual phenomena in experimental tests is challenging. Accordingly, the Phase 2 validation approach uses a combination of analytical solutions and separate and integral effects tests in an experimental reactor.

The first Phase 2 validation method will compare a mathematical solution for a stylized problem to the XSTERM TRISO particle and fuel pebble temperature distribution predictions during normal operation and simulated power transients. Research performed on local heat transfer phenomena in a pebble bed core included development of several models and documented in Reference [35]. This research will be used to demonstrate that given the thermal properties and boundary conditions representative of an HTGR pebble, an accurate prediction of the internal temperature can be obtained.

Validation activities will include selected cases from the tests performed in the SANA facility in Germany [36] to validate XSTERM prediction of pebble core temperature distributions during normal operation and simulated power transients. A description of the SANA facility can be found in [36]. Pebble bed heating in the SANA facility was provided by single or multiple electrical heaters. Some tests use shortened heaters to simulate heat generation in only the upper or lower part of the bed. Normal operation and transient temperatures, as well as values for effective solid thermal conductivity, were measured.

The HTR-10 benchmark will be used to validate XSTERM predictions of reactor core temperature distributions during normal operation and simulated power transients. HTR-10 is a 10 MW(th) HTGR with a pebble bed core that was designed, constructed, and operated by the Institute of Nuclear and New Energy Technology (INET). A description of the HTR-10 facility can be found in Reference [40]. Operational experiments and safety demonstration tests were performed in the HTR-10 with the objective to determine the technical and safety features of the modular HTGR and to establish an experimental basis for developing nuclear process heat applications and code validation. With this objective, the International Atomic Energy Agency (IAEA) has published a technical report that includes several benchmark tests [40]. The following three cases have been selected for validation: (1) normal operation temperature distribution with reactor at full power, (2) loss of primary coolant flow without scram and (3) control rod withdrawal without scram. These three tests are considered suitable for the validation of XSTERM reactor power and temperature distribution calculations. In order to simulate these tests, XSTERM requires inputs from the results of corresponding analysis performed by neutron

physics (VSOP) and thermal hydraulics (Flownex) codes. This data flow is consistent with the approach applied in the Xe-100 safety analysis.

#### 6.1.1.3 Dust Production (Phase 3)

Phase 3 validation will focus on calculations of graphite and metallic dust production during normal operation. The XSTERM dust models represented by the Dust Production Rate Calculations Model (DUSTM) described in Section 5.1.5 of this LTR performs the required calculations and forwards the resultant graphite and metallic dust amounts to the HPB Radionuclide Transport, Deposition and Lift-off Calculations Model (HPBM) described in Section 5.1.6.

The phenomenon to be validated is Dust Generation (DU-1). Since dust production is a very slow process, the key scenario to be addressed during this validation phase is the steady state, normal operation of the Xe-100 that serves as initial conditions for all other accident sequences.

The following figures of merit are proposed: (1) graphite dust production in the pebble core, (2) graphite and metallic dust production in the Fuel Handling System (FHS), and (3) graphite and dust production in the Reactivity Control System (RCS). The key parameters associated with the FOMs include dust production from pebbles, pebble bed walls, inner reflector, other core carbonaceous structure, the FHS and the RCS. These parameters will be the focus of validation activities for pre-event steady state conditions.

As reactor temperature distributions, pebble burnup/fluence, and state of other graphite core structures affect the production of graphite and metallic dust, isolation of individual properties and phenomena is not feasible. Additionally, since the dust particle size distribution and production rate are largely dependent on reactor design, the dust production parameters used by XSTERM are calibrated as documented in Section 5.1.5.1 of this LTR. This approach makes the selection of in-reactor experiments difficult since the few in-reactor tests available in open literature are directly or indirectly used during the calibration process. For this reason, the selected dust production validation methods include validation of the theoretical and mathematical basis as well as out-of-pile experiments performed in specialized facilities.

XSTERM dust models will be conceptually validated using the theoretical and mathematical basis of the metallic and graphite dust production model.

The HTR-10 Lifting-Line Platform Facility (LLPF) will be used to validate XSTERM predictions of dust generated in the FHS. Pebbles that haven't reached discharge burnup are recirculated. These pebbles are lifted pneumatically via a metal lifting pipe from the core outlet at the bottom of the reactor, to the top of the core and are then reinserted into the reactor. This function is performed by the FHS. In the HTR-10, the height of the lifting pipe is approximately 24 m [37]. Inevitably, the movement of the fuel elements as they recirculate in the reactor produces graphite and metallic dust. With the objective of measuring the dust produced in the lifting pipe [37], an experimental facility was designed to simulate this process in the HTR-10 reactor. A description of the LLPF can be found in Reference [37]. The graphite pebbles used in these tests were fabricated by the same process as that used for fabricating reactor pebbles, except that these pebbles did not contain TRISO fuel particles. Using the existing FHS model in XSTERM, the experimental setup will be reproduced to compare the XSTERM abrasion rate predictions with the LLPF results.

#### 6.1.1.4 Exposure to Oxidizing Environments (Phase 4)

As of the date of this LTR, the Phase 4 Validation Plan has not been finalized. This portion of the V&V will address oxidation of fuel and the impact on activity releases. Phase 4 will also address the production and release of tritium, as described in Section 5.1.8. This validation plan will be available at a later date.

The phenomena to be validated in Reference [27] includes various TRISO phenomena such as fuel element corrosion by coolant impurities (TRI-8) and fuel element chemical attack by water - kinetics (TRI-45). The following figures of merit are proposed (where experimental results are available): (1) TRISO particles oxidation (steam or air), (2) pebble oxidation (steam or air), and (3) activity release by corrosion. These parameters will be the focus of the validation exercises for normal operation and the SGTR event. The validation approach is to use a variety of integral tests and separate effects tests in steam and air oxidizing environments.

XSTERM will be validated against the experimental information obtained during the irradiation of the HFR-B1 test rig conducted in Petten, the Netherlands. The HFR-B1 was a separate effect in-pile test designed to provide measurements of fission gas releases and metallic FP transport in simulated, prismatic core fuel elements over the range of normal operating conditions and in the presence of significant quantities of water vapor [39]. The HFR facility is described in Reference [22]. After irradiation was completed, a partial PIE was conducted at the KFA. Details of the experiment and PIE are provided in Reference [39] and Reference [42].

As stated in Reference [43], the corrosion apparatus, KORA, was developed at the KFA to study the effect of moisture-induced increase in FP release as a function of water vapor partial pressure and temperature with different fuel samples. The KORA experimental results from various annealing tests conducted on the fuel compacts, pebbles and kernels from the HFR-B1 irradiations and the AVR-GLE3 irradiations will be compared against XSTERM simulations.

# 7. Conclusions

## 7.1 Conclusions

X-energy has developed a series of mechanistic source term models to simulate the transport of radionuclides in the Xe-100 from their birth in the reactor fuel to their potential release to, and transport in, the environment. This topical report addresses the physical transport phenomena associated with such releases up to their discharge from the plant's Reactor Building. Modelling of the release into the atmosphere, dispersion, and associated doses are addressed in Reference [14].

The theory and application of the Xe-100 mechanistic source term models has been described in detail in Appendices A through H and include:

- Appendix A: Particle **F**ailure **P**robability **M**odel (**FPM**)
- Appendix B: **Th**ermodynamics **M**odel (**THM**)
- Appendix C: **Sol**ids Fission Products Transport **M**odel (**SOLM**)
- Appendix D: Steady-State **Gas**eous Fission Products Transport **M**odel (**GASM**)
- Appendix E: **Dust** Production Rate **M**odel (**DUSTM**)
- Appendix F: **HPB** Radionuclide Transport, Deposition and Lift-off **M**odel (**HPBM**)
- Appendix G: Core **Corr**osion **M**odel (**CORRM**)
- Appendix H: MST Models Relationship Chart

These models, along with a 2D Point **K**inetics **Sim**ulation Model (**KSIM**) described in Section 5.1.9, have been incorporated in the safety analysis of the Xe-100 LBEs.

As noted in Section 1.5, X-energy is requesting the NRC review and approval of the MST models described in Section 4.1, Section 5, and Appendices A through H of this LTR as an appropriate means to evaluate radionuclide transport phenomena and estimate mechanistic source terms.

A **Trit**ium Production and Transport **M**odel (**TRITM**) model, Section 5.1.8, will be used to calculate the overall tritium mass balance in the Xe-100 and input to associated doses. This model is under development and will be submitted to the staff in a revision to this LTR. In addition, the XSTERM code V&V effort, as described in Section 6, is currently underway and will be submitted as an LTR to the NRC at a future date for review and approval to support final safety analyses.

# 8. Cross References and References

## 8.1 Cross References and References

| Document Title<br>Cross References: X-energy documents that may impact the content of this document.<br>References: X-energy or other documents that will not impact the content of this document | | Document No. | Rev./ Date of Issuance | Cross Reference/ Reference |
|---|---|---|---|---|
| [1] | Petti, D. A., Hobbins, R. R., Lowry, P. and Gougar, H. "Representative source terms and the influence of reactor attributes on functional containment in modular high-temperature gas cooled Reactors." | Nuclear Technology, 184, p.181 | November, 2013 | Reference |
| [2] | Idaho National Laboratory, "Mechanistic Source Terms White Paper | INL/EXT-10-17997 | Rev. 0 / July 2010 | Reference |
| [3] | Risk-Informed Performance-Based Technology Inclusive Guidance for Non-Light Water Reactor Licensing Basis Development | NEI 18-04 | Rev.1 / August 2019 | Reference |
| [4] | Guidance for a Technology-Inclusive, Risk-Informed, and Performance-Based Methodology to Inform the Licensing Basis and Content of Applications for Licenses, Certifications, and Approvals for Non-Light-Water Reactors | RG 1.233 | Rev. 0 / June 2020 | Reference |
| [5] | Xe-100 Licensing White Paper Probabilistic Risk Assessment Technical Adequacy Approach | XE00-P-GL-GL-GL-GL-005593 | Rev. 1 / November 2022 | Reference |
| [6] | Risk-Informed Performance-Based Licensing Basis Approach for the Xe-100 Reactor | LTR XE00-R-R1ZZ-RDZZ-L-000687 | Rev. 1 / June 2021 | Reference |
| [7] | Xe-100 Licensing Topical Report Transient and Safety Analysis Methodologies | XE00-GL-GL-GL-GL-X-007834 | Rev. 1/ April 2024 | Cross Reference |
| [8] | Xe-100 Principal Design Criteria Licensing Topical Report | XE00-GL-GL-GL-GL-GL-004799 | Rev. 3 / February 2024 | Reference |
| [9] | Fuel Qualification for Advanced Reactors | NUREG-2246 | March 2022 | Reference |
| [10] | Technology Inclusive Guidance for Non-Light Water Reactor Safety Analysis Report: Content for Applicants Using the NEI 18-04 Methodology | NEI 21-07 | Rev. 0 / August 2021 | Reference |
| [11] | Xe-100 Topical Report TRISO-X Pebble Fuel Qualification Methodology | XE00-R-R1ZZ-RDZZ-L-000633 | Rev.3 / July 2022 | Reference |
| [12] | Xe-100 Design Summary Report | XE00-R-R1ZZ-RDZZ-X-000849 | Rev. 2 / August 2021 | Reference |

| Document Title<br>Cross References: X-energy documents that may impact the content of this document.<br>References: X-energy or other documents that will not impact the content of this document | | Document No. | Rev./ Date of Issuance | Cross Reference/ Reference |
|---|---|---|---|---|
| [13] | Xe-100 200MWth Steady-State Core Design Report | XE00-N-RZZ-NSZZ-D-000288 | Rev.5 / February 2022 | Reference |
| [14] | Xe-100 Licensing Topical Report, Atmospheric Dispersion and Dose Calculation Methodology | XE00-GL-GL-GL-GL-GL-X-007116 | Rev.2 / September 2023 | Reference |
| [15] | Fuel Performance and Fission Product Behavior in Gas Cooled Reactors | IAEA-TECDOC-978 | November 1997. | Reference |
| [16] | Next Generation Nuclear Plant Defense-in-Depth Approach | INL/EXT-09-17139 | Rev. 0 / December 2009 | Reference |
| [17] | Functional Containment Performance Criteria for Non-Light-Water-Reactors | SECY-18-0096 | September 2018. | Reference |
| [18] | Issues Pertaining to the Advanced Reactor (PRISM, MHTGR, and Process Inherent Ultimately Safe [PIUS]) and CANDU 3 Designs and Their Relationship to Current Regulatory Requirements | SECY-93-092 | April 1993 | Reference |
| [19] | Quality Assurance Program Description | XEQAPD 1.0 | Rev 6 | Reference |
| [20] | Mechanistic Source Terms White Paper | XE-Y1-NS-G0-L01-100430 | Rev.1 / January 2017 | Reference |
| [21] | High Temperature Gas Cooled Reactor Fuels and Materials | IAEA-TECDOC-1645 | March 2010 | Reference |
| [22] | Advances in High Temperature Gas Cooled Reactor Fuel Technology | IAEA-TECDOC-1674 | June 2012 | Reference |
| [23] | Compilation of Fuel Performance and Fission Product Transport Models and Database for MHTGR Design Laboratory, | ORNL/NPR-91/6 | October 1993 | Reference |
| [24] | Use of ARCON Methodology for Calculation of Accident-Related Offsite Atmospheric Dispersion Factors | USNRC RG-1.249 | Rev 0 / August 2023 | Reference |
| [25] | Atmospheric Dispersion Estimates in the Vicinity of Buildings | PNL-10286 | | Reference |
| [26] | “Nuclear Reactor Analysis,” Duderstadt, James Johnson and Louis J. Hamilton,” John Wiley & Sons, Inc. | | 1976 | Reference |
| [27] | Xe-100 In-Core PIRT Report | 003834 | Rev 3 | Cross Reference |
| [28] | AGR-1 Irradiation Experiment Test Plan | INL/EXT-05-00593 | Rev. 3 (2009) | Reference |
| [29] | AGR-2 Irradiation Experiment Test Plan | PLN-3798 | Rev. 1 / 2011 | Reference |

| Document Title<br>Cross References: X-energy documents that may impact the content of this document.<br>References: X-energy or other documents that will not impact the content of this document | | Document No. | Rev./ Date of Issuance | Cross Reference/ Reference |
|---|---|---|---|---|
| [30] | The High Flux Reactor Petten, Present Status and Projects | IAEA, Record No. 36023802 | 1990 | Reference |
| [31] | Idaho National Laboratory, "AGR-1 Irradiation Test Final As-Run Report | INL/EXT-10-18097 | Rev 3 / 2015. | Reference |
| [32] | R. N. Morris, C. A. Baldwin, P. A. Demkowicz, J. D. Hunn and E. L. Reber, "Performance of AGR-1 high-temperature reactor fuel during post-irradiation heating tests," Nuclear Engineering and Design. | Vol. 306 | 2016 | Reference |
| [33] | H. Kostecka, J. Ejton, W. de Weerd and E. Toscano, "Post-Irradiation Testing of HTR-Fuel Elements Under Accident Conditions," IAEA-Technical Meeting on Gas Cooled Reactor Fuels | HTR-F1-06/09D-2.4.1 | 2004 | Reference |
| [34] | Fuel performance and fission product behaviour in gas cooled reactors | IAEA TECDOC-978 | Nov 1997 | Reference |
| [35] | Investigation of Local Heat Transfer Phenomena in a Pebble Bed HTGR Core | NR001/RP/001 | Rev. 2 / May 2009 | Reference |
| [36] | B. Stöcker and H. Nießen, "Data Sets of the SANA Experiments 1994-1996" | Jülich-3409 | July 1997 | Reference |
| [37] | K. Shen, J. Su, H. Zhou, W. Peng, B. Liu and S. Yu, "Abrasion behavior of graphite pebble in lifting pipe of pebble-bed HTR," Nuclear Engineering and Design | Vol. 293 | 2015 | Reference |
| [38] | Guidance for a Technology -Inclusive Content-of-Application Methodology to Inform the Licensing Basis and Content of Applications for Licenses, Certifications, and Approvals for Non-Light-Water Reactors | RG 1.253 | Rev. 0/ March 2024 | Reference |
| [39] | HFR-B1 Final Summary Report | General Atomics, PC-00529 | April 2006 | Reference |
| [40] | Evaluation of High Temperature Gas Cooled Reactor Performance: Benchmark Analysis Related to the PBMR-400, PBMM, GT-MHR, HTR-10 and the ASTRA Critical Facility | IAEA File No. IAEA-TECDOC-1694 | 2013 | Reference |
| [41] | Consideration of Severe Accident Risk in NRC Regulatory Decisions | SECY-97-171 | July 1997 | Reference |
| [42] | Fuel Irradiation Experiments on HFR-K6 and HFR-B1 with Intermittent Water Vapour Injections | IAEA-TECDOC-784, Pages 17 - 24 | 1995 | Reference |
| [43] | Simulation of Steam Ingress Accidents with Irradiated Fuel Elements | IAEA-TECDOC-784, Pages 37 - 44 | 1995 | Reference |

| Document Title<br>Cross References: X-energy documents that may impact the content of this document.<br>References: X-energy or other documents that will not impact the content of this document | | Document No. | Rev./ Date of Issuance | Cross Reference/ Reference |
|---|---|---|---|---|
| [44] | Software V&V for Design & Safety Analysis Procedure | QAP 3.10 | Rev.2 / July 2021 | Reference |
| [45] | Accident Source Terms for Light-Water Nuclear Power Plants | NUREG-1465 | February 1995 | Reference |
| [46] | Plan for Resolving Policy Issues Related to Licensing Nonlight Water Reactor Designs | SECY-03-0047 | March 2003 | Reference |
| [47] | Plan for Resolving Policy Issues Related to Licensing Non-Light Water Reactor Designs | SECY-03-0047 SRM | June 2003 | Reference |
| [48] | Second Status Paper on the Staff's Proposed Regulatory Structure for New Plant Licensing and Update on Policy Issues Related to New Plant Licensing | SECY-05-0006 | January 2005 | Reference |
| [49] | Sandia National Laboratories, "Mechanistic Source Term Considerations for Advanced Non-LWRs" | SAND2020-6730 | 2020 | Reference |
| [50] | US Environmental Protection Agency, "PAG Manual: Protective Action Guides and Planning Guidance for Radiological Incidents" | EPA-400/R-17/001 | January 2017 | Reference |
| [51] | Nuclear Safety Criteria and Safety Design Process for Modular Helium-Cooled Reactor Plants | ANSI/ANS-53.1-2011 | 2011 | Reference |
| [52] | Xe-100 Topical Report TRISO-X Pebble Fuel Qualification Methodology | XE00-R-R1ZZ-RDZZ-L-000633 | Revision 3 / July 26, 2022 | Reference |
| [53] | Plan for Resolving Policy Issues Related to Licensing Nonlight Water Reactor Designs | SECY-02-0139 | July 2002 | Reference |
| [54] | Probabilistic Risk Assessment Standard for Advanced Non-Light Water Reactor Nuclear Power Plants | ASME/ANS RA-S-1.4-2021 | 2021 | Reference |
| [55] | Transient and Accident Analysis Methods | RG 1.203 | December 2005 | Reference |

# Appendix A. Failure Probability Model

**Abbreviations/Acronyms**

| Short Form | Phrase |
|---|---|
| **AGR** | Advanced Gas Reactor |
| **FIMA** | Fissions per Initial Metal Atom |
| **FPM** | TRISO-Coated Particle Failure Probability Model |
| **INL** | Idaho National Laboratory |
| **IPyC** | Inner Pyrolytic Carbon |
| **OPF** | Oxygen Atoms Released Per Fission of kernels |
| **OPyC** | Outer Pyrolytic Carbon |
| **PIE** | Post Irradiation Examination |
| **RPV** | Reactor Pressure Vessel |
| **SiC** | Silicon Carbide |
| **TRISO** | TRi-ISOtropic coated-fuel particle design with three materials in coating system (low-density PyC, high-density PyC, and SiC) |
| **CO** | Uranium oxycarbide, a heterogeneous mixture of $UO_2$ and UC2 |
| **$UO_2$** | Uranium Dioxide |
| **Xe-100** | X-energy 200 MWt Pebble Bed Reactor |

**Definitions**

| Symbol | Definition |
|---|---|
| $DS$ | reduced diffusion coefficient of the fission gases ($s^{-1}$) |
| $d_0$ | original thickness of SiC layer (m) |
| $d_1$ | IPyC layer thickness (m) |
| $d_2$ | SiC layer thickness after corrosion is accounted for (m) |
| $d_3$ | OPyC layer thickness (m) |
| $dT(\tau)/dx$ | temperature gradient across the particle at time $\tau$ (K/m) |
| $F$ | burnup (Fissions per Initial Metal Atom, FIMA) |
| $F_d$ | relative fraction of fission gas release |
| $F_f$ | fission product yield |
| $F_{m,ek}$ | fraction of defective particles due to manufacturing: exposed kernels |
| $F_{m,id}$ | fraction of defective particles due to manufacturing: defective IPyC coating |
| $F_{m,sd}$ | fraction of defective particles due to manufacturing: defective SiC coating |
| $f_{SiC}$ | fission density within the volume enclosed by the SiC layer (fissions/$m^3$) |
| $\dot{g}$ | irradiation-induced shrinkage rate of PyC (dimensionless) |
| $K_{MC}(T)$ | kernel migration coefficient as a function of temperature ($m^2K/s$) |
| $k$ | irradiation-induced creep constant for PyC ($2x10^{-29}$) ($m^2$/MPa) |
| $k_c$ | corrosion frequency factor ($h^{-1}$) |
| $k_0$ | a pre-exponential constant ($h^{-1}$) |
| $k_{td}$ | thermal decomposition frequency factor ($h^{-1}$) |
| $m$ | SiC Weibull modulus of an irradiated particle |
| $m_{00}$ | SiC Weibull modulus of an unirradiated particle |
| $m_{bi}$ | mean value of the combined thickness of the buffer and IPyC layers (m) |
| $n$ | number of irradiation time intervals |
| $OPF$ | number of oxygen atoms per fission (presenting the CO pressure) |
| $p$ | pressure (Pa) |
| $Q$ | activation energy for corrosion (J/mol) |
| $R$ | gas constant (8.3143 J/mol·K) |
| $r_o$ | particle kernel radius (m) |
| $r_1$ | average radius of the IPyC layer (m) |
| $r_2$ | average radius of the SiC layer (m) |
| $r_3$ | average radius of the OPyC layer (m) |
| $T$ | temperature (K) |
| $T_B$ | particle surface temperature (K) |

| Symbol | Definition |
|---|---|
| $T_h$ | heating temperature (K) |
| $T_{irr}$ | irradiation temperature (K) |
| $T_k$ | kernel temperature (K) |
| $T_m$ | average temperature for the time interval between $t_1$ and $t_2$ |
| $T_n$ | temperature at $t_n$ (K) |
| $T(\tau)$ | volume-average particle temperature at time $\tau$ (K) |
| $t$ | time (s) |
| $t_a$ | accident time (s) |
| $t_h$ | heating time (h) |
| $\bar{t}_i$ | mid-point of $\Delta t_i$ (s) |
| $\Delta t_i$ | $i^{th}$ irradiation time interval (s) |
| $t_{irr}$ | irradiation time (s) |
| $\Delta t_n$ | time step for $n$ (hr) |
| $t_{tot}$ | total time for particle irradiation (s) |
| $u$ | integral variable |
| $V_f$ | void fraction of buffer volume ($m^3$) |
| $V_k$ | kernel volume ($m^3$) |
| $V_m$ | molar volume of the heavy metal in a particle kernel ($m^3$/mole) |
| $x(t)$ | total migration distance at time (t) |
| $\Gamma$ | fast fluence ($10^{25}$ n/$m^2$,[[ ]]$^P$) |
| $\Gamma_m$ | Weibull reference fast fluence (n/$m^2$) |
| $\Gamma_s$ | reference fast fluence (n/m2) |
| $\dot{\vartheta}$ | corrosion rate (m/s) |
| $v$ | Poisson's ratio in creep for PyC |
| $v_1$, $v_2$, and $v_3$ | IPyC, SiC, and OPyC thicknesses, respectively |
| $\Delta v$ | variation in parameter $v$ from its mean value $\bar{v}$ (μm) |
| $\sigma$ | standard deviation of the normal distribution of the buffer/IPyC thickness around the mean $m_{bi}$ |
| $\sigma_o$ | SiC tensile strength at the end of irradiation (Pa) |
| $\sigma_{00}$ | SiC tensile strength of an unirradiated particle |
| $\sigma_c(v)$ | stress in the multi-dimensional particle having parameter that varies from its mean value $\bar{v}$ by an amount $\Delta v$ (MPa) |
| $\sigma_{cr,0}$ | mean SiC strength of particle with cracked IPyC (MPa) |
| $\sigma_{c\bar{v}}$ | maximum SiC layer stress for a particle with cracked IPyC, having all parameters set at mean values ($\bar{v}$) for a particle batch (MPa); equivalent to $UMC$ |

| Symbol | Definition |
|---|---|
| $\boldsymbol{\sigma_t}$ | stress induced in the SiC layer due to the internal gas pressure (Pa) |
| $\boldsymbol{\sigma_{u\bar{v}}}$ | maximum SiC layer stress for an intact spherical particle, having all parameters set at mean values ($\bar{v}$) for a particle batch (MPa) |
| $\boldsymbol{\sigma_u(v)}$ | maximum SiC stress for an intact spherical particle whose fuel attributes such as IPyC, SiC and OPyC thicknesses ($v$) are different from the nominal values (MPa) |
| $\boldsymbol{\tau}$ | time variable (h) |
| $\boldsymbol{\chi}$ | migration distance of the kernel (m) |
| $\boldsymbol{\Omega}$ | thermal gradient across the coated fuel particle (K/m) |
| $\boldsymbol{\Omega_{init}}$ | thermal gradient at $(G_o + G_{max})/2$, an approximation for the average gradient (K/m) |
| $\boldsymbol{\emptyset}$ **or** $\boldsymbol{\emptyset_{xfp}}$ | total SiC failure probability |
| $\boldsymbol{\emptyset_{fpc}}$ | SiC failure probability due to fission product corrosion |
| $\boldsymbol{\emptyset_n}$ | $n^{\text{th}}$ failure mechanism |
| $\boldsymbol{\emptyset_{ipyc}}$ | IPyC failure probability |
| $\boldsymbol{\emptyset_{km}(\chi)}$ | the probability that a migrating kernel comes in contact with the SiC layer |
| $\boldsymbol{\emptyset_{pv}}$ | SiC failure probability due to pressure vessel model |
| $\boldsymbol{\emptyset_{pv}^{c}}$ | SiC failure probability due to pressure vessel model with the cracked IPyC |
| $\boldsymbol{\emptyset_{pv}^{c,k}}$ | SiC failure probability of a particle with cracked IPyC ($k$ = for Monte Carlo history), using Monte Carlo-Weibull hybrid approach |
| $\boldsymbol{\emptyset_{pv}^{int}}$ | SiC failure probability due to pressure vessel model for intact particles |
| $\boldsymbol{\emptyset_{td}}$ | SiC failure probability due to thermal decomposition |

## A.1. Introduction

As addressed in Section 4.1, the release fraction from fuel particles is calculated accounting for the as-manufactured fuel reliability (e.g., the allowable heavy-metal contamination and coating defects), fuel failure during irradiation, incremental fuel failure under accident conditions, and diffusion of fission products through the intact particle coatings under normal operating and accident conditions. These factors are calculated on an event specific basis, as a function of fuel burnup, maximum operating temperature, maximum post-accident temperature and, where applicable, air and/or moisture contamination in the reactor helium coolant, (e.g., as a result of a steam generator tube rupture).

The X-energy TRISO-coated particle **F**ailure **P**robability (FPM) model calculates the TRISO-coated particle failure probabilities during normal and DBA conditions for the Xe-100 pebble bed reactor. Particle failure probabilities are calculated for TRISO particle failure mechanisms, including pressure vessel failure (i.e., Silicon Carbide (SiC) layer failure due to internal gas pressure in the particle), kernel migration (amoeba), fission product corrosion, thermal decomposition, Inner Pyrolytic Carbon (IPyC) cracking models and manufacturing defects.

## A.2 Theory and Methodology

### A.2.1 Overall Mathematical Model

[[

]]$^{P}$

#### A.2.1.1 Summary of Available Models

The main mechanisms contributing to particle failure that are modeled in FPM are listed below, along with their available models and relevant sub-sections.

1. Pressure vessel failure of TRISO particles
   - [[ ]]$^{P}$
2. Kernel migration (Amoeba) [A-6] Section A.2.5.1
   - [[ ]]$^{P}$
3. Fission product corrosion
   - Goodin-Nabielek Model [A-6] – Section A.2.6.1
4. SiC thermal decomposition [A-6] – Section A.2.7
   - [[

     ]]$^{P}$

These models are specified in terms of TRISO particle geometry, material properties, temperature, fast fluence, burnup, and fission density, depending on the model.

The FPM model also incorporates manufacturing defects. Although the fuel manufacturing process has advanced over the years, manufacturing defects are still typically dominant over the other failure mechanisms because failure of standard TRISO particles has been limited by advanced core design measures. In FPM, the following manufacturing defects are included (Section A.2.4):

- Exposed kernel (i.e., defect of all coating layers)
- SiC defect (i.e., defect of the SiC layer with at least one other coating layer intact)
- IPyC defect

[[

]]$^{P}$

### A.2.2 Failure Fraction Calculation in FPM

[[

]]$^{P}$

### A.2.3 Pressure-Vessel Failure of Particle Coatings

Pressure-vessel (PV) modelling has been historically useful in particle design and understanding of the expected integrity of a pressurized particle with coating layers of varying thicknesses. In defective particles, irradiation-induced fission gas build-up causes the SiC and OPyC layers to fail as the pressure increases. Once the stress on the SiC layer exceeds the SiC layer strength, the SiC layer fails. In standard particles, calculated PV failure is negligible.

#### A.2.3.1 X-energy Pressure Vessel (X-PV) Model

The X-PV model is an advanced version of the historical Panama model. [[

]]$^{P}$

##### A.2.3.1.1 SiC Stress Model

In the FPM model, the SiC stress is calculated by [[

]]$^{P}$

#### A.2.3.1.2 Corrosion Rate

The following equation for SiC corrosion rate (m/s), $\dot{\vartheta}$ , is used [[ ]]$^{P}$ and derived from experimental data on palladium penetration [[

]]$^{P}$

#### A.2.3.1.3 Irradiation-Induced Dimensional Change of PyC

The irradiation-induced shrinkage rate of PyC, which is defined as $\dot{g}$ in Equation (A-5), is given as follows [[

]]$^{P}$

#### A.2.3.1.4 Fission Gas Pressure

To calculate the internal fission gas buildup, $p$, in Equation (A-5), the ideal gas equation, [[ ]]$^{P}$ is used as follows: [[

]]$^{P}$

In the FPM model, [[ ]]$^{P}$ and the relative fraction of fission gas release is defined by the following equations, [[ s

]]$^{P}$

### A.2.3.1.5 Reduced Diffusion Coefficient

The reduced diffusion coefficient can be calculated as a function of temperature via the following equation. The equation is valid for $UO_2$ for low burnup fuel in accordance with [[

]]$^{P}$

#### A.2.3.1.6 Number of Oxygen Atoms Released Per Fission

The number of oxygen atoms released during the fission of kernels ($OPF$), which become available for CO formation, contribute to the gas pressure. The UCO kernel was specifically designed to suppress the formation of free oxygen and the attendant CO formation [[ ]]$^{P}$. Therefore, OPF becomes zero, [[ ]]$^{P}$. The following equation is used for $OPF$ during the irradiation if the fuel type is $UO_2$, [[

]]$^{P}$

During the heating process, the following equation, [[ ]]$^{P}$, is used to calculate $OPF$: [[

]]$^{P}$

#### A.2.3.1.7 Molar Volume in a Particle Kernel

The molar volume of the heavy metal in a particle kernel, $V_m$, is defined by the ratio of the weight of one mole of the kernel to its density. The following is valid for the UCO and $UO_2$ fuel, [[

]]$^{P}$

#### A.2.3.1.8 SiC Tensile Strength

The SiC tensile strength $\sigma_{00}$ of an unirradiated particle can be measured. The lowest limit for the SiC tensile strength is [[ ]]$^{P}$ During the irradiation, the tensile strength is given by [[

]]$^{P}$

#### A.2.3.1.9 Weibull Parameter

The Weibull parameter, $m_{oo}$, for an unirradiated particle can be measured by a brittle ring [[ ]]$^{P}$ in the same way as [[ ]]$^{P}$

As documented [[ ]]$^{P}$ the Weibull parameter, $m$, determines the distribution of the SiC tensile strength over a number of particles. [[

]]$^{P}$

#### A.2.3.1.10 Kernel Irradiation-Induced Swelling

The kernel irradiation-induced swelling is also incorporated in the X-PV model, [[

]]$^{P}$

#### A.2.3.1.11 Kernel Thermal Expansion

Kernel thermal expansion, like irradiation-induced swelling, reduces the free gas volume in the particle with a resultant increase in gas pressure. A fourth order polynomial fit for fractional volume increase as a function of kernel temperature is employed in the X-PV pressure vessel failure model of the FPM model. [[

]]P

***Table A-1: Coefficients of the Fractional Volume Change Equation A-23 [A-10]***

| Coefficient | [[ ]]P | [[ ]]P |
|---|---|---|
| $a_1$ | [[ ]]P | [[ ]]P |
| $a_2$ | [[ ]]P | [[ ]]P |
| $a_3$ | [[ ]]P | [[ ]]P |
| $a_4$ | [[ ]]P | [[ ]]P |
| $b$ | [[ ]]P | [[ ]]P |

[[ ]]P

***Equations A-24 through A-26 not used***

### A.2.4 Manufacturing Defects

Three different types of manufacturing defects are included in the FPM model: exposed kernels (, SiC defects, and IPyC defects. In Table A-3, defect fractions are presented for the AGR. This data was compiled from fuel specification documents ( [[ ]]P, [A-5], [A-16], [A-11], [A-15]). [[

]]P The values currently used in FPM for safety analysis are based on [[ ]]P and listed in Table A2 as Xe-100.

***Table A-2: UCO Defect Fraction Pre-Sets in FPM***

| Reactor | Exposed Kernel ($F_{m,ek}$) | Defective SiC ($F_{m,sd}$) | Defective IPyC ($F_{m,id}$) |
|---|---|---|---|
| Xe-100 [[ ]]$^{P}$ | [[ ]]$^{P}$ | [[ ]]$^{P}$ | [[ ]]$^{P}$ |
| AGR-1 [A-5] | 2.0 x $10^{-5}$ (mean) | 2.0 x $10^{-4}$ (mean) | 2.0 x $10^{-4}$ (mean) |
| AGR-2 [A-16] | 2.0 x $10^{-5}$ (mean) | 1.2 x $10^{-5}$ (mean) | 4.8 x $10^{-5}$ (mean) |
| AGR-3/4 [A-11] | 2.0 x $10^{-5}$ (mean) | 3.5 x $10^{-5}$ (mean) | 8.7 x $10^{-5}$ (mean) |
| AGR-5/6/7 [A-15] (specification) | 5.0 x $10^{-5}$ (mean) | 1.0 x $10^{-4}$ (mean) | 1.0 x $10^{-4}$ |

Equation (A-3) shows how these fractions are included in the total particle failure fraction calculation. Manufacturing defects, exposed kernels and SiC defects, are directly added to Equation (A-3) except [[ ]]$^{P}$

### A.2.5 Kernel Migration (Amoeba Effect)

In power reactors, the local temperature gradient can be high across the fuel particles. In such cases, kernel migration can occur, and the oxide and carbide fuel kernels migrate up the thermal gradient. The kernel is pushed towards the hot side of the TRISO particle by carbon dioxide ($CO_2$) and solid-phase carbon ($C$) produced on the cold side of the particle by $CO$ migrating down the temperature gradient and reacting as $CO + CO \rightarrow CO_2 + C$. Particle failure is assumed to occur when the kernel contacts the SiC layer. This effect is prominent with $UO_2$ kernels and is insignificant with UCO kernels based upon the AGR program irradiation tests [A-7]. This phenomenon is also known as the “amoeba effect.” Failure by this mechanism is correlated as a function of temperature, thermal gradient, and thicknesses of the buffer and IPyC layers.

This process can be significant in prismatic designs because local power densities are greater than pebble bed reactors, which leads to a higher thermal gradient across the particles. Therefore, the probability of kernel migration is greater than in pebble bed reactors [[ ]]$^{P}$. In pebble bed cores, the power densities are much smaller and the temperature gradient across the pebbles is uniform because of the low particle packing fraction. Therefore, the probability of kernel migration is lower in pebble bed cores due to a low temperature gradient across the pebble.

#### A.2.5.1 Model Equations

The model calculates the distance the kernel migrates within the particle as a function of kernel material, temperature, and thermal gradient across the particle, and the probability of SiC failure due to contact with the kernel. The model is assumed to apply to all reactor operating conditions [[

]]$^{P}$

### A.2.5.2 PARFUME Model

The evaluation of the kernel migration coefficient is specific to the kernel material. The following expression is used for LEU UCO fuel in accordance with [[

]]$^{P}$

and the following expression is used for the $UO_2$ fuel, [[

]]$^{P}$

***Equation A-35 not used***

### A.2.6 Fission Product Corrosion

Post irradiation examination (PIE)[1]of TRISO fuel particles has shown that certain fission products can be transported from the kernel to the inner surface of the SiC layer where they can cause damage and potentially fail the SiC layer. In carbide fuels, the major corrosive agents are the lanthanide group fission products; in oxidic fuels, including UCO, the lanthanide group fission products are largely retained in the kernel (with the notable exception of europium (Eu) isotopes in UCO). Noble metals such as Ruthenium (Ru), Rhodium (Rh), Palladium (Pd), and Silver (Ag) do not form stable oxides and they can readily migrate out of the kernel. For example, in LEU fuel kernels, Pd has great importance when it interacts with the SiC layer (the Pd yield is much higher from plutonium (Pu) fissions than U fissions). Although the mass of the Pd [[ ]]$^{P}$ is very small compared with the total mass of SiC layer, the Pd and other corrosive agents tend to form nodules at the IPyC/SiC interface (e.g., at the apex of radial cracks in the IPyC layer) and can create worm holes in the SiC layer leading to complete penetration of the SiC layer if sufficiently high temperatures are maintained for long periods. This is a temperature dependent reaction and the rate of the penetration into the SiC layer becomes significant at high temperatures.

Studies have been conducted to understand the mechanism for the Ag migration through, and Pd attack of, the SiC layer [[ ]]$^{P}$. These fission product attack mechanisms are expected to play a more important role during normal operation in prismatic reactors where TRISO fuel particles experience higher temperatures than in pebble bed reactors.

[1] Post irradiation examination (PIE) refers to analysis in hot cells or other similar facilities outside the reactor.

As the burnup increases, some of the oxygen liberated by uranium fissions will be released from the kernel and react with the buffer layer forming predominately CO. Excessive CO not only increases the pressure-vessel and kernel-migration failure probabilities but can also corrode the SiC layer at accident-condition temperatures. Chemical attack of the SiC layer by CO has been observed in $UO_2$ particles irradiated at temperatures above approximately 1400°C [[ ]]$^{P}$. This model calculates the probability of SiC layer failure due to corrosion by fission products as a function of thermal and irradiation conditions. CO formation is suppressed in UCO kernels which is one of its major advantages over $UO_2$ [[ ]]$^{P}$.

### A.2.6.1 1985 Goodin-Nabielek Corrosion Model

In the 1985 Goodin-Nabielek SiC corrosion model, the failure probability is equated to the compound distribution of the SiC layer thickness and SiC degradation rate using the Weibull distribution. The SiC failure probability [[ ]]$^{P}$ is given in [[

]]$^{P}$ The frequency factor is represented by an Arrhenius-type equation:

[[

]]$^{P}$

### A.2.7 SiC Thermal Decomposition

At very high temperatures (> 1600°C) [[ ]]$^{P}$, thermodynamics analysis and data from German post-irradiation heating tests show that the SiC layer undergoes thermal decomposition and that SiC will decompose into its constituent elements. The silicon vaporizes and migrates to a colder location, leaving behind a porous carbon structure. The phenomenon is primarily a function of temperature and time and has not played a major role in fuel failure at lower accident temperatures. This model calculates the time dependent high-temperature failure of the SiC layer as a function of temperature and irradiation conditions.

#### A.2.7.1 1985 Goodin-Nabielek Thermal Decomposition Model

In particle heating tests, the measured cesium (Cs) release is assumed to track the progressive functional degradation of the SiC coating, $\emptyset_{td}$. This failure fraction is equated to the compound distribution of SiC layer thickness and SiC degradation rate using a Weibull distribution [[

]]$^{P}$ The frequency factor $k_{td}$ is given by:

[[

]]$^{P}$

### A.2.7.2 PANAMA Model

In the Panama model, the following SiC failure probability due to thermal decomposition [[ ]]$^{P}$ is used in accordance with [[

]]$^{P}$

***Equations 3.53 Through 3.69 not used***

### A.2.8 Overall Solution Technique

In FPM, a failure probability (fraction) is calculated for a single representative particle at every FPM mesh point of the fuel zone for a given spherical fuel element. There are [[ ]]$^{P}$ FPM mesh points in a pebble fuel zone (active pebble zone). The FPM mesh scheme for a spherical fuel element is illustrated in the left side of Figure A-1.

[[

]]$^{P}$

***Figure A-1: Computational Domain for Fuel Elements and Reactor Core***

To model a pebble-bed core, the core is divided into [[ ]]$^{P}$ radial channels, and [[ ]]$^{P}$ axial nodes in each channel. Thus, there are [[ ]]$^{P}$ nodes in the core. The left side of Figure A-1 illustrates the nodal scheme for a fuel sphere. Since there are [[ ]]$^{P}$ fuel passes in the reference Xe-100 core design [[ ]]$^{P}$, there are [[ ]]$^{P}$ representative pebbles in each of the [[ ]]$^{P}$ core nodes. Since there are [[ ]]$^{P}$ fuel mesh points in each fuel pebble, there are [[ ]]$^{P}$ representative TRISO-coated particles in each pebble. In this approach, FPM performs a total of [[ ]]$^{P}$ TRISO-coated particle failure probability calculations for every time step for the whole core as shown in Table A-3.

***Table A-3: Number of FPM Calculations***

| FPM Model Unit | Unit # | Total in core |
|---|---|---|
| FPM particle | [[ ]]$^{P}$ | [[ ]]$^{P}$ |
| FPM mesh | [[ ]]$^{P}$ | [[ ]]$^{P}$ |
| FPM pebble | [[ ]]$^{P}$ | [[ ]]$^{P}$ |
| FPM node | [[ ]]$^{P}$ | [[ ]]$^{P}$ |
| FPM channel | [[ ]]$^{P}$ | [[ ]]$^{P}$ |

## A.3 Cross References and References

| Document Title<br>Cross References: X-energy documents that may impact the content of this document.<br>References: X-energy or other documents that will not impact the content of this document | | Document No. | Rev./ Date | Cross Reference/ Reference |
|---|---|---|---|---|
| **A-1** | H. Nabielek and K. Verfondern, "The Mathematical Basis of the PANAMA-I Code for Modeling Pressure Vessel Failure of TRISO Coated Particles under Accident Conditions," HTA-IB-03/90, Germany: Julich Research Center, 1990. | HTA-IB-03/90 | 1990 | Reference |
| **A-2** | Idaho National Engineering and Environmental Laboratory, "Development of Improved Models and Designs for Coated-Particle Gas Reactor Fuels," Final Report under the International Nuclear Energy Research Initiative (INERI), INEEL/EXT-05-02615, Idaho National Laboratory, December 2004. | INEEL/EXT-05-02615 | Dec. 2004 | Reference |
| **A-3** | F. J. Homan, T. B. Lindemer, E. L. Long, T. N. Tiegs and R. L. Beatty, "Stoichiometric Effects on Performance of High-Temperature Gas-Cooled Reactor Fuels from the UCO System," Nuclear Technology, vol. 35, no. 2, p. 428, September 1977. | vol. 35, no. 2 | Sep. 1977 | Reference |
| **A-4** | "Performance Limits of Coated Particle Fuel, Part II, Mechanical Failure of Coated Particles Due to Internal Gas Pressure and Kernel Swelling." | DP Report 828, Part II | 1973 | Reference |
| **A-5** | B. P. Collin, "AGR-1 Irradiation Test Final As-Run Report," INL/EXT-10-18097 Rev. 3, Idaho National Laboratory, January 2015. | INL/EXT-10-18097 | Jan. 2015 | Reference |
| **A-6** | R. C. Martin, "Compilation of Fuel Performance and Fission Product Transport Models and Database for MHTGR Design," ORNL/NPR-91/6, Oak Ridge National Laboratory, October 1993. | ORNL/NPR-91/6 | Oct. 1993 | Reference |
| **A-7** | D. L. Knudson, J. T. Maki, G. K. Miller and D. A. Petti, "PARFUME Theory and Model Basis Report," INL/EXT-08-14497, Idaho National Laboratory, September 2009. | INL/EXT-08-14497 | Sep. 2009 | Reference |
| **A-8** | K. Bongartz, E. Gyarmati, H. Schuster and K. Täuber, "The Brittle Ring Test: A Method for Measuring Strength and Young's Modulus on Coatings of HTR Fuel Particles," Journal of Nuclear Materials, vol. 62, no. 2–3, p. 123, 1976. | vol. 62, no. 2–3 | 1976 | Reference |
| **A-9** | Gordon R. Bower, Scott A. Ploger, Paul A. Demkowicz, John D. Hunn, "Measurement of kernel swelling and buffer densification in irradiated UCO-TRISO particles," Journal of Nuclear Materials, pp. 339-349. | 486 | 2017 | Reference |
| **A-10** | J. F. a. M. Petri, Thermophysical Properties of Uranium Dioxide, ANL/RE-97/2, February 1997. | ANL/RE-97/2 | Feb. 1997 | Reference |
| **A-11** | B. P. Collin, "AGR-3/4 Irradiation Test Final As-Run Report," INL/EXT-15-35550 Rev. 1, Idaho National Laboratory, May 2016. | INL/EXT-15-35550 | May 2016 | Reference |

| | | | | |
|---|---|---|---|---|
| **A-12** | D. W. Marshall, "AGR-5/6/7 Fuel Specification," SPC-1352, Rev. 8, Idaho National Laboratory, March 2017. | SPC-1352 | Mar. 2017 | Reference |
| **A-13** | "Xe-100 Reactor Fuel Specifications, XE01-N-RZZ-GLZZ-D-000100 Revision 1, 18-Jan-2021". | 000100 | 2 | Cross Reference |
| **A-14** | EPRI, "A Review of Radionuclide Release from HTGR Cores During Normal Operation," 1009382, Palo Alto, CA, 2004. | 1009382 | 2004 | Reference |
| **A-15** | T. N. Tiegs, "Fission product Pd-SiC interaction in irradiated coated-particle fuels," Nuclear Technology, vol. 57, no. 3, pp. 389-398, June 1982. | vol. 57, no. 3 | Jun. 1982 | Reference |
| **A-16** | B. P. Collin, "AGR-2 Irradiation Test Final As-Run Report," INL/EXT-14-32277 Rev. 1, Idaho National Laboratory, August 2014. | INL/EXT-14-32277 | Aug. 2014 | Reference |
| **A-17** | K. Minato, T. Ogawa, S. Kashimura, K. Fukuda, I. Takahashi, M. Shimizu and Y. Tayama, "Carbon monoxide-silicon carbide interaction in HTGR fuel particles," Journal of Materials Science, vol. 26, no. 9, p. 2379, 1991. | vol. 26, no. 9 | 1991 | Reference |
| **A-18** | I. van Rooyen and a. et, "Progress in Solving the Elusive Ag Transport Mechanism in TRISO Coated Particles: "What is new?"," in HTR 2014, Weihai, China, 2014. | HTR 2014 | 2014 | Reference |
| **A-19** | Brian Boyer, et. Al., “Inter-Comparison of Computer Codes for TRISO-Based Fuel Micro-Modeling and Performance Assessment,” HTR-2010, | INL/CON-10-18055 | Oct. 2020 | Reference |
| **A-20** | International Atomic Energy Agency, "Fuel Performance and Fission Product Behavior in Gas Cooled Reactors," IAEA-TECDOC-978, November 1997. | IAEA-TECDOC-978 | Nov. 1997 | Reference |
| **A-21** | S. R. Penfield, "Xe-100 Plant General Design Description," 100154, Rev. 3, X energy, 2016. | 100154 | 3 | Cross Reference |
| **A-22** | E. J. Mulder, "Preliminary Steady-State Core Design Report," XE00-N-RZZ-NSZZ-D-000288 Rev 5, 2022. | 000288 | 5 | Cross Reference |

# Appendix B. Thermodynamics Model

### Abbreviations/Acronyms

| Short Form | Phrase |
|---|---|
| **AGM** | Amsted Graphite Materials |
| **AGR** | Advanced Gas Reactor |
| **BDF2** | Backward Differentiation Formula |
| **EDN** | Equivalent DIDO-Nickel |
| **FIMA** | Fissions per Initial Metal Atom |
| **FPM** | TRISO-coated Particle Failure Probability Model |
| **GASM** | Gas Fission Transport Model |
| **HM** | Heavy Metal |
| **HTGR** | High-Temperature Gas Reactor |
| **IG** | Isotropic Graphite |
| **INL** | Idaho National Laboratory |
| **KSIM** | 2D Point Kinetics Core Simulation Model |
| **IPyC** | Inner Pyrolytic Carbon |
| **MWd** | Megawatt-day |
| **MWt** | Megawatt-thermal |
| **MST** | Mechanistic Source Term |
| **OPyC** | Outer Pyrolytic Carbon |
| **PCEA** | Petroleum Coke Extruded Graphite |
| **SiC** | Silicon Carbide |
| **SGL** | Sigri Great Lakes |
| **SOLM** | Solids Fission Transport Model |
| **SOR** | Successive Over-Relaxation |
| **THM** | Thermodynamics Model |
| **TRISO** | TRIstructural-ISOtropic |
| **UCO** | Uranium oxycarbide, a heterogeneous mixture of $UO_2$ and $UC_2$ |
| **$UO_2$** | Uranium dioxide |
| **Xe-100** | X-energy 200 MWt Pebble Bed Reactor |

**Definitions**

| Symbol | Definition |
|---|---|
| $A_{cz}^{i,r}$ | Compact Zone External Radial Heat Transfer Surface ($m^2$) |
| $A_{fz}^{i,z}$ | Surface Area of the Top/Bottom of the Compact at Axial Location 'z' in Fuel Zone 'fz' ($m^2$) |
| $A_{rz}^{i,r}$ | Reactor Zone External Radial Heat Transfer Surface ($m^2$) |
| $A_{rz}^{i,z}$ | Reactor Zone External Axial Upper/Lower Heat Transfer Surface ($m^2$) |
| $\mathbf{A_f}$ | Gas flow surface area ($m^2$) |
| $A_{fz}^{i}$ | Pebble Zone External Heat Transfer Surface ($m^2$) |
| $A_{pz}^{i}$ | Particle Zone External Heat Transfer Surface ($m^2$) |
| $\Delta B_{r,n,p,MWd/tHM}$ | Pebble Burnup Increment, (MWd/tHM) |
| $\Delta B_{r,n,p,\%FIMA}$ | Pebble Burnup Increment, (FIMA) |
| $B_{r,n}$ | Burn-up in reactor node r,n (MWd/tHM) |
| $c_p$ | helium specific heat (J/kg. K) |
| $\mathbf{d_h}$ | hydraulic diameter of the pebble bed (m) |
| $\mathbf{d}_s$ | fuel pebble diameter (m) |
| $\mathbf{E_s}$ | Young's modulus for carbon [[ ]]$^P$ ($N/m^2$) |
| $E_{g,i}^{\gamma}$ | γ energy in group g [MeV] |
| $\overline{E}_{g,i}^{\gamma}$ | Average γ energy in group g [MeV] |
| $\dot{f}$ | fission rate (fissions/s) |
| $f_e$ | energy released per fission reaction (J) |
| $\dot{f}_{r,n}$ | fission rate per pebble in core node (r, n) (fission/pebbles) |
| $\mathbf{F_i}$ | fraction of fissions from fissile isotope i |
| $\mathbf{F_r^p}$ | packing factor of component r [r ≠ core channel] |
| $F_{cap}^{res}$ | U-238 Cross Section ($cm^2$) |
| $\mathbf{F_r^V}$ | volume fraction of channel r relative to core volume |
| $\mathbf{F_{r,n}^V}$ | volume fraction of node n relative to volume of channel r |
| $F_{g,i}^{\gamma}$ | Fraction of number of γ's in group g |
| $F_{abs,g}^{\gamma}$ | Fraction of γ's produced in ($r_s$,$z_s$) that is absorbed in structure at ($r_t$,$z_t$) |
| $F_{\theta,g}^{\gamma}$ | γ's Angular Fraction |

| Symbol | Definition |
|---|---|
| $\mathbf{f_i}$ | energy released per fission from fissile isotope i (J) |
| $\mathbf{h_z}$ | height of cylindrical zone z (m) |
| $H^s$ | Heavy Metal Mass per Pebble in Equation B.2.2.5.16 (kg) |
| $HM_{pebble}$ | Pebble Heavy Metal Loading (tHM) |
| $HM_{r,n}$ | Heavy Metal Loading in reactor node r,n (tHM) |
| $L_0$ | Graphite length before irradiation (m) |
| $L_{sat}$ | Saturation level of relative thermal conductivity change due to fast neutron irradiation |
| $\dot{\mathbf{m}}$ | gas mass flow rate (kg/s) |
| $N_A$ | Avogadro's Number in Equation B.2.2.5.16 (6.022E+23/mole) |
| $\mathbf{N^s_{r,n}}$ | number of pebbles in core node (r, n) |
| $N^{\gamma}_{g,no.}$ | Number of gamma rays (γ) in group g in energy range no. 1 through 3 |
| $N^{\gamma}_{tot}$ | Total number of γ's (36) in energy range 0.085 ≤ 8.0 MeV |
| $\mathbf{n_{fc}}$ | number of flow channels in radial components |
| $N_A$ | number of particles per unit area ($1/m^2$) |
| $N_L$ | number of particles per unit length (1/m) |
| $N_u$ | Nusselt Number KTA Rule |
| $N_{ul}$ | Nusselt Number Achenbach |
| $\mathbf{P^{MW}_{core}}$ | core power ($MW_t$) |
| $\mathbf{P_{r,n}}$ | relative power in core node (r, n) (%) |
| $\dot{P}^{239}_{r,n}$ | Production rate of actinide $^{239}U$ in node (r, n), (#/s) |
| $\mathbf{p_s}$ | pebble bed stack pressure (Pa) |
| $\mathbf{p}$ | gas pressure (Pa) |
| $P_r$ | Prandtl Number |
| $\dot{Q}_{av}$ | Convective heat transfer in the core Newton's law [W] |
| $\dot{Q}_{rad}$ | Radiative heat transfer (W) |
| $\dot{Q}^i_{A,0}$ | Decay power for actinide A [W] |
| $\dot{Q}^{tot}_{A,r,n}$ | Total actinide power in node r,n (W) |
| $\dot{Q}_{core}$ | Total Core Power (W) |
| $\dot{Q}_{D,r,n}$ | Total decay power in core node r,n (MW) |

| Symbol | Definition |
|---|---|
| $Q_{r,n}^{F}$ | Fractional node power in node r,n (MW) |
| $\dot{Q}_{D,tot}$ | Total core decay power (MW) |
| $\dot{Q}_{fz}$ | Heat source in active fuel zone *fz* assuming uniform power distribution over the pebble (W) |
| $\dot{Q}_{kz}$ | Heat source in kernel zone *kz* (W) |
| $\dot{Q}_{n}$ | Pebble power in reactor node *n* (MW) |
| $\dot{Q}_{r,fz}$ | Heat source in active fuel zone (*r,fz*) assuming uniform power distribution over the compact (W) |
| $\dot{Q}_{r,n}$ | Power in core node *r,n* (W) |
| $\dot{Q}_{r,n}^{\gamma}$ | γ heat source in node (*r,n*) (MW) |
| $\dot{q}_{r,n}^{s}$ | heat source density per fuel pebble in core position (*r,n*) (W/m$^3$) |
| $\dot{q}_{r,n}^{p}$ | heat source density per particle in core region (*r,n*) (W/m$^3$) |
| $R_e$ | Reynolds Number |
| $r_e^i$ | Pebble/Particle/Compact/Reactor Zone Effective Radius (m) |
| $r_e^{i'}$ | Pebble/Particle/Compact/Reactor Inter Zone Diffusion Distance (m) |
| $\mathrm{r_i}$ | inner radius of zone i (m) |
| $\mathrm{r_{i+1}}$ | inner radius of zone i+1 (m) |
| $\mathrm{r_s}$ | fuel pebble radius (m) |
| $\mathrm{S_F}$ | packing factor constant |
| $\mathrm{T_g}$ | gas temperature (K) |
| $\mathrm{T_s}$ | solid surface temperature (K) |
| $\mathrm{t_{tr}}$ | transient duration (s) |
| $V_{cz}^{i,z}$ | Compact zone (cz) volume (m$^3$) |
| $V_{fz}^{i}$ | Pebble zone Volume [m$^3$] |
| $V_p$ | Particle volume [m$^3$] |
| $V_{pz}^{i}$ | Particle zone volume [m$^3$] |
| $\mathrm{V_k^p}$ | Volume of TRISO particle kernel (m$^3$) |
| $V_s^a$ | Pebble Active Volume (m$^3$) |
| $V_s^{shell}$ | Pebble Shell Volume (m$^3$) |
| $V_0$ | Graphite volume before irradiation (m$^3$) |

| Symbol | Definition |
|---|---|
| $z_e^{i'}$ | Compact/Reactor Inter Zone Axial Diffusion Distance (m) |
| $\alpha$ | Convective heat transfer coefficient (W/m$^2$. K) |
| $\beta$ | Dimensionless deformation factor |
| $\Delta L$ | Change in graphite length after irradiation (m) |
| $\Delta V$ | Change in graphite volume after irradiation (m$^3$) |
| $\Gamma$ | fast fluence (n/cm$^2$ E > 0.1MeV) |
| $\varepsilon$ | porosity $(1 - F_r^p)$ |
| $\epsilon_p$ | pebble emissivity |
| $\gamma$ | Fast fluence $(10^{20}\ \mathrm{n/cm^2\ EDN})$ |
| $\gamma_0$ | Fast fluence for initiating irradiation-induced changes in graphite thermal conductivity $(10^{20}\ \mathrm{n/cm^2\ EDN})$ |
| $\gamma_{sat}$ | Fast fluence for saturation of graphite thermal conductivity $(10^{20}\ \mathrm{n/cm^2\ EDN})$ |
| $\gamma_{sb}$ | Fast fluence for secondary breakdown of graphite thermal conductivity $(10^{20}\ \mathrm{n/cm^2\ EDN})$ |
| h | Helium Shear Viscosity [Pa. s] |
| $\Lambda$ | Dimensionless Conduction Heat Transfer Factor |
| $\lambda$ | Heat Conduction Coefficient (W/m. K) |
| $\lambda_{irr}$ | Thermal conductivity change due to irradiation (W/m.°C) |
| $\lambda_g$ | gas heat conduction coefficient (W/m. K) |
| $\lambda_s$ | heat conduction coefficient in pebble (W/m. K) |
| $\lambda_{sc}$ | conduction through the pebbles across the contact between pebbles (W/m. K) |
| $\lambda_r$ | conduction through solid phase and radiation between pebbles (W/m. K) |
| $\lambda_e$ | conduction through solid phase and across the fluid phase (W/m. K) |
| $\lambda_{pb}$ | total effective conductivity for packed pebble bed (W/m/. K) |
| $\lambda_\beta^1$ | β decay constant U-239 (1/sec) |
| $\lambda_\beta^2$ | β decay constant Np-239 (1/sec) |
| $\rho$ | Density [kg/m$^3$] |
| $\mu_c$ | Poisson ratio for carbon $[= 0.136]$ |
| $\sigma$ | Stefan-Boltzmann constant $[5.67\ \mathrm{x}\ 10^{-8}]$ (W/m$^2$K$^4$) |
| $\sigma_a^{238}$ | Cross Section a or c in Equation B.2.2.5.16 a subscript (absorption), c subscript (capture) |

| Symbol | Definition |
|---|---|
| $\upsilon$ | gas flow velocity (m/s) |
| $\varphi_e$ | epithermal neutron flux (n/m$^2$-sec) |
| $\Phi_{r,n}$ | Single-group flux in reactor node (r,n) (n/m$^2$-sec) |

## B.1 Introduction

As discussed in Section 3.2, the functional containment system is a collection of five radionuclide (RN) release barriers, designed to limit RN release from the core to the environment to very low levels during normal operation and a broad spectrum of postulated accidents, References 1 and 2. These barriers, together with the main phenomena and processes involved in radionuclide production, retention, transport, and release for a pebble bed reactor are depicted in Figure 3 of this Topical Report. The Thermodynamics Model (THM) calculates detailed temperature profiles along these barriers for TRISO-coated particles, fuel pebbles, core, and other reactor components as required for calculations associated with the production, decay, transmutation, transport, and leakage of fission products from TRISO coated particles and fuel pebbles into the helium pressure boundary and into the Reactor Building (if required) under normal steady-state and DBA conditions.

Detailed fuel element and TRISO-coated particle temperatures are needed to perform fuel failure probability calculations in the Fuel Failure Probability Model (FPM), and radionuclide transport calculations in the Gas (GASM) and Solids (SOLM) Fission Transport Models. The fuel failure models in FPM and diffusion coefficients in GASM and SOLM are strongly dependent on TRISO-coated particle and fuel element graphite matrix temperatures, respectively. Since the neutronics design code VSOP (Reference B-2) does not calculate temperatures at this level of detail, the Thermodynamics Model (THM) performs detailed temperature calculations for the entire core using VSOP boundary conditions.

## B.2 Theory and Methodology

### B.2.1 Computational Domain

The VSOP neutronics grid model consists of five fuel pebble flow channels with varying number of axial nodes. To simplify the THM and ensure consistency with VSOP, the computational domain is divided in [[

]]$^{P}$ The computational domain for temperature calculations in the THM is shown in Figure B-1.

Fuel is discharged at the bottom of the core from all channels at the end of each pass. For simplicity, VSOP calculates data on an average pebble at the end of each pass over the discharged pebbles. Pebbles return to the core for the next pass with the averaged parameters such as burnup and fluence, thus losing the individual pebble characteristics, when the calculation is performed within VSOP. When the THM is coupled with the time-dependent solid radionuclide transport in the SOLM model, pass histories for individual fuel pebbles are traced through all passes explicitly. Thus, burnup and radionuclide spatial distribution calculations within pebbles are performed explicitly in SOLM for each pebble going through a random loading sequence, see Appendix C, thus preserving the individual pebble characteristics.

The THM is the initializing model in MST calculations. All geometric calculations such like volumes and surface areas are performed during the initialization process. The THM computational flow and mapping to and from VSOP is discussed in Section B.2.2.7.

[[

]]$^{P}$

***Figure B-1: Computational Domain for Thermodynamics Model Temperature Calculations***

### B.2.1.1 Computational Domain – Xe-100 Reactor Model

For MST calculations, the THM can be used to calculate heat removal from the fuel to the outside surface of the Reactor Pressure Vessel (RPV) where the heat is dissipated.

In Figure B-2, the reactor is depicted in a 2-D cylindrical model in 'r' radial and 'n' axial positions to make a cylindrical mesh. The reactor is configured with [[ ]]$^{P}$ radial zones and [[ ]]$^{P}$ axial nodes in each radial zone. The height of the grid is set to the height of the effective pebble bed height [[ ]]$^{P}$ and the outer radius corresponds to inner radius of the graphite reflector. The core is represented by five fuel channels as in VSOP calculations. Thus, radial channels 1 to [[ ]]$^{P}$ represents the pebble bed core and the remaining radial channels, that is [[ ]]$^{P}$ are used for the reactor structures.

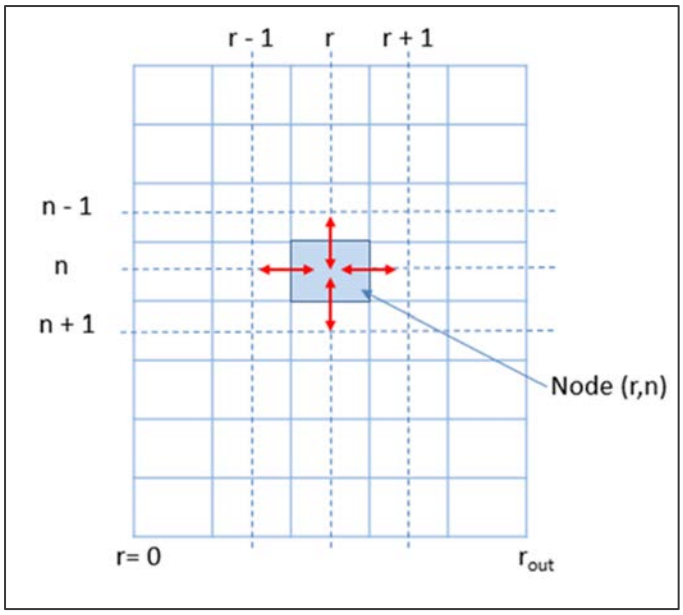


***Figure B-2: TM Xe-100 Reactor Model***

### B.2.1.2 Computational Domain – Xe-100 TRISO Coated Fuel Particle Model

The TRISO fuel particle is depicted in Figure B-1. The model is made up of five distinct components, namely a kernel containing the fissile, fertile and fissionable material, a buffer layer, and three layers, IpyC, SiC and the OpyC. The TRISO-coated fuel particles are modeled in a 1D spherical geometry. Each of the five particle components shown in Figure B-1 is divided into [[ ]]$^{P}$ equal sized radial zones (meshes). Thus, the particle is modeled in [[ ]]$^{P}$ radial zones with different volumes.

### B.2.1.3 Computational Domain – Xe-100 Fuel Pebble and Experiment Fuel Compact Models

The fuel pebbles are modeled in a 1D spherical geometry. The pebble is divided into two distinct regions as shown in Figure B-1. The first region is called the active pebble region which contains the TRISO fuel particles. The second region is called the fuel free zone (shell) which does not contain any fuel particles. Both the shell and the active pebble region may contain uranium contamination. The shell and the active pebble region are both divided into [[ ]]$^{P}$ radial zones (meshes). Thus, the pebble is modeled in [[ ]]$^{P}$ radial zones [[ ]]$^{P}$.

Fuel compacts are used in isolated fuel element calculations to simulate cylindrical-geometry fuels, such as the ones used in the Idaho National Laboratory (INL) Advanced Gas Reactor (AGR) experiments. The fuel compact is modeled in a symmetrical 2-D cylindrical geometry where the compact is divided into [[ ]]$^{P}$ radial and 10 equal-sized axial zones. Unlike the pebble, the compact does not have a fuel free zone (shell). [[
]]$^{P}$ More details about the fuel compact meshing are given in Sec. C.2.1.3.

## B.2.2 Thermodynamics Models

### B.2.2.1 Fuel Particle, Pebble, and Compact Geometry Models

Heat flow and temperature distributions in the TRISO particles, fuel pebbles and fuel compacts require knowledge of the heat sources in each fuel zone, heat transfer properties, geometry, and boundary conditions. The geometrical values of importance for determining the pebble temperature distributions are described herein and generally calculated by means of standard geometry equations expressed in Table B-1, Table B-2, and Table B-3 for TRISO particles, fuel pebbles and fuel compacts respectively.

***Table B-1: TRISO Particle Geometry Equations***

| Description | Equation | Number |
|---|---|---|
| Particle Zone Volume [m$^3$] | $V_{pz}^i = \frac{4}{3}\pi\left(r_{i+1}^3 - r_i^3\right)$ [[ ]]$^P$ $r_0 = 0, pz = Particle\ Zone$ | B-2.2.1-1 |
| Particle Zone External Heat Transfer Surface (m$^2$) | $A_{pz}^i = 4\pi r_{i+1}^2$ | B-2.2.1-2 |
| Particle Zone Effective Radius (m) | $r_e^i = \left(\frac{r_i^3 + r_{i+1}^3}{2}\right)^{\frac{1}{3}}$ | B-2.2.1-3 |
| Particle Inter Zone Diffusion Distance (m) | $r_e^{i'} = r_e^{i+1} - r_e^i$ | B-2.2.1-4 |
| Particle Volume (m$^3$) | $V_p = \frac{4}{3}\pi r^3$ | B-2.2.1-5 |

***Table B-2: Pebble Geometry Equations***

| Description | Equation | Number |
|---|---|---|
| Pebble Zone Volume [m$^3$] | $V_{fz}^i = \frac{4}{3}\pi\left(r_{i+1}^3 - r_i^3\right)$ [[ ]]$^P$ $r_0 = 0, fz = Fuel\ Zone$ | B-2.2.1-6 |
| Pebble Zone External Heat Transfer Surface (m$^2$) | $A_{fz}^i = 4\pi r_{i+1}^2$ | B-2.2.1-7 |
| Pebble Zone Effective Radius (m) | $r_e^i = \left(\frac{r_i^3 + r_{i+1}^3}{2}\right)^{\frac{1}{3}}$ | B-2.2.1-8 |
| Particle Inter Zone Diffusion Distance (m) | $r_e^{i'} = r_e^{i+1} - r_e^i$ | B-2.2.1-9 |
| Pebble Active Volume (m$^3$)<br>$r_{as}$ is the external radius of the active zone | $V_s^a = \frac{4}{3}\pi {r_{as}}^3$ | B-2.2.1-10 |
| Pebble Shell Volume (m$^3$)<br>R is the external radius of the pebble | $V_s^{shell} = \frac{4}{3}\pi(R^3 - {r_{as}}^3)$ | B-2.2.1-11 |

***Table B-3: Compact Geometry Equations***

| Description | Equation | Number |
|---|---|---|
| Compact Zone (cz) Volume ($m^3$) | $V_{cz}^{i,z} = h_z\pi(r_{i+1}^2 - r_i^2)$ [[ ]]$^P$ $r_0 = 0$ | B-2.2.1-12 |
| Compact Zone External Radial Heat Transfer Surface ($m^2$) | $A_{cz}^{i,r} = 2h_z\pi r_{i+1}$ | B-2.2.1-13 |
| Surface Area of the Top of the Compact at Axial Location 'z' in Fuel Zone 'fz' ($m^2$) | $A_{fz}^{i,z} = \pi(r_{i+1}^2 - r_i^2)$ | B-2.2.1-14 |
| Surface Area of the Bottom of the Compact at Axial Location 'z' in Fuel Zone 'fz' ($m^2$) | $A_{fz}^{i,z} = \pi(r_{i+1}^2 - r_i^2)$ | B-2.2.1-15 |
| Compact Zone Effective Radius (m) | $r_e^i = \sqrt{\frac{r_i^2 + r_{i+1}^2}{2}}$ | B-2.2.1-16 |
| Compact Inter Zone Radial Diffusion Distance (m) | $r_e^{i'} = r_e^{i+1} - r_e^i$ | B-2.2.117 |
| Compact Inter Zone Axial Diffusion Distance (m) | $z_e^{i'} = h_z$ | B-2.2.1-18 |

### B.2.2.2 Reactor Geometry Model

The geometry adopted for the reactor model considers the physical processes involved in heat transport during normal operations and postulated accidents. The geometry models consider coolant flow channels, reactor fuel, and structural components to adequately simulate convection, conduction, and radiation heat transfer. The corresponding geometry equations are listed in Table B-4.

***Table B-4: Reactor Geometry Equations***

| Description | Equation | Number |
|---|---|---|
| Reactor Zone Volume ($m^3$) | $V_{rz}^{i,z} = h_z\pi(r_{i+1}^2 - r_i^2)$ [[ ]]$^P r_0 = 0, rz = Reactor\ Zone$ | B-2.2.2-1 |
| Reactor Zone External Radial Heat Transfer Surface ($m^2$) | $A_{rz}^{i,r} = 2h_z\pi r_{i+1}$ | B-2.2.2-2 |
| Reactor Zone External Axial Upper/Lower Heat Transfer Surface ($m^2$) | $A_{rz}^{i,z} = F_r^p\pi(r_{i+1}^2 - r_i^2)$ | B-2.2.2-3 |
| Reactor Zone Effective Radius (m) | $r_e^i = \sqrt{\frac{r_i^2 + r_{i+1}^2}{2}}$ | B-2.2.2-4 |
| Reactor Inter Zone Radial Diffusion Distance (m) | $r_e^{i'} = r_e^{i+1} - r_e^i$ | B-2.2.2-5 |
| Reactor Inter Zone Axial Diffusion Distance (m) | $z_e^{i'} = h_z$ | B-2.2.2-6 |

### B.2.2.3 Helium Properties

The thermodynamics model computes heat transfer coefficients between the solid surfaces and the helium coolant. The solid-to-gas heat transfer coefficients are used to determine fuel temperatures

during both normal operations and transients where coolant or air flow is present. The coefficients are dependent on the flow channel geometry, gas dynamics, and temperature/pressure dependent gas properties.

Heat transfer between the coolant gas and the hotter solid surfaces is based on heat transfer coefficients dependent on multiple input parameters such as gas properties and system geometry as discussed in Section B.2.2.4.

The heat transfer rate between the coolant gas flow and the solid surface is expressed in terms of Newton's Law of cooling as follows:

$$\dot{Q} = \alpha A(T_s - T_g) \qquad \text{B-2.2.3-1}$$

where α is the convective heat transfer coefficient in W/m$^2$K, $T_s$ is the solid surface temperature in °K, $T_g$ is the coolant gas temperature in °K and A is the heat transfer surface area in m$^2$.

In general, thermodynamics parameters can be calculated using well established empirical correlations. For a pebble bed reactor, specific correlations have been established over years of research and development. Helium property correlations used in the THM for determining reactor component temperature distributions are listed in Table B-5.

***Table B-5: Helium Property Correlations***

| Description | Equation | Reference | Number |
|---|---|---|---|
| Helium Shear Viscosity [Pa. s] | $\eta = 3.674 \times 10^{-7} T_g^{0.7}$ | [B-1] | B-2.2.3-2 |
| Helium Specific Heat [J/kg. K] (p is in bar) | $c_p = 5195$ | [B-4] | B-2.2.3-3 |
| Helium Density [kg/m$^3$] (p in bar) | $\rho = 48.14 \frac{p}{T_g}\left(1 + \frac{0.4446p}{T_g^{1.2}}\right)^{-1}$ | [B-1] | B-2.2.3-4 |
| Hydraulic Diameter of a Pebble Bed [m] | $d_h = \frac{2}{3} d_s \frac{\varepsilon}{1-\varepsilon}$ | [B-3] | B-2.2.3-5 |
| Reynolds Number | $R_e = \frac{\dot{m} d_h}{\eta A_f} = \frac{\rho v d_h}{\eta}$ | [B-4] | B-2.2.3-6 |
| Prandtl Number | $P_r = \frac{\eta c_p}{\lambda_g}$ | [B-4] | B-2.2.3-7 |
| Nusselt Number KTA rule | $N_u = 1.27 \frac{P_r^{1/3}}{\varepsilon^{1.18}} R_e^{0.36} + 0.033 \frac{P_r^{1/2}}{\varepsilon^{1.07}} R_e^{0.86}$ | [B-1] | B-2.2.3-8 |
| Nusselt Number Achenbach | $N_u = f_\varepsilon \times N_{lt}$<br>$f_\varepsilon = 1 + 1.5(1-\varepsilon)$<br>$N_{ul} = 0.664 \left(\frac{R_e}{\varepsilon}\right)^{1/2} P_r^{1/3}$<br>$N_{ut} = \frac{0.037 \left(\frac{R_e}{\varepsilon}\right)^{0.8} P_r}{1 + 2.443 \left(\frac{R_e}{\varepsilon}\right)^{-0.1} \left(P_r^{2/3} - 1\right)}$ | [B-5] | B-2.2.3-9 |

| Description | Equation | Reference | Number |
|---|---|---|---|
| | $N_{lt} = 2 + \sqrt{N_{ul}^2 + N_{ut}^2}$ | | |
| Helium Flow Rate in Axial Direction [kg/s] | $\dot{m} = \frac{n_{fc} A_f}{A_t}\left(\dot{m}_t - \dot{m}_{bp}\right)$ | | B-2.2.3-10 |
| Helium Flow Velocity in Axial Direction [m/s] | $v = \frac{\dot{m}}{\rho n_{fc} A_f \left(1 - F_r^p\right)}$ | | B-2.2.3-11 |

### B.2.2.4 Heat Transfer

The following heat transfer mechanisms are modelled in THM. They are based on empirical correlations applicable to HTGR materials and conditions.

- Conductive linear heat transfer
- Convective heat transfer
- Radiative heat transfer

Heat transfer between adjacent bodies (or regions in the same body) takes place when there is a temperature gradient between the bodies as illustrated in Figure B-6, Figure B-7, and Figure B-8. The heat transfer coefficient can be interpreted as a coupling coefficient between the two bodies. For steady state conditions, a temperature balance is achieved between adjacent bodies dependent on the heat transfer coefficient under prevailing steady state conditions.

#### B.2.2.4.1 Conductive Heat Transfer

The process of heat conduction, Figure B-6, is dependent on:

- The temperature gradient
- The interface cross section of the materials
- The path length
- Material heat conduction properties

In all regions and components of the reactor model, these values are inputs in the form of constants and correlations so that reactor and coolant temperature distributions can be calculated. Because the heat transfer coefficients depend on temperature, they generally vary between the neighboring nodes in the discrete model. To capture this variation, an effective heat transfer coefficient between adjacent nodes is calculated by imposing the physical constraint of continuity of heat flux across the interface.

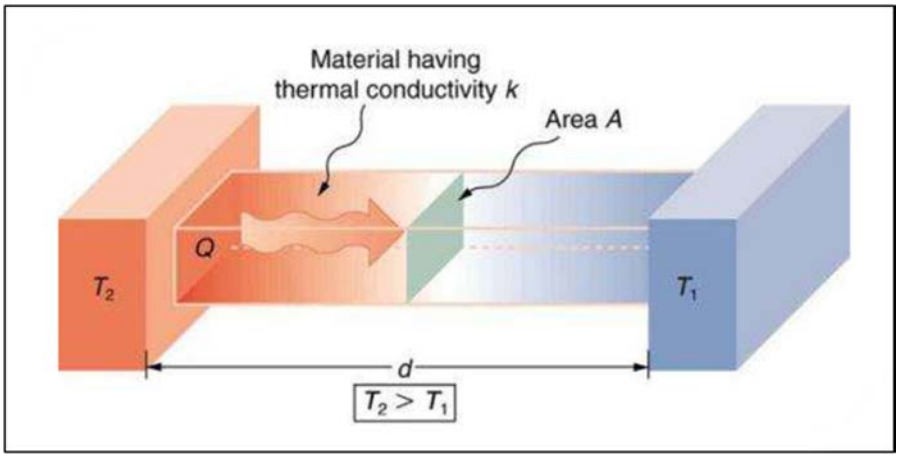


***Figure B-6: Conductive Heat Transfer***

#### B.2.2.4.2 Convective Heat Transfer

The reactor coolant gas flows next to a solid surface where the surface temperature is higher than the bulk gas temperature removing heat from the solid body as depicted in Figure B-7. The convective heat transfer coefficient is dependent on the gas physical and heat transfer properties and flow rate. In a steady-state condition, an iterative numerical procedure is applied to determine the equilibrium state between the solid body and gas temperatures.

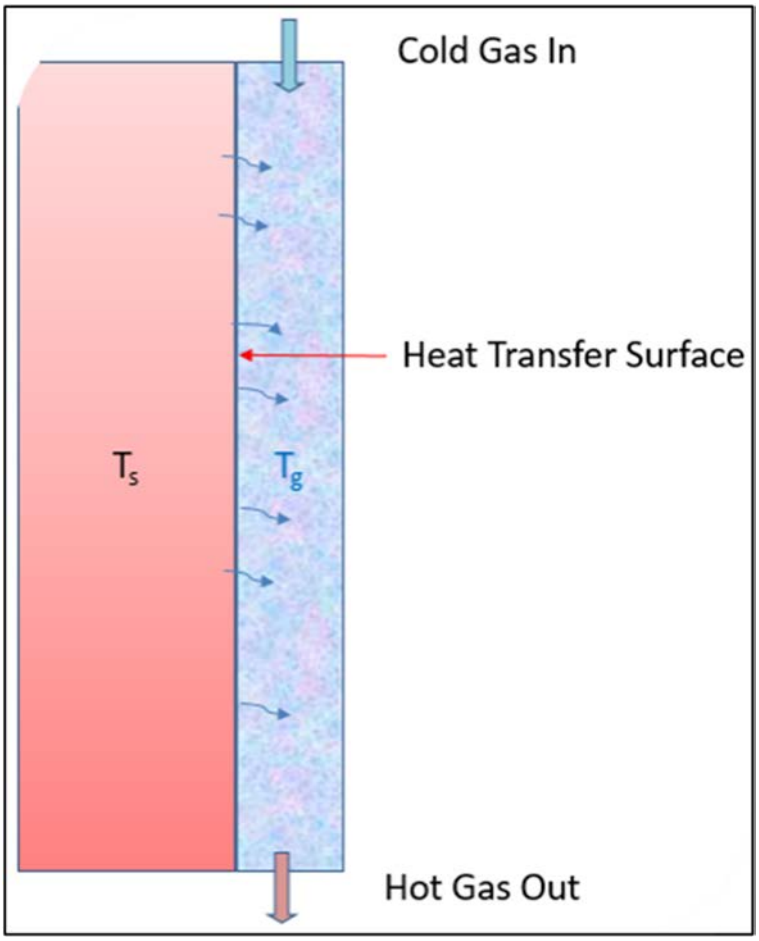


***Figure B-7: Convective Heat Transfer***

### B.2.2.4.3 Radiative Heat Transfer

Radiation heat transfer does not require direct contact between adjacent bodies but rather dependent on the properties of the media between the bodies (normally a gas) as shown in Figure B-8. The net radiation from a body with surface area A is given by:

$$\dot{Q}_{rad} = \varepsilon_p \sigma A T^4 \qquad \text{B-2.2.4.-1}$$

Thus, the net radiative heat transfer between $A_1$ when present in the radiative heat flux of body $A_2$ can be written as:

$$\dot{Q}_{rad} = \varepsilon_p \sigma (A_2 T_2^4 - A_1 T_1^4) \qquad \text{B-2.2.4-2}$$

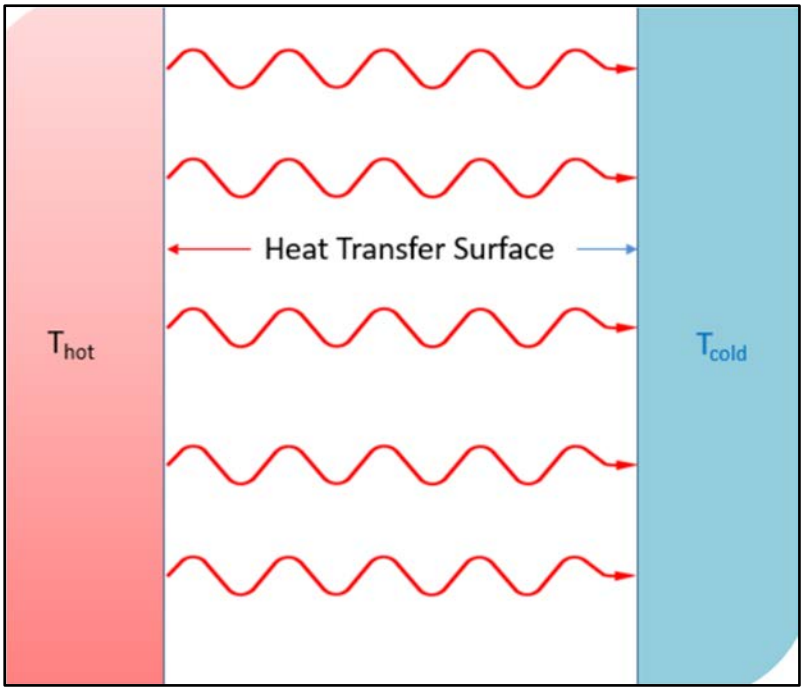


***Figure B-8: Radiative Heat Transfer***

### B.2.2.4.4 Heat Transfer Correlations

The heat transfer correlations used in determining the reactor core and reactor component temperature distributions are shown in Table B-6.

***Table B-6: Heat Transfer Correlations***

| Description | Equation | Reference | Number |
|---|---|---|---|
| Conduction through the pebbles and across the contact between pebbles [W/m. K] | [[ ]]$^{P}$ | [[ ]]$^{P}$ | B-2.2.4-3 |

| Description | Equation | Reference | Number |
|---|---|---|---|
| Conduction through the solid Phase and radiation between pebbles [W/m.K] (Zehner-Schlunder Model) | [[ ]]P | [[ ]]P | B-2.2.4-4 |
| [[ ]]P | [[ ]]P | [[ ]]P | B-2.2.4-5 |
| [[ ]]P | [[ ]]P | [[ ]]P | B-2.2.4-6 |
| Conduction through the solid phase and across the fluid phase [W/m.K] | [[ ]]P | [[ ]]P | B-2.2.4-7 |
| [[ ]]P | [[ ]]P | [[ ]]P | B-2.2.4-7a |
| Total effective conductivity for packed pebble bed [W/m. K] | $\lambda_{pb} = \lambda_{sc} + \lambda_r + \lambda_f$ | [B-6], Section 4.2.2.2 Item 3. | B-2.2.4-8 |
| [[ ]]P | [[ ]]P | [[ ]]P | B-2.2.4-9 |
| [[ ]]P | [[ ]]P | [[ ]]P | B-2.2.4-10 |
| Convective heat transfer in the core Newton's law [W] | $\dot{Q}_{av} = A_s\alpha(T_s - T_g)$ | [B-4], Chapter 12 | B-2.2.4-11 |

| Description | Equation | Reference | Number |
|---|---|---|---|
| Convective heat transfer coefficient [W/m². K] | $\alpha = \frac{N_u \lambda_g}{d_h}$ | [B-4], Chapter 12 | B-2.2.4-12 |
| Radiative heat transfer [W] | $\dot{Q}_{rad} = \varepsilon_p \sigma \left( A_2 T_2^4 - A_1 T_1^4 \right)$ | | B-2.2.4-13 |

The material property correlations used in heat transfer and temperature calculations are shown in Table B-7.

***Table B-7: Material Properties Correlations***

| Description | Equation |
|---|---|
| Density of [[ ]]$^P$ Steel [kg/m³] | [[ ]]$^P$ |
| Density of [[ ]]$^P$ Steel [kg/m³] | [[ ]]$^P$ |
| Density of Graphite [kg/m³] | $\rho = 1800$ |
| Density of A3-3 Graphite [kg/m³] | [[ ]]$^P$ |
| Heat conduction coefficient of [[ ]]$^P$ Steel [W/m. °K] | [[ ]]$^P$ |
| Heat conduction coefficient of [[ ]]$^P$ Steel [W/m. °K] | [[ ]]$^P$ |
| Heat conduction coefficient of Reflector Graphite [W/m. °C] | The Mitchell-Haag Model is used, see Section B.2.2.4.1. [[ ]]$^P$ |
| Heat conduction coefficient of $UO_2$ [W/m. K] | [[ ]]$^P$ |
| Heat conduction coefficient of UCO [W/m. K] | [[ |

| Description | Equation |
|---|---|
| | [[ ]]P |
| Heat conduction coefficient of Buffer [W/m. K] | [[ ]]P |
| Heat conduction coefficient of PyC [W/m. K] | [[ ]]P |
| Heat conduction coefficient of SiC [W/m.°K] | [[ ]]P |
| Specific heat of A3-3 Graphite [J/kg.K] | [[ ]]P |

#### B.2.2.4.4.1 Derivation of Mitchell-Haag Model for Heat Conduction Coefficient of Reflector Graphite

[[

]]P

#### B.2.2.4.4.1 Thermal Conductivity of Unirradiated Graphite, $\lambda_0$

The thermal conductivity of unirradiated (virgin) graphite as a function of temperature is obtained as an exponential fit to Figure 29 of Reference [B-13]:

$$\lambda_0(T) = \lambda_0(20) \cdot \left[a + (1-a) \cdot \mathrm{e}^{k\cdot(T-20)}\right],$$

where:

$\lambda_0(20) = 132$ W/m.°C (thermal conductivity of virgin graphite at room temperature[3])

$a = 0.29$,

$k = -0.00229$,

$T =$ temperature (°C)

#### B.2.2.4.4.2 Heat Capacity of Unirradiated Graphite, $c_p$

$$c_p(T) = 1.75\ (0.645 + 3.14 \times 10^{-3}\ T - 2.809 \times 10^{-6}\ T^2 + 0.959 \times 10^{-9}\ T^3),$$

where the validity range is for $T < 1200$°C.

#### B.2.2.4.4.3 Irradiation-induced Change in Thermal Conductivity at Irradiation Temperature, $\frac{\lambda(T_{irr})}{\lambda_0(T_{irr})}$

As indicated in References [B-11] through [B-14], the thermal conductivity of irradiated graphite as a function of fast neutron fluence is characterized by a decrease in conductivity with increasing fluence, reaching a saturation level beyond which the conductivity stays constant, and potentially undergoing a secondary breakdown at very high fluence levels, beyond which the conductivity starts decreasing again.

[3] Exponential fit obtained from the VSOP source code, in agreement with typical values reported for various nuclear graphite grades in literature.

This is illustrated in Figure B-9. The exact behavior and values depend on the specific type of graphite, irradiation conditions, and temperature range. The correlations used in the THM model are in agreement with the plots pertaining to the AGM PCEA, SGL NBG-18 and Toyo Tanso IG-110 graphites used in the current stage of the Xe-100 graphite core structure design (see Sec. 7.9 [B-15] and [B-16]).

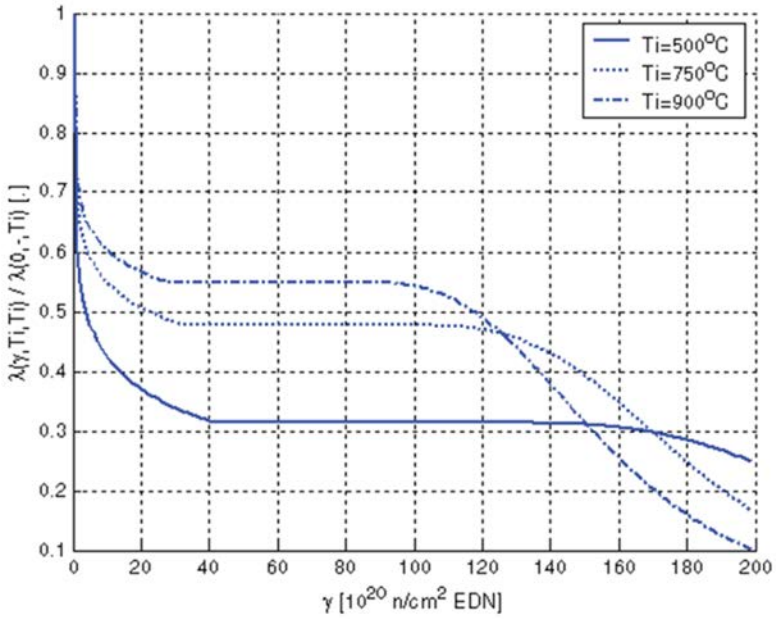


***Figure B-9: Typical irradiation-induced thermal conductivity changes in reactor graphite (Figure B-5, [B-14]).***

### B.2.2.4.4.4 Fluence Thresholds

While the mechanism of graphite initial shrinkage is not well understood, the effects causing shrinkage reversal to growth are at least qualitatively known. The secondary breakdown of thermal conductivity at high fluences is related to the relative volume change after turn-around as confirmed in Reference [B-13], the onset of the secondary breakdown of thermal conductivity coincides with the turn-around of the dimensional or volume changes due to irradiation, which can be formally written as:

$$\gamma_{sb}(T_{irr}) = \text{argmin}_{\gamma}\left(\left[\frac{\Delta V(\gamma)}{V_0}\right]_{T_{irr}}\right)$$

where $\Delta V$ is the change in volume after irradiation and $V_0$ is the volume before irradiation, measured at a specific temperature. A functional dependence from the VSOP code is used in the THM model:

$$\gamma_{sb}(T_{irr}) = -0.1082\, T_{irr} + 179.17$$

which agrees with Figures B-3 and B-4 of Reference [B-14] for a typical reactor graphite[4].

Similarly, the approach adopted by the VSOP code is used to estimate the saturation limit in the THM model, whereby the saturation fluence is set to be one third of the secondary breakdown limit (see the plots in Figure B-9):

$$\gamma_{sat}(T_{irr}) = \frac{1}{3}\gamma_{sb}(T_{irr}).$$

### B.2.2.4.4.5 Thermal Conductivity as a Function of Fluence

The fluence thresholds established in the previous subsection, along with an initial threshold for the onset of irradiation effects, divides the dependence of the ratio of the irradiated and unirradiated thermal conductivity $\lambda/\lambda_0$ (the inverse of which appears in the last term of the Equation for $\lambda(T)$ in Section B.2.2.4.1) on fluence into 4 regions as described below.[5]

$$\Gamma \leq \gamma_0:$$

$$\frac{\lambda(T_{irr})}{\lambda_0(T_{irr})} = 1$$

where $\gamma_0 = 0.0059\ [10^{20}\ \mathrm{n/cm^2\ \ EDN}]$ is an initial threshold for irradiation-induced changes in graphite thermal conductivity (per VSOP source code).

$$\gamma_0 < \gamma \leq \gamma_{sat}:$$

The approach to the saturation level is approximated by a linear fit on a semi-logarithmic $\gamma$-axis (see the initial steep decrease of the curves in FigureB-9 before plateauing at the saturation level), using the two end values:

$$\gamma = \gamma_0 \quad \Rightarrow \quad \frac{\lambda(T_{irr})}{\lambda_0(T_{irr})} = 1,$$

$$\gamma = \gamma_{sat} \ \Rightarrow \ \frac{\lambda(T_{irr})}{\lambda_0(T_{irr})} = \left[\frac{\lambda(T_{irr})}{\lambda_0(T_{irr})}\right]_{sat} \equiv L_{sat}(T_{irr}),$$

where the saturation level of relative thermal conductivity changes due to fast neutron irradiation is obtained as a function of irradiation temperature by fitting the data empirically derived for different nuclear graphites and presented in Table 4 of Reference [B-13]:

---

[4] If dimensional changes $\left(\frac{\Delta L}{L_0}\right)^{\perp}$ and $\left(\frac{\Delta L}{L_0}\right)^{\parallel}$ in perpendicular/parallel directions are available as in Reference [B-14], the volumetric change is obtained as

$$\frac{\mathrm{V}_0 + \Delta V}{V_0} = \left(\frac{L_0 + \Delta L}{L_0}\right)^{\perp 2} \times \left(\frac{L_0 + \Delta L}{L_0}\right)^{\parallel} \Rightarrow \frac{\Delta V}{V_0} = \left(1 + \frac{\Delta L}{L_0}\right)^{\perp 2} \times \left(1 + \frac{\Delta L}{L_0}\right)^{\parallel} - 1$$

[5] The fast fluence in the units of $10^{20}$ n/cm$^2$ EDN is most commonly encountered in the literature relevant to the present discussion. The conversion from the fast fluence is performed using the following formula:

$$\gamma[10^{20}\ \mathrm{n/cm^2\ \ EDN}] = 0.557 \times 10^{-20} \times \Gamma[\mathrm{n/cm^2}, [[\qquad\qquad]]^{\mathrm{P}}$$

$$L_{sat}(T_{irr}) = 0.4025\ln(T_{irr}) - 2.188.$$

This results in the following expression applicable in this fast fluence range:

$$\frac{\lambda(T_{irr})}{\lambda_0(T_{irr})} = 1 + \frac{L_{sat}(T_{irr}) - 1}{\ln(\gamma_{sat}) - \ln(\gamma_0)} \cdot [\ln(\gamma) - \ln(\gamma_0)].$$

$$\gamma_{sat} < \gamma \leq \gamma_{sb}:$$

$$\frac{\lambda(T_{irr})}{\lambda_0(T_{irr})} = L_{sat}(T_{irr}).$$

$$\gamma_{sb} < \gamma:$$

After the secondary breakdown, the inverse of the irradiation-induced thermal conductivity change is given by an equation on p. 56 of Reference [B-13], used in the THM model as follows:

$$\frac{\lambda_0(T_{irr})}{\lambda(T_{irr})} = \frac{1}{L_{sat}(T_{irr})} + A \cdot V_R(\gamma, T_{irr}) \cdot (\gamma - \gamma_{sb}),$$

where $A = -0.015$ is an empirically determined parameter obtained by converting the parameter $A$ from Reference [B-13] into the units of $\gamma$ ($10^{20}$ n/cm$^2$ EDN), and $V_R$ is computed as

$$V_R(\gamma, T_{irr}) = \left[\frac{\frac{\Delta V(\gamma)}{V_0}}{\min_{\gamma} \frac{\Delta V(\gamma)}{V_0}}\right]_{T_{irr}} - 1,$$

or, using the Equation for $\gamma_{sb}(T_{irr})$ from Section B.2.2.4.1.4, as

$$V_R(\gamma, T_{irr}) = \left[\frac{\frac{\Delta V(\gamma)}{V_0}}{\frac{\Delta V(\gamma_{sb})}{V_0}}\right]_{T_{irr}} - 1.$$

The relative volume change due to fast neutron irradiation is obtained by combining the two relative dimensional changes presented for different temperatures in figures B-3 and B-4 of Reference [B-14], respectively, into relative volume changes (as described in footnote [4]), performing a quadratic fit with respect to the fluence, and a piecewise-linear interpolation of the resulting curves to obtain the temperature dependence.

### B.2.2.5 Heat Sources

The heat sources in the THM model are generated from nuclear reactions and grouped into local and non-local sources. Local heat sources are those where the energy released is absorbed in the direct vicinity of the reaction. A small percentage of energy, notably from interactions of neutrons and gamma rays with structural materials, can dissipate at a considerable distance from their birth position. These

interactions can heat up reflectors and other reactor components and referred to as non-local heat sources.

The primary heat source in a nuclear reactor is the fission of fissile material where the energy is released in the form of kinetic energy of the fission fragments. A significant portion of energy is also carried by the neutrons and gammas. Furthermore, the decay of radioactive fission products contributes approximately [[ ]]$^{P}$ of the total core energy. Depending on the half-life of the fission products, the decay heat after shutdown is released over a long period.

The heat sources in the THM model are grouped into the following three categories:

- Direct fission reactions
- Gamma heating of structural material
- Decay heat

### B.2.2.5.1 Direct Fission Energy Equations

The equations used to determine the heat source from direct fission are presented in Table B-8 below.

***Table B-8: Heat Source from Direct Fission***

| Description | Equation | Number |
|---|---|---|
| General equation for fission rate [fissions/s] | $\dot{f} = \frac{\dot{Q}}{f_e}$ | B-2.2.5-1 |
| Energy released per fission reaction [J] | $f_e = \sum_{i=1}^{n} F_i \cdot f_i$ | B-2.2.5-2 |
| Fission rate per fuel pebble in core node (r, n) as used in the THM [fission/pebble-s] | $\dot{f}_{r,n} = \frac{P_{r,n} \times 0.01 \times P_{core}^{MW} \times 10^6 \times F_r^V \cdot F_{r,n}^V}{f_e N_{r,n}^s}$ | B-2.2.5-3 |
| Heat source density per fuel pebble in core position (r, n) [W/m$^3$] | $\dot{q}_{r,n}^s = \frac{\dot{f}_{r,n} \times f_e}{V_A^s}$ | B-2.2.5-4 |
| Heat source density per particle in core region (r, n) [W/m$^3$] | $\dot{q}_{r,n}^p = \frac{\dot{q}_{r,n}^s V_A^s}{V_k^p N_s^p}$ | B-2.2.5-5 |

### B.2.2.5.2 Gamma Heating Correlations

Non-local heat sources (heat generated outside the fuel) such as gamma heating of structural materials are modelled in accordance with the correlations listed in Table B-9. Gamma energy spectra and transport cross-sections through matrix and structural graphite are required as gamma radiation is a source of significant non-local heat source modelled by the THM [B-7].

Derivation of Equation B.2.2.5-12 is provided following Table B-9.

***Table B-9: Gamma Heating Correlations***

| Description | Equation | Reference | Number |
|---|---|---|---|
| Number of gamma rays (γ) in group *g* in energy range<br>0.085 ≤ E < 0.3 [MeV] | [[ ]]P | [[ ]]P | B.2.2.5-6 |
| Number of γ's in group *g* in energy range<br>0.3 ≤ E < 1.0 [MeV] | [[ ]]P | [[ ]]P | B.2.2.5-7 |
| Number of γ's in group *g* in energy range<br>1.0 ≤ E ≤ 8.0 [MeV] | [[ ]]P | [[ ]]P | B.2.2.5-8 |
| Total number of γ's (36) in energy range 0.085 ≤ 8.0 [MeV] | [[ ]]P | [[ ]]P | B.2.2.5-9 |
| Fraction of number of γ's in group g | [[ ]]P | | B.2.2.5-10 |
| Average γ energy in group g [MeV] | [[ ]]P | | B.2.2.5-11 |
| Fraction of γ's produced in $(r_s,z_s)$ that is absorbed in structure at $(r_t,z_t)$<br>s = source<br>t = target | [[ ]]P | | B.2.2.5-12 |
| Angular fraction | [[ ]]P | | B.2.2.5-13 |
| γ-heat source in node (r,n) [MW] | [[ ]]P | | B.2.2.5-14 |

Equation B.2.2.5-12 was derived as follows:

[[

]]$^{P}$

### B.2.2.5.3 Decay Heat Equations

The THM Xe-100 reactor decay heat model is based on the [[ ]]$^{P}$. Decay heat sources are grouped into three contributors:

- Heat from fission product decay (from fission of [[ ]]$^{P}$)
- Heat from decay of actinides [[ ]]$^{P}$
- Neutron capture by [[ ]]$^{P}$

The equations used to determine decay heat in the THM are presented in Table B-10.

***Table B-10: Decay Heat Equations***

| Description | Equation | Reference | Number |
|---|---|---|---|
| Fractional node power | [[ ]]$^{P}$ | | B.2.2.5-15 |
| Production rate of actinide [[ ]]$^{P}$ in node (r, n) [#/s] | $P_{r,n}^{239} = \varphi_e F_{cap}^{res} N_A N_{r,n}^{s} H^{s} \times 1000\left(\frac{1 - \square^{235} \times 0.01}{238}\right) \cdot \frac{\sigma_a^{238}}{\sigma_c^{238}}$ | | B.2.2.5-16 |
| Transient decay time + time to reach node (r, n) for pass p [s] | $t_0 = t_{tr} + t_{r,n,p}$ | | B.2.2.5-17 |
| Total at power time for channel r for at start of pass p [s] | $t_0^r = t_{r,0,p}$ | | B.2.2.5-18 |
| Decay time elapsed + time to reach node (r, n) for current pass p [s] | $t_1 = t_{tr} + \left(t_{r,n,p} - t_{r,d,p}\right)$ | | B.2.2.5-19 |

| Description | Equation | Reference | Number |
|---|---|---|---|
| Difference between accumulated residence time of a pebble in nodes n and n–- 1 in fuel channel r for pass p [s] | $t_1^r = t_{r,n,p} - t_{r,n-1,p}$ | | B.2.2.5-20 |
| [[ ]]$^P$ | [[ ]]$^P$ | [[ ]]$^P$ | B.2.2.5-21 |
| [[ ]]$^P$ | [[ ]]$^P$ | [[ ]]$^P$ | B.2.2.5-22 |
| [[ ]]$^P$ | [[ ]]$^P$ | [[ ]]$^P$ | B.2.2.5-23 |
| [[ ]]$^P$ | [[ ]]$^P$ | [[ ]]$^P$ | B.2.2.5-24 |
| [[ ]]$^P$ | [[ ]]$^P$ | [[ ]]$^P$ | B.2.2.5-25 |
| [[ ]]$^P$ | [[ ]]$^P$ | [[ ]]$^P$ | B.2.2.5-26 |
| [[ ]]$^P$ | [[ ]]$^P$ | [[ ]]$^P$ | B.2.2.5-27 |
| [[ ]]$^P$ | [[ ]]$^P$ | [[ ]]$^P$ | B.2.2.5-28 |
| [[ ]]$^P$ | [[ ]]$^P$ | [[ ]]$^P$ | B.2.2.5-29 |
| [[ ]]$^P$ | [[ ]]$^P$ | [[ ]]$^P$ | B.2.2.5-30 |
| [[ ]]$^P$ | [[ ]]$^P$ | [[ ]]$^P$ | B.2.2.5-31 |
| [[ ]]$^P$ | [[ ]]$^P$ | [[ ]]$^P$ | B.2.2.5-32 |

| Description | Equation | Reference | Number |
|---|---|---|---|
| [[ ]]P | [[ ]]P | [[ ]]P | B.2.2.5-33 |
| [[ ]]P | [[ ]]P | [[ ]]P | B.2.2.5-34 |
| [[ ]]P | [[ ]]P | [[ ]]P | B.2.2.5-35 |

### B.2.2.6 Core Residence Times

In the Xe-100 reactor, fuel moves downwards through the core and, in case of the multi-pass system, fuel pebbles that have not yet reached a predetermined burnup value will be reloaded at the top of the core to complete another pass. This process is repeated until the pebble predetermined discharge burnup level is reached. The radial location where the fuel pebble ends after being loaded impacts the time spent to complete the pass. Generally, fuel pebbles loaded radially towards the center move faster than those closer to the side reflectors. These velocity differences between pebbles translate to different residence times for different fuel flow channels.

[[

]]P

Parameters required to calculate the residence times are:

- Heavy metal loading per pebble in tonne (metric ton)
- Pebble power in MW
- Burnup acquired in the current node

The residence times are calculated in VSOP using the equations in Table B-11.

***Table B-11: Core Residence Time Equations***

| Description | Equation | Number |
|---|---|---|
| Fuel residence time in reactor node (r, n) in a multi-pass fueling scheme [days] | $t_{r,n} = \frac{HM_{r,n}}{\dot{Q}_{r,n}}\left(B_{r,n} - B_{r,n-1}\right)$ | B-2.2.6-1 |
| Fuel residence time in reactor flow channel r [days] | $t_r = \sum_{n=1}^{N_r} t_{r,n}$ | B-2.2.6-2 |
| Accumulated residence time over p passes [days] | $t_p = \sum_{p=1}^{P}\sum_{n=1}^{N_{r_p}} t_{r_p,n}$<br>$r_p$ = *flow channel in pass p* | B-2.2.6-3 |
| Average core residence time [days] | $\bar{t}_{core} = \sum_{r=1}^{FC} F_r t_r$<br>$F_r$ = *flow channel volume fraction* | B-2.2.6-4 |

[[

]]$^{P}$

### B.2.2.7 VSOP Mapping

[[

]]$^{P}$

These parameters are used in downstream calculation models (see Appendix H) and as initial conditions for transients modelled by the KSIM model (see Section 5.1.9). [[

]]$^{P}$

[6] [[

]]$^{P}$

### B.2.2.8 Fuel Burnup

[[

]]$^{P}$

### B.2.2.9 4-Group Neutron Flux

[[

]]$^{P}$

### B.2.2.10 Fast Fluence

[[

]]P

### B.2.2.11 Particle Temperature

The TRISO fuel particle performance and radionuclide transport and release from fuel elements are influenced by the fuel temperature. The THM calculates fuel temperatures using two methods depending on the application. Under reactor steady state conditions, the particle temperatures can be determined by means of a steady state analytical solution for heat transfer in a spherical geometry with an internal power source, where the matrix temperatures are used as a given boundary condition. Due to high heat dissipation through the particle zones, large number of inner iterations would be needed to calculate particle temperature dynamics in transient conditions. Therefore, in transient simulations, a quasi-steady-state approach is adopted whereby time-dependent pebble temperature is used to update boundary conditions for steady-state particle temperature calculation in each time step.

The particle temperature distribution is dependent on particle power density. Heat is mostly generated in the kernel from fission. The kernel temperature is higher than the surrounding particle layer temperatures and heat flows towards the outside surface of the particle where thermal energy is transferred to the matrix material. The matrix material temperature serves as a boundary condition determined by the helium coolant temperature.

[[

]]$^{P}$

***Table B-16: Steady State Particle Temperature Equations***

| Description | Equation | Number |
|---|---|---|
| Heat source in kernel zone kz [W] | [[ ]]$^{P}$ | B.2.2.11-3 |
| $\Delta T_{kz}$ over the kernel zone kz [K] | [[ ]]$^{P}$ | B.2.2.11-4 |
| $\Delta T_{k}$ over the kernel [K] | [[ ]]$^{P}$ | B.2.2.11-5 |
| $\Delta T_{pz}$ over the particle layer zone pz [K] | [[ ]]$^{P}$ | B.2.2.11-6 |
| Particle temperature distribution [K] | [[ where, ]]$^{P}$ | B.2.2.11-7 |

### B.2.2.12 Fuel Element Temperature

The THM models two fuel element geometries. A spherical (pebble) geometry is available for both full core and experiment calculations while compact (cylindrical) geometry is used in experiment simulations. The temperature distribution calculation principles are similar to those of particles described in Section B.2.2.11. The steady state fuel pebble temperature equations are presented in Table B-18. Power transient temperature calculations are performed for fuel pebbles only and described in Section B.2.2.13.

As described in Section B.2.2.5, heat generated in the fuel particles is transferred by conduction to the surrounding matrix material. The fuel pebble geometry consists of a number of [[ ]]$^{P}$ concentric shells in the active fuel zone and similarly in the fuel free zone (shell). An [[ ]]$^{P}$ power distribution is assumed [[ ]]$^{P}$ in each shell of the active zone. The fuel free zone also has a [[ ]]$^{P}$ power distribution from heavy metal contamination of the matrix material.

***Table B-18: Steady State Fuel Pebble Temperature Equations***

| Description | Equation | Number |
|---|---|---|
| Heat source in active fuel zone fz assuming [[ ]]$^{P}$ power distribution over the pebble [W] | [[ ]]$^{P}$ | B.2.2.12-1 |
| $\Delta T_{fz}$ over the active fuel pebble zone fz [K] | [[ ]]$^{P}$ | B.2.2.12-2 |
| $\Delta T_{\text{pebble}}^{active}$ over the active fuel pebble [K] | [[ ]]$^{P}$ | B.2.2.12-3 |
| $\Delta T_{sz}$ over the fuel free zone zone sz [K] | [[ ]]$^{P}$ | B.2.2.12-4 |
| $\Delta T_{gap}$ over the fuel surface and bulk helium temperatures [K] | [[ ]]$^{P}$ | B.2.2.12-5 |
| Fuel temperature in shell zone sz [K] | [[ ]]$^{P}$ | B.2.2.12-6 |
| Fuel surface temperature [K] | [[ ]]$^{P}$ | B.2.2.12-7 |
| Volume weighted average fuel temperature [K] | [[ ]]$^{P}$ | B.2.2.12-8 |
| Fuel center zone temperature [K] | [[ ]]$^{P}$ | B.2.2.12-9 |

The fuel compact geometry consists of a number of concentric cylindrical shells of equal thickness and height in the active (fuel containing) zone and a number of concentric cylindrical shells with varying thicknesses and equal height in the fuel free zones (capsule structures). As in the pebble case, it is assumed that the power density in each shell of the active zone is equal, thus a uniform power distribution is assumed for the active zone.

[[

]]$^{P}$

In the radial dimension, the time dependent heat conduction in 1-D cylindrical geometry can be expressed as:

[[ ]]$^{P}$ B.2.2.12-10

In the case of experiments, steady state irradiation conditions normally prevail, and this equation reduces to:

[[ ]]P B.2.2.12-11

The discretized tridiagonal matrix coefficients representing the steady state radial heat transport equations in compacts are given in Table B-19.

***Table B-19: Steady State Fuel Compact Temperature Equations in Radial Dimension***

| Description | Equation | Number |
|---|---|---|
| Heat source in active fuel zone (r,fz) assuming [[ ]]P power distribution over the compact [W] | [[ ]]P | B.2.2.12-12 |
| Effective heat conduction coefficient between two adjacent volumes [W/m.K] | [[ ]]P | B.2.2.12-13 |
| Gauss matrix coefficients for 1-D cylindrical radial heat conduction to and from volume I [W/m.K] | [[ ]]P | B.2.2.12-14 |

For fuel pebble transients, the time dependent pebble temperature is calculated using an iterative time-stepping solver (see Section B.3.1). The equations for calculating transient fuel pebble temperatures using the Backward Implicit-Explicit Iterative method are presented in Table B-20.

***Table B-20: Transient Fuel Pebble Temperature Equations***

| Description | Equation | Number |
|---|---|---|
| Backward Implicit-Explicit Iterative solver for T [K] | [[ ]]P | B.2.2.12.-15 |
| Effective heat transfer coefficients between neighboring particle zones [W/m.K] | [[ ]]P | B.2.2.12-16 |
| Heat flow density from inner neighbor zone [W/m$^3$] | [[ ]]P | B.2.2.12-17 |
| Heat flow density to outer neighbor zone [W/m$^3$] | [[ ]]P | B.2.2.12-18 |

| Description | Equation | Number |
|---|---|---|
| Temperature change due to heat inflow from inner neighbor over time step $\Delta t$ [K] | [[ if then else ]]$^{P}$ | B.2.2.12.-19 |
| Temperature change due to heat outflow to outer neighbor over time step $\Delta t$ [K] | [[ if then else ]]$^{P}$ | B.2.2.12-20 |

### B.2.2.13 Reactor Component Temperature

The reactor geometry is represented by a 2-D cylindrical configuration with [[ ]]$^{P}$ radial zonesI) and [[ ]]$^{P}$ axial nodes (n) in each radial zone as described in Section B.2.1.1. Temperatures are calculated for steady state operation, power transients and loss of coolant accidents where the power transient is determined from decay heat. For convection cooling, if gas temperatures are known, they may be used as boundary conditions for determining the solid component temperatures.

The bulk of the heat source in the reactor is situated in the core; analytical provisions are made for non-local heat sources from ϒ- and n-heating. From the VSOP core power distribution, the power densities in all the reactor nodes can be calculated using the pebble's power, pebble's volume packing factors, node volumes, etc. Relevant material properties for all components and reactor nodes are provided by the KSIM model. Generally, these properties are temperature dependent, and the corresponding correlations and equations are provided in Section B.2.2.4.

Steady state calculations can be performed using either analytical solutions or time-dependent numerical solvers where the power does not change with time. The latter requires longer execution time.

### B.2.2.14 Coolant Temperature

The THM has several options available for determining the helium temperature used in the reactor temperature calculations. The model provides an option to use the helium temperature and mass flow rates imported from the VSOP output or the helium temperatures may be calculated by the THM using either the VSOP mass flow rates or those determined by the THM along with node power from the KSIM model.

[[

]]$^{P}$

During normal operation, the convective heat removal mechanism dominates the total heat removed from the core. The heat removal rate depends on the temperature difference between the fuel surface and the bulk helium temperature, the convective heat transfer surface area and, and the heat transfer coefficient, and is expressed in terms of Newton's Law as addressed in Section B.2.2.3.

## B.3 Overall Solution Technique

The overall calculation flow following the THM methodology is shown in Figure B-12. Calculations are performed over a specified period of time. In each time step, the reactor component and helium temperatures are converged by means of a selected iterative time-stepping method (see the subsections below).

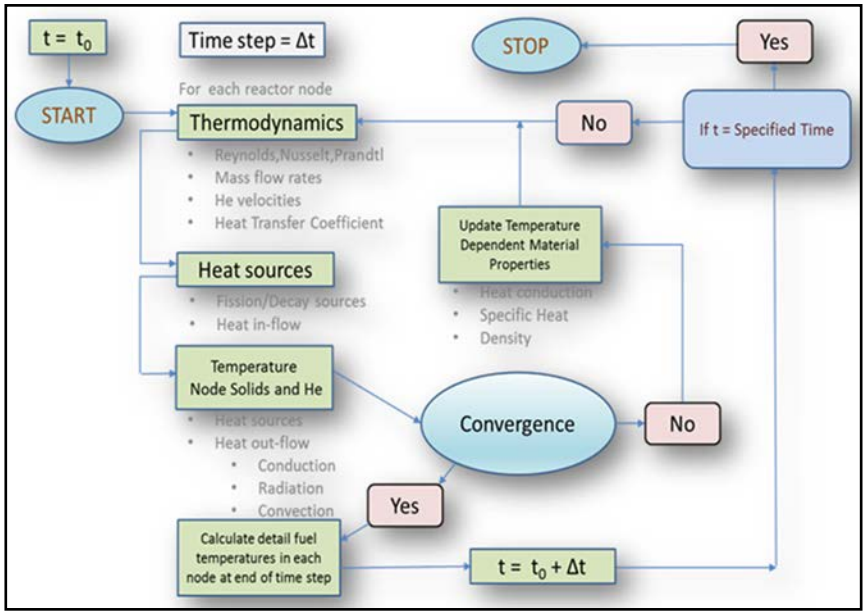


***Figure B-12: Calculation Flow***

Either the Backward Implicit-Explicit method (Euler) or the 2$^{nd}$-order Backward Differentiation Formula (BDF2) can be used to calculate the helium temperatures distributions in the reactor components. The computational process depicted in Figure B-13 is employed in an iterative loop to calculate the convective heat transfer to the coolant and converged reactor component temperatures.

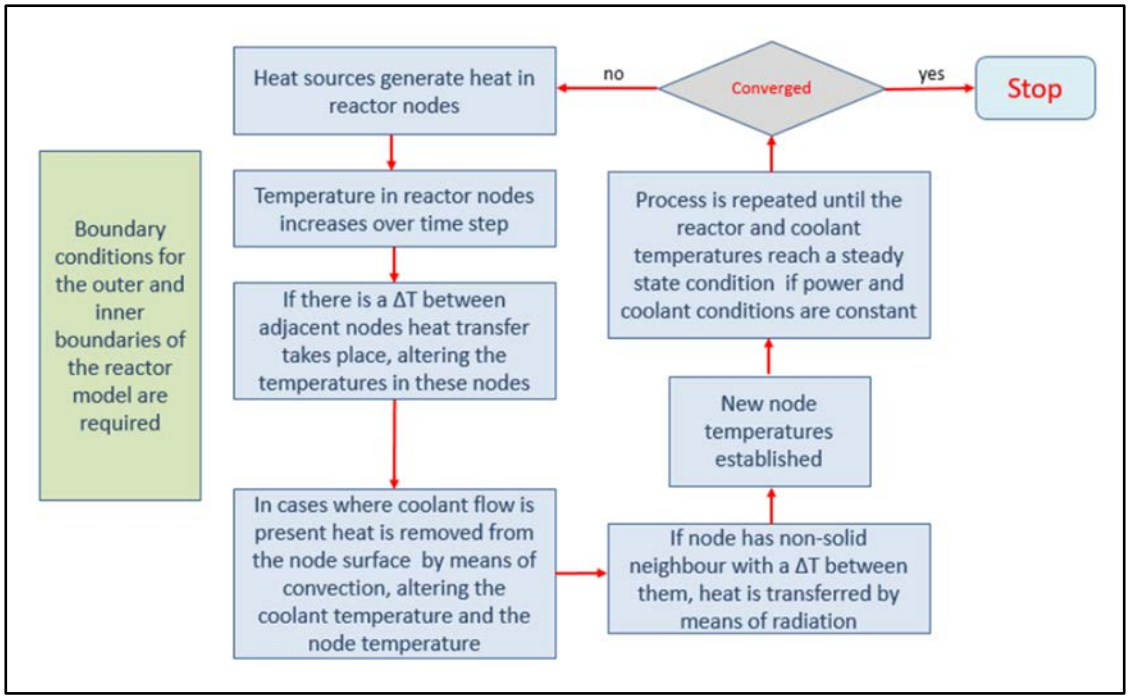


***Figure B-13: Reactor Temperature Calculation Process***

### B.3.1 Backward Explicit-Implicit Iterative Method

The THM calculates the node temperatures by means of a backward implicit-explicit method expressed in the following equation:

[[

]]$^{P}$

### B.3.2 Backward Differentiation Formula Method

The second order Backward Differentiation Formula (BDF2) method [B-9] can be applied to numerically solve ordinary differential equations using the following expression:

[[

]]$^{P}$

### B.3.3 Fuel Compact Steady State Temperature Solver

[[

]]$^{P}$

For each mesh-zone, there is an equation (as above) which represents the coupling of neighboring zones together with their internal sources and removal terms. These can be expressed in a tri-diagonal matrix and solved by Gauss elimination to determine the temperature in each zone.

This methodology represents a numerical solution of a heat transport equation in the radial direction of cylindrical geometry, which is the dominating heat flow direction. Upon adding the axial heat flow matrix coefficients, a 5-element diagonal matrix is obtained, which is more efficiently solved by an iterative method like SOR [B-9].

## B.4 Cross References and References

| Document Title<br>Cross References: X-energy documents that may impact the content of this document.<br>References: X-energy or other documents that will not impact the content of this document | | Document No. | Rev./ Date of Issuance | Cross Reference/ Reference |
|---|---|---|---|---|
| **B-1** | Reactor core design of High Temperature Gas-Cooled Reactors | KTA standards 3102.1, 3102.2, 3102.3 | 1978, 1983, 1981 | Reference |
| **B-2** | V.S.O.P. (99/05) Computer Code System | Jul-4189 | 10-2005 | Reference |
| **B-3** | Feasibility of a Radially Cooled Thorium Breeder Pebble Bed Type High Temperature Reactor | | 6-2014 | Reference |
| **B-4** | Nuclear Reactor Analysis | | 1976 | Reference |
| **B-5** | Heat-and-flow-characteristics-of-packed-beds | Vol. 10, Issue 1 | 1995 | Reference |
| **B-6** | Heat Transport and Afterheat Removal for Gas Cooled Reactors under Accident Conditions | IAEA-TECDOC-1163 | 2000 | Reference |
| **B-7** | Simulation of Neutron and Gamma Ray Emission from Fission and Photofission | UCRL-AR-228518 | 1-17-2014 | Reference |
| **B-8** | Berechnung der Nachzerfallsleistung der Kernbrennstoffe von Hochtemperaturreaktoren mit kugelförmigen Brennelementen | | 5-1990 | Reference |
| **B-9** | A First Course in the Numerical Analysis of Differential Equations | ISBN 978-0-521-55655-2 | 1996 | Reference |
| **B-10** | "Reverse Engineering of GETTER a Fission Product Release Code for PBMR," J B Keshaw | | November, 2007 | Reference |
| **B-11** | *G. Haag: Thermal Conductivity of Graphite Irradiated with Medium and High Neutron Fluences* | N/A | May 2003 | Reference |
| **B-12** | *R. J. Price: Review of the Thermal Conductivity of Nuclear Graphite under HTGR Conditions* | Gulf-GA-A12615 | Sep 7, 1973 | Reference |
| **B-13** | *G. Haag: Properties of ATR-2E Graphite and Property Changes due to Fast Neutron Irradiation* | Juel-4183 | Oct 2005 | Reference |
| **B-14** | *NGNP High Temperature Materials White Paper* | INL/EXT-09-17187, Rev 1 | Aug 2012 | Reference |
| **B-15** | Reactor System Design Description | 000002 | 5/April, 2022 | Reference |
| **B-16** | M.C.R. Heijna, S. de Groot, J.A. Vreeling, Comparison of irradiation behaviour of HTR graphite grades, Journal of Nuclear Materials | | May, 2017 | Reference |

# Appendix C. Solids Fission Transport Model

## Abbreviations/Acronyms

| Short Form | Phrase |
|---|---|
| 1D | One-Dimensional |
| 2D | Two-Dimensional |
| AGR | Advanced Gas Reactor |
| FIMA | Fissions per Initial Metal Atom |
| FPM | Particle Failure Probability Model |
| GASM | Gaseous Fission Product Transport Model |
| HPB | Helium Pressure Boundary |
| HPBM | Helium Pressure Boundary Model |
| HTGR | High Temperature Gas Reactor |
| IAEA | International Atomic Energy Agency |
| IPyC | Inner Pyrolytic Carbon |
| OPyC | Outer Pyrolytic Carbon |
| PFM | Particle Failure Probability Model |
| R/B | Release Over Birth Ratio |
| RCCS | Reactor Cavity Core Cooling System |
| RPV | Reactor Pressure Vessel |
| RN | Radionuclide |
| SiC | Silicon Carbide |
| SOLM | Solids Fission Transport Model |
| THM | Thermodynamics Calculation Model |
| TRIsO | TRi-ISOtropic coated-fuel particle design with three materials in coating system (low-density PyC, high-density PyC, and SiC) |
| UCO | Uranium oxycarbide, a heterogeneous mixture of $UO_2$ and $UC_2$ |
| $UO_2$ | Uranium Dioxide |
| VSOP | Very Superior Old Program Neutronics Code |
| Xe-100 | X-energy 200 $MW_{th}$ Pebble Bed Reactor |

**Definitions**

| Symbol | Definition |
|---|---|
| $A_{cz}^{i,r}$ | external radial mass transfer surface of compact zone ($i$, $z$) or leakage surface of a fuel compact (m$^2$) |
| $A_{cz}^{i,z}$ | external axial mass transfer surface of compact zone ($i$, $z$) (m$^2$) |
| $A_F, B_F, D_F, E_F$ | coefficients for the non-linear range of sorption isotherm (Freundlich) |
| $A_{fz}^{i}$ | external mass transfer surface area of fuel sphere zone $i$ or leakage surface area of a fuel sphere (m$^2$) |
| $A_H, B_H$ | coefficients for the linear range of sorption isotherm (Henry) |
| $A_{pz}^{i}$ | external mass transfer surface area of particle zone $i$ (m$^2$) |
| $A_s(r)$ | surface area (m$^2$) |
| $a_{z,z-1}, a_{z,z}, a_{z,z+1}$ | spherical Gauss matrix coefficients (m$^3$/s) |
| $BU$ | sphere burnup (MWd/TU) |
| $C$ | isotope concentration (#/m$^3$) |
| $C_{bc}$ | isotope concentration at the graphite surface layer (#/m$^3$) |
| $C_{bl}$ | isotope concentration in the helium boundary layer (#/m$^3$) |
| $C_{gr}$ | concentration of sorbate species (mmol/kg C) as in equation C-35 |
| $C_j$ | concentration of isotope $j$ (#/m$^3$) |
| $C_s$ | concentration at the surface of pebble or compact (#/m$^3$) |
| $C_{ts}$ | thin-shell isotope density (#/m$^3$) |
| $\Delta C_{ts}$ | isotope density gradient at the surface (#/m$^3$) |
| $\overline{C}_{ts}$ | average isotope density in the thin shell (#/m$^3$) |
| $C_z$ | isotope concentration in zone $z$ (#/m$^3$) |
| $D_1, D_2$ | pre-exponential factor (m$^2$/s |
| $D$ | diffusion coefficient (m$^2$/s) |
| $D_{eff}$ | effective diffusion coefficient in a zone (m$^2$/s) |
| $D_{eff}^{z,z+1}$ | effective diffusion coefficient between adjacent zones (m$^2$/s) |
| $D_{gb}$ | isotopic diffusion coefficient in the gas boundary layer (m$^2$/s) |
| $D_z, D_{z+1}$ | diffusion coefficient (m$^2$/s) for zones $z$ and $z+1$, respectively |
| $D(r)$ | diffusion coefficient (m$^2$/s) at position $r$ |
| $d_h$ | characteristic dimension (diameter of pebble or compact) (m) |
| $F_i$ | power fraction produced by fissile isotope $i$ |
| $F_{fp}$ | failed particle fraction in the sphere |
| $F_{ts}$ | thin-shell factor to extent inwards from the fuel element surface (set to 0.99) |
| $f_e$ | number of spheres in core zone (r,n) |

| Symbol | Definition |
|---|---|
| $\dot{f}_k$ | fission rate in the fuel kernel (fissions/s) |
| $\dot{f}_m$ | fission rate in the active fuel pebble matrix (fissions/s) |
| $\dot{f}_{shell}$ | fission rate in the fuel sphere shell matrix (fissions/s) |
| $\dot{f}_Z$ | fission rate in zone Z (where Z can be in the kernel, matrix or shell) (fissions/s) |
| $HM$ | heavy metal mass (tHM) |
| $h_z$ | axial length of the axial compact zone $z$ or axial reactor zone $z$ (m) |
| $J_1, J_2$ | current from volumes 1 and 2, respectively (#/s) |
| $J_{net}$ | net current into a volume with two adjacent volumes (#/s) |
| $J(r)$ | current between two adjacent volumes (#/s) |
| $J_s$ | leakage current (#/s) |
| $M$ | molecular weight (g/mol) |
| $N_{fz}^{p}$ | is the number of fuel particles in fuel zone *fz* |
| $Nu$ | Nusselt number |
| $P$ | pressure (MPa) |
| $P_c$ | pressure (atm) |
| $P_{\delta(t)}$ | local power for fuel pass p in core zone (fc, n) (MW) |
| $Pr$ | Prandtl Number |
| $Q_1, Q_2$ | activation energy (J/mol) |
| $\dot{Q}_{s,p}^{r,n}$ | is the fission rate in core zone (r,n) (fissions/s) |
| $R$ | gas constant (8.3143 J/mol·K) |
| $Re$ | Reynolds number |
| $R_j^A$ | average removal rate over $\Delta t$ of isotope $j$ by neutron absorption (#/s) |
| $R_j^D$ | average removal rate over $\Delta t$ of isotope $j$ by decay (#/s) |
| $r$ | radial position (m) |
| $r_e^i$ | effective (center of mass) radius of particle zone $i$ or fuel sphere zone $i$ or radial compact zone $i$ (m) |
| $r_e^{i'}$ | inter-zone radial diffusion distance of particle zone $i$ or fuel sphere zone $i$ or radial compact zone $i$ (m) |
| $i$ | inner radius of particle zone $i$ or fuel sphere zone $i$ or radial compact zone $i$ or radial reactor zone $i$ (m) |
| $r_{i+1}$ | outer radius of particle zone $i$ or fuel sphere zone $i$ or radial compact zone $i$ or radial reactor zone $i$ (m) |
| $r_{fa}$ | outer radius of active fuel zone (m) |
| $r_{fe}$ | outer radius of the fuel element, pebble (m) |
| $r_n$ | outer radius of a TRISO particle or pebble (m) |
| $r_{ts}$ | thin-shell fuel element radius (m) |

| Symbol | Definition |
|---|---|
| $r_z$ | radius of zone $z$ |
| $r^e_{z-1}, r^e_z, r^e_{z+1}$ | effective radius (m) of zones $z-1$, $z$, and $z+1$, respectively |
| $Sc$ | Schmidt Number |
| $Sh$ | Sherwood Number |
| $S(r)$ | source rate at point *r* (#/s) |
| $S^A_{i,j}$ | average activation source over $\Delta t$ for isotope $i$ from the neutron absorption of the parent isotope $j$ (#/s) |
| $S^D_{i,j}$ | average decay source over $\Delta t$ for isotope $i$ from the decay of isotope $j$ (#/s) |
| $S^F_{i,j}$ | fission source of isotope $j$ in $Z$ (kernel, matrix or shell) (#/s) |
| $S_z$ | sum of sources and removals in zone $z$ (#/s) |
| $s_z$ and $s_{z-1}$ | outer and inner surface areas of zone z ($m^2$) |
| $T$ | temperature (K) |
| $T_c$ | He temperature (K) |
| $T_{fc}$ | time required for the sphere to complete a full movement through all axial nodes in core channel *fc* (d) |
| $T_{fc,n}$ | time required for the sphere to complete movements from axial node 1 to axial node *n* in core channel *fc* (d) |
| $t$ | time (s) |
| $\Delta r$ | diffusion distance (m) |
| $\Delta t$ | time increment or irradiation time (s) |
| $\Delta t_k$ | irradiation time increment (d) |
| $\Delta t_i$ | time a sphere stays in a core node *n* in a core channel *fc* (d) |
| $U_c$ | is the heavy metal contamination fraction in the sphere |
| $V^s_A$ | is the volume of the active fuel region (sphere volume – shell volume) ($m^3$) |
| $V_{buf}$ | buffer volume ($m^3$) |
| $V^{i,z}_{cz}$ | volume of compact zone ($i$, $z$) ($m^3$) |
| $V_{fz}$ | volume of the fuel sphere zone $i$ ($m^3$) |
| $V_{ker}$ | kernel volume ($m^3$) |
| $V_p$ | particle volume ($m^3$) |
| $V_{pz}$ | volume of the kernel zone ($m^3$) |
| $V^i_{pz}$ | volume of the particle zone $i$ ($m^3$) |
| $V_s$ | total volume of the sphere ($m^3$) |
| $V^a_s$ | volume of the active (containing TRISO particles) sphere region ($m^3$) |
| $V^{shell}_s$ | volume of the fuel-free shell region ($m^3$) |

| Symbol | Definition |
|---|---|
| $V_{ts}$ | thin-shell volume ($m^3$) |
| $V_z$ | volume of zone $z$ ($m^3$) |
| $z_e^{i'}$ | inter-zone axial diffusion distance of axial compact zone $z$ (m) |
| $\alpha_F$ | Freundlich sorption coefficient |
| $\alpha_H$ | Henry sorption coefficient |
| $\alpha_R$ | sorption coefficient |
| $\beta$ | mass transfer coefficient ($m^3/s$) |
| $\beta_{i,j}$ | branching ratio of isotope *i* from transmutation of isotope *j* |
| $\Gamma$ | fast fluence ($\#/m^2$) |
| $\gamma_{i,j}$ | independent fission yield of fission product *j* from fissile isotope *i* |
| $\gamma_k$ | index of core zone (fc, n) where the pebble is located during irradiation interval $\Delta t_k$ |
| $\delta_k$ | index of core zone (fc, n) and pass of a pebble during irradiation interval $\Delta t_k$ |
| $\varepsilon$ | packing factor (i.e., void fraction or porosity of the pebble bed) |
| $\lambda_i, \lambda_j$ | decay constant of isotope $i$ $or$ $j$ ($s^{-1}$) |
| $\mu_g$ | dynamic viscosity of He (kg/m·s) |
| $\rho_{buf}$ | a density factor of the buffer relative to the theoretical density of graphite (0.5) |
| $\rho_g$ | density of He ($kg/m^3$) |
| $\sigma_a^i$ | 1-group neutron absorption cross-section of isotope $i$ ($m^2$) |
| $\phi_0$ | 1-group neutron flux ($n/m^2$ s) |

## C.1. Introduction

As discussed in Section 3.2, the functional containment system is a collection of five radionuclide (RN) release barriers, designed to limit RN release from the core to the environment to very low levels during normal operation and a broad spectrum of postulated accidents, References 1 and 2. These barriers, together with the main phenomena and processes involved in radionuclide production, retention, transport, and release for a pebble bed reactor are depicted in Figure 3 of this Topical Report. The Solids Fission Transport Model (SOLM) calculates the production, decay, transmutation, transport, and leakage of gaseous and solid fission products from fuel pebbles into the helium pressure boundary under normal steady-state and accident conditions via the first three barriers.

## C.2. Theory and Methodology

The Solids Fission Transport Model (SOLM) is a radionuclide diffusion model used for calculating the production, decay, transmutation, transport, and leakage of gaseous and solid fission products from fuel pebbles into the helium pressure boundary under steady-state and accident conditions. The model is normally used for pebble calculations for various fuel paths through the core and coupled with the Thermodynamics Calculation Model (THM) to update the temperature distribution in the pebbles. The Particle Failure Probability Model (FPM) provides the TRISO-coated particle failure probabilities. In an integrated calculation, the SOLM is coupled with the THM, FPM, and the HPBM models.

The fission product release from the pebbles is calculated for a 2D core configuration, containing the fission product history at each point in the core. A fission product distribution library is generated for all particle and pebble radial zones in all core regions, accounting for fuel movement in a multi-pass fueling regime.

The SOLM model performs the following functions:

models the fuel elements and particles in a fine mesh [[
]]$^{P}$

- Calculates the production of metallic fission products in the fine meshes, accounting for direct fission, decay, transmutation, and activation sources
- Calculates removal by means of decay and neutron capture
- Models transport and release of fission products from particles and fuel elements by means of diffusion calculations, using the time-dependent diffusion equations with temperature-dependent effective diffusion coefficients
- Accounts for the effects on isotope transport and retention from as-manufactured particle defects, contamination and particle failure fractions that may occur during operation from the FPM model
- Calculates isotope concentrations in the fuel elements and particle meshes in all core nodes
- Creates an isotope library with the concentration distributions for the core, which is used as the initial condition for transient calculations, selects and calculates isotope reaction chains used in source, decay and removal calculations

- Models irradiation and safety (annealing) experiments for both spherical and compact geometries
- Can be used for Monte Carlo uncertainty calculations

Gaseous and solid fission product densities in the TRISO particles and graphite matrix are calculated in this model. The transport and release behavior of these radionuclides is strongly dependent on the fuel temperature. A diffusion transport model is executed in SOLM to calculate the radionuclide distribution in the TRISO-coated particles and fuel pebbles as well as the leakage rates from the fuel surfaces into the helium pressure boundary (HPB).

The SOLM can also simulate gaseous and halogen radionuclide releases during temperature transients. The model receives input data such as fuel temperature, burnup, and fluence levels from the THM and failed particle fractions from FPM. During steady state irradiations, release over birth ratios (R/B) are estimated by dividing the rate of releases by the generation rate for the isotopes of interest. Also, during temperature transients and annealing experiments, fractional releases are estimated by dividing the amount released during the transient or annealing by the initial sample inventory for each measured isotope.

The SOLM can be used for TRISO fuel experiments as well as full-core analysis of the Xe-100 reactor. The reference fuel for the Xe-100 reactor is uranium oxycarbide (UCO), however, historic experiments used uranium dioxide ($UO_2$) fuel. In addition, many experiments, including Advanced Gas Reactor (AGR) experiments, were performed using fuel compacts instead of fuel spheres. The SOLM can be used to calculate releases from the following:

1. TRISO fuel particles with UCO or $UO_2$ kernels
2. Graphite fuel spheres for High Temperature Gas Reactors (HTGRs) and fuel experiments
3. Graphite fuel compacts for fuel experiments
4. Pebble-bed HTGRs with multi-pass fuel management schemes

### C.2.1 Reactor Geometry Models

The SOLM calculates radionuclide production chains to determine the radionuclide densities in the fuel particles and fuel pebbles. It accounts for the transport of radionuclides from birth to the fuel element surface via the diffusion process. At the fuel element surface, the radionuclide mass transfer rate into the coolant gas is then calculated. As indicated earlier, the diffusion rate depends on radionuclide density gradients, fuel temperatures, fast neutron fluence, and the transport characteristics of the isotopes in the fuel materials. The SOLM follows the operating history of individual fuel spheres in a multi-pass system through the fuel channels defined in the reactor model and can also model irradiation and annealing experiments.

#### C.2.1.1 TRISO Particles

The TRISO fuel particle, depicted in Figure C-1, is comprised of five distinct regions:

- A kernel containing the fissile fuel material
- A porous buffer layer
- A dense inner pyrocarbon layer (IPyC)
- A silicon carbide layer (SiC)
- A dense outer pyrocarbon layer (OPyC)

Radionuclides are predominantly produced in the kernel from where they are transported outwards by means of diffusion or direct recoil into the buffer layer. From the buffer layer, diffusion occurs through the outer layers.

The TRISO fuel particle is modeled in a one-dimensional (1D) spherical geometry. The kernel and particle layers, shown in Figure C-1, are divided into [[ ]]$^{P}$ radial zones (meshes). Thus, the particle is modeled in [[ ]]$^{P}$ radial zones with different volumes. The inter-zone interface surface areas and the distance between two adjacent zones are the geometrical parameters used in diffusion calculations.

The geometric equations used to calculate the radionuclide transport in the TRISO particles are provided below (see also Appendix B, Table B-1). In the equations, $r_i$ is the radius of particle zone $i$ (m), and $r_{i+1}$ is the radius of particle zone $(i + 1)$ (m).

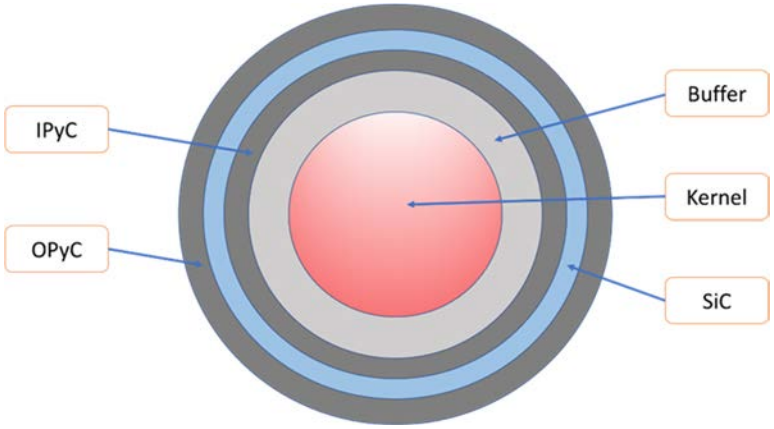


***Figure C-1: TRISO Fuel Particle Model***

The volume of particle zone $i$ (m$^3$), $V_{pz}^i$, is calculated as:

$$V_{pz}^i = \frac{4}{3}\pi\left(r_{i+1}^3 - r_i^3\right) \quad \text{(C-1)}$$

The external mass transfer surface area of particle zone $i$ (m$^2$), $A_{pz}^i$, is calculated as:

$$A_{pz}^i = 4\pi r_{i+1}^2 \quad \text{(C-2)}$$

The effective radius of particle zone $i$ (m), $r_e^i$, is calculated as:

$$r_e^i = \left(\frac{r_i^3 + r_{i+1}^3}{2}\right)^{\frac{1}{3}} \quad \text{(C-3)}$$

The inter-zone radial diffusion distance of particle zone $i$ (m), $r_e^{i'}$, is calculated as:

$$r_e^{i'} = r_e^{i+1} - r_e^i \quad \text{(C-4)}$$

The particle volume (m$^3$), $V_p$, is calculated as:

$$V_p = \sum_{i=1}^{n} V_{pz}^i = \frac{4}{3}\pi r_n^3 \quad \text{(C-5)}$$

where $r_n$ is the outer radius of the particle (m).

### C.2.1.2 Fuel Sphere

The fuel sphere is modeled, like the TRISO particle, in a 1D spherical geometry where the pebble is divided into two distinct regions as shown in Figure C-2. The first region that contains the TRISO-coated

fuel particles is called the “active sphere” region. The second region that does not contain any fuel particles is called the “shell” region. Both the shell and the active sphere regions may have uranium contamination. The shell and active sphere regions are each divided into [[ ]]$^{P}$ radial zones (meshes). Thus, the sphere is modeled in [[ ]]$^{P}$ radial zones with different volumes. Similar to the TRISO particle, the inter-zone interface surface areas and the distance between two adjacent zones are the geometrical parameters used in diffusion calculations.

[[

]]$^{P}$

***Figure C-2: Fuel Pebble Model***

The geometric equations used to calculate the radionuclide transport in the fuel spheres are provided below (see also Appendix B, Table B-2). In the equations, $r_i$ is the radius of fuel sphere zone $i$ (m), and $r_{i+1}$ is the radius of fuel sphere zone $(i+1)$ (m).

The volume of fuel sphere zone $i$ (m$^3$), $V_{fz}^{i}$, is calculated as:

$$V_{fz}^{i} = \frac{4}{3}\pi\left(r_{i+1}^{3} - r_{i}^{3}\right) \quad \text{(C-6)}$$

The external mass transfer surface area of fuel sphere zone $i$ (m$^2$), $A_{fz}^{i}$, is calculated as:

$$A_{fz}^{i} = 4\pi r_{i+1}^{2} \quad \text{(C-7)}$$

The effective radius of fuel sphere zone $i$ (m), $r_e^i$, is calculated as:

$$r_e^i = \left(\frac{r_i^3 + r_{i+1}^3}{2}\right)^{\frac{1}{3}} \quad \text{(C-8)}$$

The inter-zone radial diffusion distance of fuel sphere zone $i$ (m), $r_e^{i'}$, is calculated as:

$$r_e^{i'} = r_e^{i+1} - r_e^i \quad \text{(C-9)}$$

The active (containing TRISO particles) sphere volume (m$^3$), $V_s^a$, is calculated as follows:

$$V_s^a = \frac{4}{3}\pi\left(r_{fa}\right)^3. \quad \text{(C-10)}$$

Similarly, the shell volume (m$^3$), $V_s^{shell}$, is calculated as the difference between the volume of the pebble minus the active sphere volume:

$$V_s^{shell} = \frac{4}{3}\pi(r_{fe}^3 - r_{fa}^3). \quad \text{(C-11)}$$

Where:

$r_{fa}$ is the active fuel zone (where TRISO particles are present) radius (m)
$r_{fe}$ is the radius of fuel pebble (m) .

### C.2.1.3 Fuel Compact

The fuel compact is modeled in a symmetrical two-dimensional (2D) cylindrical geometry where the compact is divided into radial and axial zones as shown in Figure C-3. Unlike the fuel sphere, the compact does not have a fuel-free shell. The mesh distribution includes [[ ]]$^{P}$ radial zones [[ ]]$^{P}$ and [[ ]]$^{P}$ axial zones. The [[ ]]$^{P}$ radial zones closest to the centerline are active zones filled with TRISO particles in graphite matrix. The radial zone adjacent to the last active radial zone (zone 4) models the graphite holder material. Radial zone [[ ]]$^{P}$ represents a gas zone where leaked radionuclides are collected. [[ ]]$^{P}$ The inter-zone interface surface areas and the distance between two adjacent zones are the geometrical parameters used in diffusion calculations.

The geometric equations used to calculate the radionuclide transport in the fuel compacts are provided below (see also Appendix B, Table B-3). In the equations, $r_i$ is the inner radius of radial compact zone $i$ (m), and $r_{i+1}$ is the outer radius of radial compact zone $i$ (m).

[[

]]$^{P}$

***Figure C-3: Fuel Compact Mesh Model***

The volume of compact zone $(i, z)$ (m$^3$), $V_{cz}^{i,z}$, is calculated as:

$$V_{cz}^{i,z} = h_z \pi \left(r_{i+1}^2 - r_i^2\right) \quad \text{(C-12)}$$

The external radial mass transfer surface of compact zone $(i, z)$ (m$^2$), $A_{cz}^{i,r}$, is:

$$A_{cz}^{i,r} = 2h_z \pi r_{i+1} \quad \text{(C-13)}$$

The external axial mass transfer surface of compact zone $(i, z)$ (m$^2$), $A_{cz}^{i,z}$, is:

$$A_{cz}^{i,z} = \pi \left(r_{i+1}^2 - r_i^2\right) \quad \text{(C-14)}$$

The effective radius of radial compact zone $i$ (m), $r_e^i$, is calculated as:

$$r_e^i = \sqrt{\frac{r_i^2 + r_{i+1}^2}{2}} \quad \text{(C-15)}$$

The inter-zone radial diffusion distance of radial compact zone $i$ (m), $r_e^{i'}$, is calculated as:

$$r_e^{i'} = r_e^{i+1} - r_e^i \quad \text{(C-16)}$$

The inter-zone axial diffusion distance of axial compact zone $z$ (m), $z_e^{i'}$, is calculated as:

$$z_e^{i'} = h_z \quad \text{(C-17)}$$

where $h_z$ is the length of axial compact zone $z$ (m).

#### C.2.1.4 Xe-100 Reactor

The Xe-100 reactor model is applied when full-core, detailed fuel sphere histories are constructed and saved in an isotopic library. The reactor model is consistent with that in the THM model (Appendix B, Section B.2.1.1), which provides operational data such as sphere power, fission rates, burnup, fluence and residence times. The tracking of fuel sphere histories is described in more detail in Section C.2.6.

### C.2.2 Diffusion Model

Fick's second law of diffusion is applied to model radionuclide transport in all TRISO fuel components [C-2]. Fick's second law assumes that the driving force for radionuclide transport between adjacent zones is the density or concentration difference between zones. The rate at which transport takes place for a given density gradient is determined by diffusion coefficients. Each isotope has unique diffusion characteristics which are specific to the material through which the diffusion is to take place. These diffusion coefficients are generally dependent on the temperature in the base material as well as the activation energy associated with the isotope in that material. Effective diffusion coefficients are usually expressed in an Arrhenius formulation where a diffusion constant, activation energy and the temperature determine the diffusivity of the isotope in the material (see equation C-22). The SOLM model uses an effective diffusion coefficient for neighboring zones which accounts for the differences in temperatures and material attributes as well as the diffusion length in each zone (see equation C-23).

[[

]]$^{P}$

### C.2.3 Failed TRISO Particles

Failed particle fractions are calculated by the FPM and passed to SOLM. [[ ]]$^{P}$ In SOLM, the failed particle fraction is used to calculate the fraction of fissions taking place within intact and failed particles. [[

]]$^{P}$

### C.2.4 Leakage Models

For spheres, any one of the following leakage models can be executed within the SOLM:

- Diffusion with a fixed zero surface concentration [[ ]]$^{P}$ this model used for safety analysis, others below are optional.
- Diffusion with a fixed non-zero surface concentration, and
- Mass transfer model with sorption coefficients [[ ]]$^{P}$ (International Atomic Energy Agency November 1997)).

To determine the leakage, the net current of the radionuclide at the surface of the fuel element is calculated. The net RN current is dependent on the concentration gradient near the surface of the fuel element and the model used (which in turn may also depend on the concentration of the radionuclide in the cooling gas and any sorption characteristics of the radionuclide).

### C.2.4.1 Diffusion Leakage Model

The process of radionuclide diffusion transport depends on four basic factors:

- The concentration gradient between adjacent zones
- The interface cross-section of the materials involved
- The path length
- Isotope effective diffusion coefficients in the fuel materials under prevailing conditions

In cases where the fixed surface concentration diffusion model is selected, the diffusion methodology described in Section C.3 is applied to a thin-shell model at the surface of the fuel element. From the thin-shell model, a concentration gradient near the surface is determined that is then used in equation C-20 to determine the leakage current. The thin-shell equations used to determine the isotope leakage current in the fixed (i.e., zero or non-zero) surface density diffusion model are provided below.

[[

]]$^{P}$

### C.2.4.2 Sorption Mass Transfer

At the boundary between a solid and a gas, the transition of diffusing atoms occurs due to sorption processes. These processes are presumed to be fast enough such that a local equilibrium is established between the concentration of atoms at the solid surface and the thin gas layer. The relationship between these concentrations is expressed as an isotherm, i.e., the vapor pressure in the gas is related to the surface concentration of isotopes on the solid. At low concentrations, the sorption conforms to Henry's law (constant heat of adsorption, direct proportionality between vapor pressure and concentration of sorbed species on the solid surface) and at higher concentrations the Freundlich sorption holds (characterized by decreasing heat of absorption with increasing concentration of sorbed species).

[[

[[

]]$^{P}$

]]$^{P}$

### C.2.5 Radionuclide Production, Decay, and Transmutation

The SOLM model explicitly calculates the reaction chains in each of the particle and fuel element diffusion volumes to determine the time-dependent radionuclide source and removal terms.

#### C.2.5.1 Fission Sources

Fission sources are defined in cases when radionuclides are produced directly from a fission reaction. The model considers fission reactions from [[ ]]$^{P}$ and takes into account the radionuclide fission yields from these fissile isotopes. The contribution to power from [[ ]]$^{P}$ fissions is a function of burnup. In cases where a radionuclide is produced from a fission product precursor decay reaction where the precursor has a short half-life, the cumulative fission yield could also be applicable.

[[

]]$^{P}$

### C.2.5.2 Decay Sources and Removal Rates

Decay sources are defined in cases where a radionuclide is produced from a precursor decay reaction. Similarly, if the radionuclide is radioactive, it is removed by means of radioactive decay. The equations for these reactions are provided below.

[[

]]$^{P}$

### C.2.5.3 Activation Sources and Removal Rates

Radionuclides can be formed as a result of the absorption of neutrons by fission products, impurities in fuel or reactor materials, or the materials themselves. Likewise, radionuclides can be transmuted by neutron absorption reactions to another isotope, meaning that it has been removed. These source and removal phenomena are accounted in the SOLM model. The equations for these reactions are provided below.

[[

]]$^{P}$

## C.2.6 Multi-Pass Fuel History

To create isotopic libraries that are representative of the Xe-100 equilibrium core, the irradiation histories of a significant number of individual spheres must be tracked. Since the VSOP neutronics code averages the fuel burnups and isotopic compositions after the first pass into a lumped batch, the unique isotopic composition, burnup, fluence, and sphere power are lost. Thus, a methodology was developed to determine the unique irradiation history for a sphere during its full irradiation period in the Xe-100 core.

The SOLM model calculates the fuel sphere movement history through the pebble bed core. Most of the operational parameters, including the core model, are obtained from the THM model (Section B.2.1.1).

The actinide densities in each core position (i.e., each fuel channel and axial node) and fuel pass are used to determine corresponding pebble power and burnup data. These values are unique to the Xe-100 equilibrium core since the flux distribution is fixed and stable under these conditions. Using this data for the six passes in each core location, unique irradiation histories are possible in the SOLM model when combined with the THM equilibrium core calculations.

### C.2.6.1 Multi-Pass Fuel Movement Model

In the SOLM model, the core is divided into 5 flow channels analogously to the VSOP core model[8]. The fuel sphere moves downwards along these flow channels. In multi-pass fuel management schemes, the fuel sphere is reloaded at the top of the core after it has been discharged at the bottom of the core. This process is repeated until the fuel has reached a specified discharge burnup level after which it is moved to the spent fuel tank.

In practice, the channel path through which the fuel travels[9] is considered a random selection depending on the cylindrical top surface area of each core channel. The SOLM model can be used with fixed pre-selected flow patterns, or randomly selected patterns. Each channel has a different surface area thus the channel's loading probabilities are different. Thus, the multi-pass history of a fuel pebble is random and the fuel pebble burnup and radionuclide production and distribution vary. This methodology is used to model a sufficient number of individual pebble histories to realistically represent the Xe-100 core burnup and fluence. The fuel sphere burnup, temperature, and fluence history are input to the transport and leakage calculations of radionuclides from the fuel particles and spheres, according to the SOLM model.

[[

]]$^{P}$

[8] In contrast to the VSOP model, SOLM uses fixed number of axial nodes in each flow channel, and a mapping of VSOP nodal values is performed to obtain equivalent THM/SOLM parameters, see Appendix B, Section B.2.2.7.
[9] That is, which channel the fuel sphere enters in each pass – it is assumed that the fuel sphere does not migrate to another flow channel during the pass.

[[

]]$^{P}$

**Figure C-4: Fuel Channel Numbering (Top View of the Reactor Core)**

[[

]]$^{P}$

As described above, the fuel sphere is loaded at the top into one of the defined or random flow channels. The residence time for the fuel in each of the axial nodes is calculated by the THM model from VSOP input data and is integrated in the SOLM model. When the integrated time exceeds the residence time, the sphere moves to the next node in the same channel. Once the last core node in a fuel channel has been reached and the integrated time exceeds the sum of the individual node residence times in that channel, the sphere is reloaded into node 1 of the next channel determined by the loading sequence. The process is repeated until the fuel sphere reaches the bottom of the core. The fuel sphere burnup is compared to a pre-set burnup limit level;[10] if the burnup is below the limit it is reloaded at the

[10] The pre-set burnup level is selected such that a sphere would not exceed the fuel discharge burnup limit in the last pass.

top of the core for its next pass, else it is discharged to the spent fuel tank. The process is repeated until the pebble is discharged, or all passes in the loading sequence have been completed.

During the above process, the SOLM model performs the isotopic production, migration (in TRISO particles and pebbles), and release to the cooling fluid. In each core node, the power and temperatures differ (as well as for each pass). Thus, a complete radionuclide inventory for a pebble must be built from the beginning to the end of life.

[[

]]$^{P}$

The criterion used for a pebble to move in a channel from one core axial node to next node is:

$$\sum_{i=1}^{k} \Delta t_i \geq T_{fc,n},\ k = \frac{T_{fc,n}}{\Delta t_i} \quad \text{(C-48)}$$

Where:

$\Delta t_i$ is the time in days a sphere stays in a core node *n* in a core channel *fc* (d)

$T_{fc,n}$ is the time required for the sphere to complete movements from axial node 1 to axial node *n* in core channel *fc* (d).

The criterion to move to the next pass (d) is:

$$\sum_{i=1}^{K} \Delta t_i \geq T_{fc},\ K = \frac{T_{fc}}{\Delta t_i} \quad \text{(C-49)}$$

Where $T_{fc}$ is the time required for the sphere to complete a full movement through all axial nodes in a core channel *fc* (d).

### C.2.6.3 Fuel Burnup

The fuel sphere burnup is calculated in the SOLM model by taking into account the sphere power and residence times for its whole operating history. It is dependent upon the loading sequence the sphere has followed during its life in the core.

The burnup is expressed either in units of FIMA (fissions per initial metal atom) or MWd/tHM and is a measure of energy extracted from the fuel relative to its original heavy metal content before irradiation started.

The burnup is calculated as the summation of the product of sphere power and time at power over the total sphere life in the core. The sphere burnup (MWd/tHM), $BU$, is calculated as:

$$\mathrm{BU} = \sum_k \frac{P_{\delta_k} \Delta t_k}{HM} \tag{C-50}$$

Where:

$\Delta t_k$ is the irradiation time increment (d), $\sum_k \Delta t_k$ = total irradiation time;
$\delta_k$ is the index of fuel pass p and core zone (fc, n) where the pebble is located during $\Delta t_k$;
$P_{\delta_k}$ is the local power for current fuel pass and pebble location in the core (MW), calculated from the local fission rate, actinide fission energy and local actinide densities; and
$HM$ is the mass of heavy metals (tHM).

### C.2.6.4 Fast Fluence

Fast fluence represents the total fast flux neutron dose that the sphere has been subjected to. The fast fluence is calculated in SOLM when building the pebble irradiation history profile, using the neutron flux and residence times for a sphere in each node and considering its loading sequence. The fluence is calculated using the fast neutron flux [[ ]]$^{P}$ The [[ ]]$^{P}$ of the VSOP 4-group neutron flux, mapped to the THM model grid as described in Sec. B.2.2.10, are used in the fast fluence calculations in SOLM.

The fast fluence (#/m$^2$), $\Gamma$, is calculated as:

$$\Gamma = \sum_k \varphi_{\gamma_k} \Delta t_k \tag{C-51}$$

Where:

$\Delta t_k$ is the irradiation time increment (d), $\sum_k \Delta t_k$ = total irradiation time;
$\gamma_k$ is the index of core zone (fc, n) where the pebble is located at time during $\Delta t_k$; and
$\varphi_{\gamma_k}$ is the local neutron flux (fuel channel *fc*, node *n*) with [[ ]]$^{P}$

## C.2.7 Overall Solution Technique

The SOLM model is coupled with the FPM and THM models for inputs such as fuel failure fractions, fuel temperatures, and fission rates. Either full-core or single sphere/compact options are available.

SOLM is a transient model performing time-dependent calculations for radionuclide production, decay, transmutation, transport, and leakage. Furthermore, in multi-pass full core analysis, the fuel flow and pebble power model are integrated with the radionuclide calculations to obtain radionuclide density distributions in individual fuel spheres. Figure C-6 shows a typical calculation flow sequence for a sphere in a pebble bed core.

[[

]]$^{P}$

***Figure C-6 Typical SOLM Calculation Flow for a Pebble Bed Core***

### C.2.10.1 Numerical Solution Procedure

#### C.2.10.1.1 1-D Spherical Geometries (Pebbles/Particles)

The implicit Euler method is used to numerically solve the time-dependent diffusion Equation C-19. At each time step, this method requires a solution of the system of linear algebraic equations arising from the spatial discretization of the diffusion and source terms as per Equation C-24.

[[

]]$^{P}$

For each mesh zone, an equation (as above) exists which represents the coupling of neighboring zones together with their internal sources and removal terms. The resulting tri-diagonal matrix is solved by Gauss elimination to determine the isotopic concentrations in each zone at each time step. This methodology provides a numerical solution of Fick's second law of diffusion in spherical geometry.

#### C.2.10.1.2 2D Cylindrical Geometry (Compacts)

In cylindrical geometry, either an implicit Euler method or the second order backward-difference method (BDF2) [C-6] can be used to advance in time. Both methods require a time step a solution of a system of algebraic equations with a 5-diagonal matrix which represents the inter-node coupling in both radial and axial directions. The standard Gauss-Seidel iterative method is used to solve the algebraic system in each time step, [[

]]$^{P}$

## C.3 Cross References and References

| Document Title<br>Cross References: X-energy documents that may impact the content of this document.<br>References: X-energy or other documents that will not impact the content of this document | | Document No. | Rev./ Date of Issuance | Cross Reference/ Reference |
|---|---|---|---|---|
| **C-1** | H. Rutten, K. Haas, H. Brockmann and W.Scherer, "V.S.O.P.(99/05) Computer Code System," Forschungszentrum FZJ, Julich. | jul-4189 | October 2005 | Reference |
| **C-2** | L. J. H. James J. Duderstadt, "Nuclear Reactor Analysis," John Wiley & Sons, Canada. | | 1976 | Reference |
| **C-3** | International Atomic Energy Agency, "Fuel Performance and Fission Product Behavior in Gas Cooled Reactors." | IAEA-TECDOC-978 | November 1997 | Reference |
| **C-4** | G. K. Miller, D. A. Petti, J. T. Maki, D. L. Knudson and W. F. Skerjanc, "PARFUME Theory and Model Basis Report." | INL/EXT-08-14497 | Revision 1/ September 2018 | Reference |
| **C-5** | “Reactor Core Design of High-Temperature Gas-Cooled Reactors, Part 2: Heat Transfer in Spherical Fuel Elements” | KTA 3102.2 | June 1983 | Reference |
| **C-6** | L. S. M.E. Hosea, "Analysis and Implementation of TR-BDF2," *Applied Numerical Mathematics 20,* vol. 20, no. 1-2, pp. 21-37 | | 1996 | Reference |

# Appendix D. Gaseous Fission Product Transport Model

### Abbreviations/Acronyms

| Short Form | Phrase |
|---|---|
| **FPM** | Coated Particle Failure Probability Model |
| **FGR** | Fission-Gas Release |
| **FPM** | Fuel Performance Model |
| **GASM** | Gaseous Fission Product Transport Model |
| **HPBM** | Helium Pressure Boundary Model |
| **R/B** | Release-to-birth Ratio |
| **RN** | Radionuclide |
| **SOLM** | Solid Fission Product Transport Model |
| **THM** | Thermodynamics Model |
| **TRIGA** | Test/Research Reactor (Training, Research, Isotopes - GA) |
| **UCO** | Uranium oxycarbide, a heterogeneous mixture of $UO_2$ and $UC_2$ |
| **UO2** | Uranium Dioxide |
| **Xe-100** | X-energy 200 $MW_{th}$ Pebble Bed Reactor |

**Definitions**

| Symbol | Definition |
|---|---|
| $A$ | atomic mass number |
| $A_0$ | pre-exponential for kernel diffusion coefficient ($cm^2/s$) |
| $A_{O,T}$ | pre-exponential for thermal re-solution frequency ($cm^2/s$) |
| $a$ | radius of kernel grain (cm) |
| $a_g$ | ratio of kernel geometric surface area to kernel volume |
| $B$ | birth (fission) rate (atoms/s) |
| $b_f$ | fission-induced re-solution frequency ($s^{-1}$) |
| $b_T$ | thermal re-solution frequency ($s^{-1}$) |
| $C$ | concentration of non-trapped fission gas in a kernel grain ($atoms/cm^3$) |
| $c_1$ | trapping frequency constant ($1x10^{-14}$ $cm^3$/fission) |
| $c_2$ | fission-induced re-solution frequency constant ($1x10^{-14}$ $cm^3$/fission) |
| $C_t$ | concentration of trapped fission gas in a kernel grain ($atoms/cm^3$) |
| $D$ | kernel diffusion coefficient ($s^{-1}$) |
| $D_o$ | kernel reduced diffusion coefficient ($\frac{D}{a^2}$) |
| $D_0^{Kr}$ | diffusion constant for Kr ($s^{-1}$) |
| $D_0^{Xe}$ | diffusion constant for Xe ($s^{-1}$) |
| $D_B$ | binary gas diffusion coefficient of Kr and Xe in matrix pores ($cm^2/s$) |
| $D_B^P$ | effective binary diffusion coefficient ($s^{-1}$) |
| $D_{bami}$ | reduced diffusion coefficient in buffer binder for $i^{th}$ isotope ($s^{-1}$) |
| $D_{bgi}$ | reduced diffusion coefficient in buffer grains for $i^{th}$ isotope ($s^{-1}$) |
| $D_E$ | effective diffusion coefficient of Kr and Xe in matrix pores ($s^{-1}$) |
| $D_E^P$ | effective diffusion coefficient of Kr and Xe in matrix pores in presence of helium ($s^{-1}$) |
| $D_g$ | gas-phase diffusion coefficient ($s^{-1}$) |
| $D_{g,o}$ | Constant used to calculate $D_g$ |
| $D_K$ | derived Knudsen diffusion coefficient ($cm^2/s$) |
| $D_{kgi}$ | reduced diffusion coefficient in kernel grains for $i^{th}$ isotope ($s^{-1}$) |
| $D_{mami}$ | diffusion coefficient in matrix binder for the $i^{th}$ isotope ($s^{-1}$) |
| $D_{mgi}$ | reduced diffusion coefficient in matrix grains for the $i^{th}$ isotope ($s^{-1}$) |
| $\dot{F}$ | kernel fission-rate density ($fissions/s/cm^3$) |
| $F_0^{Kr,Xe}$ | recoil fraction constant for either Kr or Xe |
| $F_{bam}$ | fraction of binder (amorphous) material in the buffer |

| Symbol | Definition |
|---|---|
| $F_{cont}$ | fraction of heavy metal contamination in the matrix |
| $F_{mami}$ | fraction of binder in matrix $(1 - F_{mg})$ |
| $F_{mg}$ | fraction of graphite material (grains) in the matrix |
| $F_p$ | particle failure fraction (simplified GASM model) |
| $F_{pret}$ | pebble retention factor |
| $F_{rb}$ | recoil fraction into buffer (pores or grains) |
| $F_{rbp}$ | temperature dependent recoil fraction kernel into buffer pores |
| $f_{gas}$ | factor to account for decay during gas-phase transport |
| $f_{rec}$ | recoil fraction |
| $f_{sm}$ | fraction of fission-gas inventory in surrounding materials (from embedded recoils) that is released by diffusion |
| $fz$ | pebble fueled zone (1 to 10) |
| $G$ | trapping parameter |
| $g$ | trapping frequency ($s^{-1}$) |
| $H$ | thermal re-solution parameter |
| $i$ | $i^{th}$ isotope |
| $k_1$ | structural parameter for Knudsen diffusion in A3 matrix (function of tortuosity, shape, diameter, and volume fraction of pores) (cm) |
| $k_2$ | structural parameter for binary gas diffusion A3 matrix (function of tortuosity, shape, diameter, and volume fraction of pores) (cm) |
| $\ell$ | characteristic dimension for gas-phase diffusion (cm) |
| $M$ | molecular weight of diffusing species (g/mol) |
| $M_g$ | molecular weight of surrounding gas (g/mol) |
| $m$ | exponent used for calculating tortuosity coefficient $\phi$ |
| $m^*$ | reduced mass of binary gas mixture (g/mol) |
| $P$ | total pressure (MPa) |
| $P_g$ | helium pressure ratio $\frac{P}{P_o}$ where $P_o = 101$ kPa (dimensionless) |
| $P_{He}$ | helium pressure (bar) |
| $p$ | nuclide production (birth) rate per unit volume in a kernel grain |
| $Q^{Kr}$ | activation energy for Kr (J) |
| $Q^{Xe}$ | activation energy for Xe (J) |
| $R$ | nuclide release rate to the coolant or sweep gas (atoms/s) |
| $R^*$ | the gas constant (8.3143 J/mol·K) |

| Symbol | Definition |
|---|---|
| $R_T$ | kernel release rate from thermal re-solution |
| $(R/B)$ | ratio of nuclide release rate to coolant to birth rate in exposed kernels |
| $\left(\frac{R}{B}\right)_{bam}$ | release-to-birth ratio from buffer binder grains into the buffer pores |
| $\left(\frac{R}{B}\right)_{bg}$ | release-to-birth ratio from buffer grains into the buffer pores |
| $(R/B)_D$ | ratio of kernel release rate from diffusion to birth rate |
| $(R/B)_{DR}$ | kernel fractional release by diffusion and bubble resolution mechanisms |
| $(R/B)_{fp}$ | release-to-birth ratio into buffer pores (so matrix pores) due to failed particles |
| $(R/B)_K$ | kernel fractional release byknockout |
| $\left(\frac{R}{B}\right)_{kg}$ | release-to-birth ratio from kernel grains into the buffer pores |
| $(R/B)_R$ | kernel fractional release by thermal re-solution |
| $(R/B)_{matrix}$ | release-to-birth ratio into matrix pores due to heavy metal contamination in the matrix |
| $\left(\frac{R}{B}\right)_{mami}$ | release-to-birth ratio from matrix binder into the matrix pores for the $i^{th}$ isotope |
| $\left(\frac{R}{B}\right)_{mgi}$ | release-to-birth ratio from matrix grains into the matrix pores for the $i^{th}$ isotope |
| $\left(\frac{R}{B}\right)_{mrc}$ | release-to-birth ratio due to direct recoil from grains and binder into the matrix pores for the $i^{th}$ isotope |
| $(R/B)_{tot}$ | total release-to-birth ratio |
| $r$ | radial position from the center of a kernel grain (cm) |
| $r_p$ | fuel pebble radius (cm) |
| $r_k$ | kernel radius (µm) |
| $r_m$ | matrix binder grain radius (µm) |
| $T_o$ | reference temperature ( = 273.15 K) |
| $T_A$ | activation temperature for diffusion in kernel grains (K) |
| $T_{A,T}$ | activation temperature for thermal re-solution (K) |
| $T_{fz}$ | temperature in fuel zone (K) |
| $T_g$ | gas temperature (K) |
| $T_k$ | kernel temperature (K) |
| $T_m$ | matrix grain temperature (K) |
| $V_{fz}$ | pebble fuel zone volume ($m^3$) |
| $V_{pebble}$ | pebble volume ($m^3$) |

| Symbol | Definition |
|---|---|
| $Y_B$ | binary gas diffusion constant ($m^2/s$) |
| $Y_K$ | mean thermal speed of gas atoms with mass number $m$ at temperature $T$, $v = \left(\frac{8R^*T}{\pi m}\right)^{1/2}$ (m/s) |
| $\beta$ | parameter used to calculate $f_{gas}$ |
| $\Gamma$ | parameter $(D_o/\lambda)$ used to calculate $(R/B)_D$ |
| $\epsilon$ | void fraction of surrounding porous medium |
| $\eta_{rec}$ | fraction of recoiled atoms that do not embed in surrounding materials |
| $\lambda$ | radioactive decay constant |
| $\lambda_i$ | half-life for the $i^{th}$ isotope (s) |
| $\mu_{ff}$ | fission-fragment range in kernel material (μm) |
| $\phi$ | tortuosity coefficient of surrounding porous medium |

## D.1 Introduction

As discussed in Section 3.2, the functional containment system is a collection of five radionuclide (RN) release barriers, designed to limit RN release from the core to the environment to very low levels during normal operation and a broad spectrum of postulated accidents, References 1 and 2. These barriers, together with the main phenomena and processes involved in radionuclide production, retention, transport, and release for a pebble bed reactor are depicted in Figure 3 of this Topical Report. The Gaseous Fission Product Transport Model (GASM) calculates the gaseous fractional (release-to-birth ratio) fission product release from TRISO-coated fuel particles and pebbles (spheres) into the helium pressure boundary under steady-state power conditions.

## D.2 Theory and Methodology

Two gaseous fission product transport models are implemented in GASM. The first approach is based on the Röllig model [D-1] also used in the NOBLEG code. The model was derived in 1977 from German Low Enriched Uranium (LEU) uranium dioxide ($UO_2$) data. Fission product release codes based on this Röllig model, including NOBLEG, have been used with good success by the German High Temperature Reactor (HTR) programs [D-7] and the Pebble Bed Modular Reactor (PBMR) [D-3]. This approach is useful for validation against experiments that use $UO_2$ fuel. The second approach, the Richards uranium oxycarbide (UCO) Fission-Gas Release (FGR) model [D-4], is primarily based upon UCO release-to-birth (R/B) data from the High Flux Reactor (HFR)-B1 experiment [D-5].

Both the Richards and Röllig models are applicable for gaseous fission product release from fuel elements (pebbles) under irradiation and in the absence of oxidants. [[

]]$^{P}$

GASM is capable of modeling:

- Fuel geometry
- Uranium contamination in the matrix material and particle layers
- Recoil of fission gases from the fuel kernel
- Combined release of fission gases from the amorphous binder and the matrix material grains into matrix material open porosity volumes
- Gas-phase diffusion through the matrix material open porosity volumes to the fuel element surface
- Release-to-birth ratio (R/B) for fission gases (noble gases, halogens and chalcogens)
- Coolant gas activity

### D.2.1 Röllig Model

Prior to the GASM calculations, the following core node parameters are calculated by the thermodynamics model THM:

- Detailed temperature distribution
- Number of fuel pebbles
- Fuel pebble fission rate
- Fuel pebble burnup

For each isotope, the total isotopic release-to-birth ratio is calculated by summing up the contributions from the failed/defective particles and contaminated fuel element matrix:

$$\left(\frac{R}{B}\right)_{tot} = \left(\frac{R}{B}\right)_{matrix} + \left(\frac{R}{B}\right)_{fp} \quad \text{(D-1)}$$

Where:

$R$ is release rate (atoms/s),
$B$ is fission (birth) rate (atoms/s),
$\left(\frac{R}{B}\right)_{matrix}$ is the $\left(\frac{R}{B}\right)$ contribution from the pebble due to heavy metal contamination in the matrix,
$\left(\frac{R}{B}\right)_{fp}$ is the $\left(\frac{R}{B}\right)$ contribution from the fuel pebble due to failed particles, and
$\left(\frac{R}{B}\right)_{tot}$ represents the total ratio for the pebble.

#### D.2.1.1 Releases Due to Heavy Metal Contamination

The release-to-birth ratio contribution from heavy metal contamination in the matrix, $\left(\frac{R}{B}\right)_{matrix}$ in Equation D-1 is calculated with Equation D-2:

$$(R/B)_{matrix} = F_{pret}\left((R/B)_{mgi} + (R/B)_{mami} + (R/B)_{mrc}\right) \sum_{fz=1}^{[[\ \ ]]^P} \frac{V_{fz}}{V_{pebble}} \quad \text{(D-2)}$$

Where:

$F_{pret}$ is the pebble retention factor,
$\left(\frac{R}{B}\right)_{mgi}$ is the release-to-birth ratio from matrix grains into the matrix pores for the $i^{th}$ isotope,
$\left(\frac{R}{B}\right)_{mami}$ is the release-to-birth ratio from matrix binder into the matrix pores for the $i^{th}$ isotope,
$\left(\frac{R}{B}\right)_{mrc}$ is the release-to-birth ratio due to direct recoil from grains and binder into the matrix pores for the $i^{th}$ isotope,

$fz$ is the pebble fueled zone [[ ]][P]
$V_{fz}$ is the pebble fuel zone volume (m$^3$), and
$V_{pebble}$ is the pebble volume (m$^3$).

### D.2.1.2. Retention Factor, $F_{pret}$

The pressure-dependent retention factor (van der Merwe June 2004), $F_{pret}$ in Equation D-2, is calculated by Equation D-3 per Reference [D-3], Section 4.3.2.1:

$$F_{pret} = \frac{D_E^P \left( \frac{\sqrt{\lambda_i / D_E^P}}{tanh\left(\sqrt{\lambda_i / D_E^P}\right)} - 1 \right)}{D_E \left( \frac{\sqrt{\lambda_i / D_E}}{tanh\left(\sqrt{\lambda_i / D_E}\right)} - 1 \right)} \quad \text{(D-3)}$$

Where:

$$D_E^P = \frac{D_B^P D_K}{(D_B^P + D_K) r_p^2} \quad \text{(D-4)}$$

$$D_E = \frac{D_B D_K}{(D_B + D_K) r_p^2} \quad \text{(D-5)}$$

$$D_B^P = \frac{D_B}{P_g} \quad \text{(D-6)}$$

$$D_K = k_1 Y_K \sqrt{T_{fz} / T_o} \quad \text{(D-7)}$$

$$D_B = k_2 Y_B \left( T_{fz} / T_o \right)^{3/2} \quad \text{(D-8)}$$

and:

$D_E^P$ is the effective diffusion coefficient of krypton (Kr) and xenon (Xe) in matrix pores in the presence of helium (s$^{-1}$),
$D_B^P$ is the effective binary diffusion coefficient (s$^{-1}$),
$D_E$ is the effective diffusion coefficient of Kr and Xe in matrix pores (s$^{-1}$),
$\lambda_i$ is the half-life for the $i^{th}$ isotope (s),
$D_B$ is the binary gas diffusion coefficient (Hirschfelder, Curtiss and Bird 1954) of Kr and Xe in matrix pores, Appendix A, per Reference [D-8].,

$D_K$ is the derived Knudsen diffusion coefficient (van der Merwe June 2004)per Reference [D-3]
$r_p$ is the fuel pebble radius (cm),
$k_1$ is the structural parameter for Knudsen diffusion in A3 matrix (function of tortuosity, shape, diameter and volume fraction of pores, 6 x $10^{-7}$ cm, Appendix A, Reference [D-3].,
$k_2$ is the structural parameter for binary gas diffusion A3 matrix (function of tortuosity, shape, diameter and volume fraction of pores, 1.4 x $10^{-2}$ cm, Appendix A, Reference [D-3],
$Y_K$ is the arithmetic mean thermal speed of gas atoms (in cm/s) with mass number $m$ at temperature $T$, $Y_K = \left(\frac{8R^*T}{\pi m}\right)^{1/2}$, where $R^*$ is the gas constant (8.3143 J/mol·K), Chapter 2, Problem 4, Reference [D-2]
$Y_B$ is the binary gas diffusion constant (0.556 $m^2$/s), for Kr, Appendix A, Reference [D-3].
$T_o$ is the reference temperature (273.15 K) (van der Merwe June 2004),
$T_{fz}$ is the temperature in fuel zone (K), and
$P_g$ is the helium pressure ratio $\frac{P}{P_o}$ with $P_o$=101 kPa.

### D.2.1.3 R/B Calculation from Matrix Grains into Matrix Pores

Release-to-birth ratio, $\left(\frac{R}{B}\right)_{\text{mgi}}$ in Equation D-2, from matrix grains into the matrix pores for the $i^{\text{th}}$ is calculated by the following equation, Reference [D-3], Section 3.2.1.

$$\left(\frac{R}{B}\right)_{mgi} = 3F_{mg}F_{cont}\frac{D_{mgi}}{\lambda_i}\left(\frac{\sqrt{\lambda_i/D_{mgi}}}{tanh\left(\sqrt{\lambda_i/D_{mgi}}\right)} - 1\right) \quad \text{(D-9)}$$

Where:

$R$ is the release rate (atoms/s),
$B$ is the fission (birth) rate (atoms/s),
$i$ is the $i^{\text{th}}$ isotope,
$F_{mg}$ is the fraction of graphite material (grains) in the matrix (0.995) (van der Merwe June 2004),
$F_{cont}$ is the fraction of heavy metal contamination in the matrix (consistent with the Xe-100 fuel specification)
$D_{mgi} \equiv \frac{D'_{mgi}}{r_m^2}$ is the reduced diffusion coefficient in matrix grains for the $i^{\text{th}}$ isotope, where $r_m$ is the matrix binder grain radius, and
$\lambda_i$ is the half-life for the $i^{\text{th}}$ isotope (s).

The reduced diffusion coefficient, $D_{mgi}$ in Equation D-9, in matrix grains for the $i^{\text{th}}$ isotope is calculated by an Arrhenius form given by Reference [D-3], Section 3.2.4:

$$D_{mgi} = D_0^{Kr,Xe} e^{-Q^{Kr,Xe}/R^*T_m} \quad \text{(D-10)}$$

Where:

$D_0^{Kr}$ is the diffusion constant for Kr (3.0 x $10^{-5}$ $s^{-1}$) (van der Merwe June 2004),
$D_0^{Xe}$ is the diffusion constant for Xe (1.7 x $10^{-7}$ $s^{-1}$),[D-3]
$Q^{Kr}$ is the activation energy (1.063 x $10^5$ J/mol) (van der Merwe June 2004),
$Q^{Xe}$ is the activation energy (7.87 x $10^4$J/mol) (van der Merwe June 2004),
$T_m$ is the temperature of the matrix grain (K), and
$R^*$ is the gas constant (8.3143 J/mol·K).

[[

]]$^P$

### D.2.1.4 R/B Calculation from Matrix Binder into Matrix Pores

Release-to-birth ratio, $\left(\frac{R}{B}\right)_{mami}$ in Equation D-2, from matrix binder into the matrix pores for the $i^{th}$ isotope is calculated by, Reference [D-3], Section 3.2.1 :

$$\left(\frac{R}{B}\right)_{mami} = 3F_{mami}F_{cont}\frac{D_{mami}}{\lambda_i}\left(\frac{\sqrt{\lambda_i/D_{mami}}}{tanh\left(\sqrt{\lambda_i/D_{mami}}\right)} - 1\right) \quad \text{(D-11)}$$

Where:

$F_{mami}$ is the fraction of binder in matrix $(1 - F_{mg})$,
$F_{cont}$ is the fraction of heavy metal contamination in the matrix [[
]]$^P$
$D_{mami} \equiv \frac{D'_{mami}}{r_m^2}$ is the reduced diffusion coefficient in matrix binder for the $i^{th}$ isotope ($s^{-1}$), where
$r_m$ is the matrix binder grain radius, and
$\lambda_i$ is the half-life for the $i^{th}$ isotope (s).

The reduced diffusion coefficient, $D_{mami}$ in Equation D-2, in matrix binder for the $i^{th}$ isotope is calculated by:

$$D_{mami} = D_0^{Kr,Xe} e^{-Q^{Kr,Xe}/R^*T_m} \quad \text{(D-12)}$$

Where:

$D_0^{Kr}$ is the diffusion constant for Kr (1.7 x $10^{-2}$ $s^{-1}$) (van der Merwe June 2004),
$D_0^{Xe}$ is the diffusion constant for Xe (1.7 x $10^{-2}$ $s^{-1}$),[D-3]
$Q^{Kr}$ is the activation energy (5.44 x $10^4$J/mol) (van der Merwe June 2004),

$Q^{Xe}$ is the activation energy (5.44 x $10^4$J/mol), [D-3]
$T_m$ is the temperature of the matrix grain (K), and
$R^*$ is the gas constant (8.3143 J/mol·K).

#### D.2.1.5 R/B Calculation from Matrix Material into Matrix Pores due to Direct Recoil

Release-to-birth ratio, $\left(\frac{R}{B}\right)_{mrc}$ in Equation D-2, due to direct recoil from grains and binder into the matrix pores for the $i^{th}$ isotope is calculated by Reference [D-3] of Section 3.2.5 (van der Merwe June 2004):

$$\left(\frac{R}{B}\right)_{mrc} = \frac{RF\ P_{He} F_{cont}}{T_{fz}} \quad \text{(D-13)}$$

Where:

RF is the recoil fraction into open porosity per [[ ]]$^P$
$F_{cont}$ is the fraction of heavy metal contamination in the matrix pores [[ ]]$^P$
$P_{He}$ is the helium pressure (bar), and
$T_{fz}$ is the temperature in fuel zone (K).

### D.2.2 Releases from Failed Particles

Release-to-birth ratio, $\left(\frac{R}{B}\right)_{fp}$ in Equation D-1, from the fuel sphere due to failed particles is calculated by: [[

]]$^{P}$

***Equations D-22 and D-23 not used***

## D.3. Richards Model

A second model is available in GASM for gaseous fission product release from non-hydrolyzed LEU-UCO fuel during steady-state operations. [[

]]$^{P}$ (Hanson April 2006). The theoretical basis of the new model allows for accurate predictions of release over a wide range of temperatures, isotope half-life, and fission-rate density.

The model was derived from an overall mass balance for gaseous fission products and includes components that account for low-temperature release, high-temperature release, and gas-phase transport to the coolant or sweep gas.

[[

]]$^{P}$

### D.2.3.1 Low Temperature Release

#### D.3.1.1 Direct Recoil

In the direct-recoil mechanism, high-energy fission-fragments generated near and directed toward the surface of the kernel are released. [[

]]$^{P}$

### D.3.2 High Temperature Release

[[ ]]$^{P}$ For high-temperature release, the fuel kernel is modeled as a collection of spherical grains. The fission process creates traps which delay and reduce (due to decay) the diffusive release. Due to trapping, the total fission-gas inventory is divided into a non-trapped inventory and a trapped inventory consisting of gas bubbles. Two mechanisms of re-solution of gas in the trapped bubbles are considered: [[

]]$^{P}$

### D.3.2.1 Mass Balance Equations

At steady-state, the balance equations for the non-trapped concentration $C$ and the trapped concentration $C_t$ are given by:

[[

]]$^{P}$

### D.3.2.2 Diffusive Release

[[

]]$^{P}$

### D.3.2.3 Release from Thermal Re-Solution

[[

]]$^{P}$

### D.3.2.4 Functional Dependencies of Model Parameters

[[

]]$^{P}$

### D.3.3 Gas-Phase Transport

Released fission gases from fuel kernels can diffuse through the porosity of surrounding matrix materials to the helium coolant. For shorter-lived isotopes, it may be important to account for radioactive decay during this transport process [[

]]$^{P}$

[[

]]$^{P}$

***Figure D-1: Fractional Release $\left(\frac{R}{B}\right)$ of Krypton Isotopes as a Function of the Product of Pressure and Reduced Mass at Low Temperature (300 K)***

### D.3.3.1 Decay During Transport

Subject to appropriate boundary conditions, expressions for [[ ]]$^{P}$ can be derived from steady-state solutions of the nuclide mass conservation (Equation D-25), accounting for diffusion, decay, and source terms. [[

]]$^{P}$

### D.3.3.2 Gas-Phase Diffusion Coefficient

[[

]]$^{P}$

### D.3.3.3 Tortuosity Coefficient

[[

]]$^{P}$

### D.3.3.4 Model Parameters

[[

]]$^{P}$

## D.4 Overall Calculation Method

The core model consists of several flow channels and fuel elements divided into several layers in each core region. The fission product release is calculated in each core region to determine the total core gaseous release. The GASM model receives input from the Thermodynamics Model THM (Appendix B), and the TRISO-coated Particle Failure Probability Model FPM (Appendix A). The gaseous release rates calculated by GASM serve as input to the helium pressure boundary model HPBM (Appendix F).

## D.5 Cross References and References

| Document Title<br>Cross References: X-energy documents that may impact the content of this document.<br>References: X-energy or other documents that will not impact the content of this document | | Document No. | Rev./ Date of Issuance | Cross Reference/ Reference |
|---|---|---|---|---|
| **D-1** | K. Röllig, "Release of Rare Fission Gases from Spherical Elements with Coated Fuel Particles," *Nuclear Technology*. | Vol. 35, No. 2 | September, 1977 | Reference |
| **D-2** | J. O. Hirschfelder, C. F. Curtiss and R. B. Bird, "Molecular Theory of Gases and Liquids" | | 1954 | Reference |
| **D-3** | [[ ]]$^{P}$ | | June, 2004 | Reference |
| **D-4** | [[ ]]$^{P}$ | [[ ]]$^{P}$ | 1994 | Reference |
| **D-5** | D. L. Hanson, "HFR-B1 Final Summary Report," General Atomics. | PC-000529 | Rev. 0/ April, 2006 | Reference |
| **D-6** | J. M. Smith and N. Wakao, "Diffusion in Catalyst Pellets," *Chemical Engineering Science.* | Vol. 17, No. 11 | 1962 | Reference |
| **D-7** | D. R. Olander, "Fundamental Aspects of Nuclear Reactor Fuel Elements,", National Technical Information Service, U.S. Department of Commerce, Springfield, Virginia, | TID-26711-PI | April, 1976. | Reference |
| **D-8** | N. L. Baldwin, W. E. Bell and C. F. Myers, "Fission Gas Release from Fuel Particles and Fuel Rods," *Nuclear Technology*. | Vol. 35 | September, 1977 | Reference |
| **D-9** | M. Richards, "A Theoretical Model for Fission Gas Release from UC TRISO Fuel," Ultra Safe Nuclear Corporation, Warsaw, Poland. | HTR 2018-0006 | October, 2018 | Reference |
| **D-10** | [[ ]]$^{P}$ | [[ ]]$^{P}$ | 1990 | Reference |
| **D-11** | R. N. Morris, Et. al., TRISO-Coated Particle Fuel Phenomenon Identification and Ranking Tables (PIRTs) for Fission Product Transport Due to Manufacturing, Operations, and Accidents | NUREG/CR-6844, Vol. 1 | October, 2003 | Reference |

| | | | | |
|---|---|---|---|---|
| **D-12** | Xe-100 Reactor Fuel Specifications | XE01-N-RZZ-GLZZ-D-000100 | 2/ June, 2023 | Cross Reference |

# Appendix E. Dust Production Model

### Abbreviations/Acronyms

| Short Form | Phrase |
|---|---|
| **AVR** | Arbeitsgemeinschaft Versuchs Reaktor |
| **DUSTM** | Dust Production Model |
| **EFPY** | Effective Full Power Years |
| **FHS** | Fuel Handling System |
| **HPB** | Helium Pressure Boundary |
| **HTGR** | High Temperature Gas Reactor |
| **HTR** | High Temperature Reactor |
| **RCS** | Reactivity Control System |
| **THTR** | Thorium Hochtemperatur Reaktor |

**Definitions**

| Symbol | Definition |
|---|---|
| $A_{hex}$ | floor surface area of the hexagon ($m^2$) |
| $a$ | side of hexagon (m) |
| $D_{RCS}$ | distance travelled per control rod per EFPY (m) |
| $D_{eff}$ | effective hydraulic diameter of the core (m) |
| $D$ | total dust production in the core (kg) |
| $d_{FHS}$ | dust generation per meter in the FHS (mg) |
| $d_{RCS}$ | dust generation per meter travelled per RCS (mg/m) |
| $d$ | dust production rate (kg/m-N-pebble) |
| $EFPY$ | effective full power years |
| $L_f$ | load factor [%] |
| $F_{gd}$ | graphite dust fraction [%] |
| $FHS_{dust}$ | dust generated in the FHS over the reactor lifetime (kg) |
| $F_z$ | friction force at $z^{th}$ axial zone (N) |
| $g$ | gravitational acceleration ($m/s^2$) |
| $H$ | core height (m) |
| $h$ | height of hexagon (m) |
| $k$ | pressure ratio coefficient |
| $L_{FHS}$ | length of FHS feed line (m) |
| $M$ | total number of axial nodes in the core |
| $N_{RCS}$ | number of control rods |
| $N_f$ | total number of fuel pebbles over the reactor lifetime |
| $N_{fd}$ | number of fresh fuel pebbles used per full power day |
| $N_{pebble}$ | number of pebbles per hexagon |
| $N_{psm}$ | number of pebbles per $m^2$ |
| $PF$ | pebble bed packing factor |
| $P_N(z, T_z)$ | normal pressure (Pa) |
| $P_f$ | number of fuel passes |
| $p$ | pebble bed density ($kg/m^3$) |
| $RCS_{dust}$ | dust generated in the RCS over the reactor lifetime (kg) |
| $r$ | pebble radius (m) |
| $T_z$ | pebble surface temperature at the $z^{th}$ axial zone (°C) |
| $V_{hex}$ | volume of hexagon ($m^3$) |

| Symbol | Definition |
|---|---|
| $V_{pebble}$ | volume of pebble ($m^3$) |
| $z$ | height of the core (m) or axial zone |
| $\mu (T_z)$ | temperature dependent friction coefficient for graphite at the $z^{th}$ axial zone |
| $v_d$ | design average pebble velocity in FHS feedline (m/s) |
| $v_{nom}$ | nominal average pebble velocity in FHS feedline (m/s) |
| $\Delta p$ | helium pressure drop (Pa) |
| $\rho$ | pebble bed density (kg/m3) |

## E.1 Introduction

As discussed in Section 3.2, the functional containment system is a collection of five radionuclide (RN) release barriers, designed to limit RN release from the core to the environment to very low levels during normal operation and a broad spectrum of DBAs, References 1 and 2. These barriers, together with the main phenomena and processes involved in radionuclide production, retention, transport, and release for a pebble bed reactor are depicted in Figure 3 of this Topical Report.

The Dust Production Model (DUSTM) model calculates the graphite and metallic dust production rates in the core, FHS, and RCS. Radionuclides produced in the core can be transported with dust entrained in the helium coolant throughout the helium pressure boundary (HPB). Dust is produced from mechanical wear such as the pebble-to-pebble and pebble-to-reflector interactions in the core, pebble-to-pipe interactions in the fuel handling system (FHS), and control rod-to-reflector interactions in the reactivity control system (RCS). Mechanical wear is the only mechanism accounted as a major source of dust. Other potential sources such as oxidation from impurities in the helium coolant are neglected.

## E.2 Theory and Methodology

Graphite dust in the Xe-100 core is produced from sliding friction forces between the moving pebbles as well as pebbles rubbing against the side graphite reflector. Friction forces are calculated using the normal force and friction coefficient as function of axial core position. Pressure on the pebbles is determined by a modified Janssen silo pressure theory including the effect of the helium pressure drop over the pebble bed. The average number of pebbles per square meter of contact surface area in a hexagonal geometry, packing factor included, is calculated to convert the pressure on the pebbles to a normal force. The friction coefficient and normal force are then used to calculate the friction force per pebble. The friction force along with operating parameters such as the number of passes and the number of daily fresh fuel pebbles are used to determine the total number of pebbles used over a given operating period. Once the distance each pebble travels during its core lifetime is calculated, the core's graphite dust production can be determined based on the axial friction forces. This methodology allows for the calculation of a dust production coefficient which can be calibrated against operating pebble bed reactors with known dust production.

At the end of each FHS fuel pass, the pebble's burnup is determined. If the pebble is determined to return to the core for another pass, it is transported pneumatically by helium in a pipe run of several meters in length and reloaded at the top of the core. During this relatively high velocity transport phase, interaction between the fuel pebble and the walls of the transport piping leads to abrasion and dust production during transport.

Abrasion of the pipeline can also lead to metallic dust production. Metallic dust production rates per meter travelled in the FHS pipelines can be determined by means of experiments. The number of fuel pebble movements through the FHS reload pipeline is determined from the number of fuel passes, the number of fresh fuel pebbles added per day and the operating period.

The dust produced from the movement of control rods in the reflectors is calculated from the number control rods and an estimate of the distance of control rod movements over the operating period under

consideration. In this case, both graphite and metallic dust are generated. The metallic dust originates from the control rod cladding material. Dust production coefficients per unit length travelled are established via experiments.

### E.2.1 Dust Production in Pebble Bed Core

In DUSTM, the reactor core dust production rate is calculated for [[ ]]$^{P}$ axial mesh points. For each mesh point, the average pebble surface temperatures are calculated over the five radial flow channels. The DUSTM core computational domain is illustrated in Figure E-1.

[[

]]$^{P}$

***Figure E-1: DUSTM Computational Domain in the Core***

[[

]]$^{P}$

### E.2.2 Dust Production in Fuel Handling System

[[

]]$^{P}$

### E.2.3 Dust Production in the Reactivity Control System

[[

]]$^{P}$

### E.2.4 Calibration of the Dust Production Model

The dust production rate [[ ]]$^{P}$ can be calibrated against a known pebble bed configuration such as [[ ]]$^{P}$ for which best estimates of the dust production over the lifetime are known. [[

]]$^{P}$

### E.2.4.1 Calibration Inputs and Assumptions

[[

]]$^{P}$

### E.2.3.2 Calibration Calculations

[[

]]$^{P}$

## E.3 Cross References and References

| Document Title<br>Cross References: X-energy documents that may impact the content of this document.<br>References: X-energy or other documents that will not impact the content of this document | | Document No. | Rev./ Date of Issuance | Cross Reference/ Reference |
|---|---|---|---|---|
| **E-1** | "Contact and Rubbing of Flat Surfaces," J. F. Archard, Journal of Applied Physics | Volume 24, No. 8 | August 1953 | Reference |
| **E-2** | "Computational prediction of dust production in pebble bed reactors, Part II," M. Hiruta Et. al., Nuclear Engineering and Design. | | April 2013 | Reference |
| **E-3** | Xe-100 200MWt, Fuel Handling System (FHS) Design Description | 000052 | 5/May 2022 | Reference |
| **E-4** | Fuel performance and fission product behaviour in gas cooled reactors | IAEA-TECDOC-978 | Nov 1997 | Reference |
| **E-5** | Final Report about Operation of the AVR Experimental Nuclear Power Station | Julich Report 3448 | Oct 1997 | Reference |
| **E-6** | Xe-100 200MWth Preliminary Steady-State Core Design Report | 000288 | 5/February 2022 | Reference |
| **E-7** | AVR- Experimental High-Temperature Reactor: 21 Years of Successful Operation For A Future Energy Technology | ISBN 3-18401015-5 | 1990 | Reference |
| **E-8** | Fuel Handling System Process Layout Design Comparison Report | 000591 | 1/March 2022 | Reference |

# Appendix F. Helium Pressure Boundary Model

### Abbreviations/Acronyms

| Short Form | Phrase |
|---|---|
| **AVR** | Arbeitsgemeinschaft Versuchsreaktor |
| **DAMD** | Dust and Activity Migration and Distribution |
| **DUSTM** | Dust Production Model |
| **EFPD** | Effective Full Power Days |
| **FHS** | Fuel Handling System |
| **FP** | Fission Product |
| **FPM** | Failure Probability Model |
| **FRF** | Fission Product Release Factor |
| **GASM** | Gaseous Fission Product Model |
| **HPB** | Helium Pressure Boundary |
| **HPBM** | Helium Pressure Boundary Model |
| **HTGR** | High Temperature Gas-cooled Reactor |
| **HTR** | High Temperature Reactor |
| **LTR** | Licensing Topical Report |
| **MCNP** | Monte Carlo N-Particle Transport Code |
| **MST** | Mechanistic Source Term |
| **ORIGEN** | Oak Ridge Isotope Generation |
| **RB** | Reactor Building |
| **RCS** | Reactivity Control System |
| **RN** | Radionuclide |
| **ROT** | Reactor Outlet Temperature |
| **SFT** | Spent Fuel Tank |
| **SOLM** | Solid Fission Product Model |
| **SSC** | Structures, Systems and Components |

| Short Form | Phrase |
|---|---|
| **THM** | Thermodynamics Model |
| **TRISO** | Tri-structural Isotropic |
| **VSOP** | Very Superior Old Programs Code |

**Definitions**

| Symbol | Definition |
|---|---|
| $A$ | flow surface of the control volume ($m^2$) |
| $A_i$ | production rate (kg/s) |
| $A_f$ | outward pointing face area vector ($m^2$) |
| $A_n$ | flow area ($m^2$) |
| $A_F$ | coefficient for the non-linear range of sorption isotherm |
| $A_H$ | coefficient for the linear range of sorption isotherm |
| $A^C_{comp,n,k}$ | rate of gain in coolant (He) in component comp, node n for FP k ($kg/m^3$-d) |
| $A^G_{comp,n,p,k}$ | rate of gain in graphite in component comp, node n for FP k, for particle size p (kg/d) |
| $a_g$ | fluid acceleration between two adjacent nodes ($m/s^2$) |
| $amu_k$ | atomic mass unit of isotope *k* (g/mol) |
| $B_F$ | coefficient for the non-linear range of sorption isotherm |
| $B_H$ | coefficient for the linear range of sorption isotherm |
| $C$ | circulating dust concentration ($kg/m^3$) |
| $CI$ | number of component inlets |
| $CO$ | number of component outlets |
| $C_t$ | concentration of the entrained target isotopes ($kg/m^3$) |
| $C^i_n$ | circulating particle density of isotope “i” in node “n” ($kg/m^3$) |
| $C^G_{t'}$ | circulating concentration of nuclide “t’” in graphite dust ($kg/m^3$) |
| $C^G_{t''}$ | circulating concentration of nuclide “t’’” in graphite dust ($kg/m^3$) |
| $C^M_{m'}$ | circulating concentration of isotopes m’ in metallic dust ($kg/m^3$) |
| $C^M_{t''}$ | circulating concentration of isotope t” in metallic dust ($kg/m^3$) |
| $C_L$ | liftoff scaling factor |
| $C_S$ | deposition scaling factor |
| $C_{LT}$ | transient liftoff scaling factor |
| $c_{C,k}$ | concentration of FP k in the coolant (He) ($atoms/m^3$) |

| Symbol | Definition |
|---|---|
| $c_{G,k}$ | concentration of FP k in graphite (atoms/m$^3$) |
| $c_t$ | transition concentration of sorbate species (mmol/kg-C) |
| $D$ | deposited dust mass (kg) |
| $D_{coreN}$ | dust mass on pebble surface in bottom core node (kg) |
| $D_h$ | hydraulic diameter of component node (m) |
| $D_t$ | mass of the deposited target isotopes (kg) |
| $D_F$ | coefficient for the non-linear range of sorption isotherm |
| $D_n^i$ | deposited particle mass of nuclide “i” in node “n” (kg) |
| $D_{n'}^F$ | ratio of dust layer thickness to average particle thickness |
| $D_{m'}^G$ | precursor isotope m’ mass in deposited graphite dust (kg) |
| $D_{t'}^G$ | isotope “t” mass in deposited graphite dust (kg) |
| $D_{t,sphere,n}^G$ | isotope “t” mass in deposited graphite sphere in node n (kg) |
| $D_{t,core,n,p}^G$ | isotope “t” mass in deposited graphite in node n for particle size p (kg) |
| $D_{t'}^M$ | isotope t’ mass in metallic dust (kg) |
| $\mathrm{d_p}$ | particle diameter (m) |
| $d_p^{avg}$ | average node dimension (m) |
| $d_{k,n}^h$ | the hydraulic diameter of the flow channel (m) |
| $d_{comp,n}^{layer}$ | layer thickness for component comp in node n (m) |
| $E_F$ | coefficient for the non-linear range of sorption isotherm |
| $F_{cd}$ | removal rate of core dust attached to fuel pebbles (kg/d) |
| $F_{efpd}$ | new fuel elements loaded per effective full power days (1/d) |
| $F_{fhs}$ | dust mass generated and deposited on the FHS fueling line surface during its transit in the FHS (kg) |
| $F_{pass}$ | number of times fuel element passes through core |
| $F_{pd}$ | fuel pebbles passing through FHS per day (1/d) |
| $F_t$ | transient force (N) or transport of slid target isotope of fuel pebbles (kg/d) |

| Symbol | Definition |
|---|---|
| $F_{tci}$ | transport of solid target isotope on fuel pebbles (kg/d) |
| $F_{core \rightarrow fhs}$ | removal rate of dust attached to fuel pebbles that are entering the FHS (kg/d) |
| $F_{core \rightarrow sft}$ | removal rate of dust attached to fuel pebbles that are being discharged to the SFT (kg/d) |
| $F_{fhs \rightarrow core}$ | dust Fraction from FHS to Core (1/d) |
| $F_{pebble \rightarrow fhs}$ | dust mass transferred from pebble surface to the FHS fueling line surface during the transit from the bottom of the core to the top (kg) |
| $F_D$ | Total deposition force (N) |
| $F_M$ | ratio of metal dust to total dust |
| $F_{LO}$ | total liftoff force (N) |
| $F_{gas,fhs}$ | dust mass generated and released directly into carrier gas during pebble transit in the FHS (kg) |
| $F_{pebble,fhs}$ | dust mass generated and retained on the fuel pebble during its transit in the FHS (kg) |
| $F_{D,n}$ | FHS Dust Deposition Factor in node “n” |
| $F_{fhs}^{d}$ | FHS flow time fraction |
| $F_{z,n}^{G}$ | fractional removal rate in deposited graphite in component z, in node n (1/d) |
| $F_{D}^{g}$ | gravity deposition force on particle (N) |
| $F_{D}^{h}$ | hydraulic deposition force on particle (N) |
| $F_{D}^{p}$ | lumped deposition force on particle “p” (N) [user input] |
| $F_{AD}^{p}$ | adhesion force on particle “p” on material ‘’mat’’ (N) |
| $F_{LO}^{h}$ | hydraulic liftoff force (N) |
| $F_{LO}^{p}$ | lumped liftoff force for particle “p” (N) [user input] |
| $F_{t'}^{G}$ | net rate at which isotope “t” contained in graphite dust are added from fuel movements (kg/d) |
| $F_{t'}^{M}$ | rate of change of isotope t’ mass in deposited metal (kg/d) |
| $F_{co,comp-1}^{O}$ | flow fraction |
| $F_{fhs,fhs}^{G}$ | fraction of graphite dust produced in FHS that are deposited on FHS fueling line |

| Symbol | Definition |
|---|---|
| $F^{M}_{fhs,fhs}$ | fraction of metal dust produced in FHS that are deposited on FHS fueling line |
| $F^{G,z}_{t,core,n,p}$ | rate of change of isotope "t" mass in deposited graphite in node n for particle size p (kg/d) |
| $f_{AD}$ | adhesion force coefficient |
| $f_{d}$ | lumped deposition constant |
| $f_{p}$ | dust removal fraction from base material |
| $f_{r}$ | dust retention factor on pebble in FHS |
| $f_{LO}$ | liftoff constant (1/N.d) |
| $f_{gas,fhs}$ | fraction of dust produced in node n released into carrier gas [user input] |
| $f_{pebble,fhs}$ | fraction of dust produced in node "n" remaining on the pebble [user input] |
| $f^{\ell}_{LO}$ | lumped liftoff constant [user input] |
| $\mathrm{G}$ | graphite |
| $\mathrm{g}$ | gravity constant (m/s$^2$) |
| $\mathrm{g_c}$ | mass to force conversion constant (kg-m/N-sec2) |
| $I^{G}_{t}$ | impurity level of isotope "t" in matrix graphite (mg/kg) |
| $I^{M}_{t}$ | impurity level of isotope "t" in metal dust (mg/kg) |
| $I^{G}_{comp,n,p}$ | impurity level of isotope "t" in matrix graphite in component node "n" (mg/kg) |
| $\mathrm{i}$ | Nuclide |
| $\mathrm{j}$ | precursor nuclide for absorption reaction |
| $k$ | phase number or precursor nuclide for decay reaction |
| $L$ | liftoff coefficient |
| $L_{m}$ | particle fractional liftoff rate in node m (1/m.d) |
| $L_{n}$ | fractional removal rate of deposited particle mass per unit length in node "n" (1/m.d) |
| $L_{n'}$ | length of node "n" (m), |
| $L^{G}_{t,n'}$ | liftoff rate of isotope "t" contained in graphite dust in node *n* (kg/m.d) |
| $L^{M}_{t,n'}$ | liftoff rate of isotope "t" contained in metal dust in node *n* (kg/m.d) |

| Symbol | Definition |
|---|---|
| $L_n = L_{lo}^{p}$ | particle fractional liftoff rate in node n (1/m.d) |
| $l_0$ | FHS pipe length (m) |
| $l_i$ | length of node “i” (m) |
| $l_n$ | length of node “n” (m) |
| $l_{core,n}$ | Core node length (m) |
| $M_{Core}^{G}$ | graphite dust mass in the core (kg) |
| $M_{FHS}^{G}$ | graphite dust mass in FHS (kg), |
| $M_{FHS}^{M}$ | metal dust mass in FHS (k |
| $M_{comp}^{M}$ | metal dust mass in the component (kg) |
| $\dot{M}_{comp}^{n}$ | mass flow rate for component in node “n” (kg/s) |
| $m$ | precursor isotope |
| $m_{comp,n,k}$ | mass of FP k in graphite component comp, node n (kg) |
| $m_p$ | particle mass (kg) |
| $\dot{m}_{gn}$ | fluid mass flow rate in node “n” (kg/s) |
| $m_{t'}^{C}$ | mass of isotope t’ in He coolant C (kg) |
| $m_{comp,n,k}^{C}$ | FP mass in coolant (He) in component comp, in node n for FP k (kg) |
| $m_{comp,n,k}^{C'}$ | equilibrium mass of FP k in coolant (He) component comp, node n (kg) |
| $m_{n'}^{G}$ | mass of isotopes in graphite in node n’ (kg) |
| $m_{n',p}^{G}$ | mass of isotopes in graphite in node n’ for particle size p (kg) |
| $m_{comp,n}^{G}$ | dust particle mass in graphite in component comp, in node n (kg) |
| $m_{comp,n,p}^{G}$ | FP mass in graphite in component comp, in node n for particle size p (kg) |
| $m_{comp,n,p,k}^{G}$ | mass of FP k in graphite component comp, node n for particle size p (kg) |
| $m_{comp,n,k}^{G}$ | FP mass in graphite in component comp, in node n for FP k (kg) |
| $m_{comp,n,k}^{G'}$ | equilibrium mass of FP k in graphite component comp, node n |
| $m_{comp,n,p,k}^{G'}$ | equilibrium mass of FP k in graphite component comp, node n for particle size p |

| Symbol | Definition |
|---|---|
| $m^{G}_{sphere,n}$ | mass of graphite sphere in node n (kg) |
| $N$ | total number of phases |
| $N_i$ | mass of activation nuclide “i” mass (kg) |
| $N_k$ | density for FP k (nMole/kg) |
| $N_{pi}$ | atomic density of precursor p (atoms/m$^3$) |
| $N_t$ | target isotope mass (kg) |
| $N^{core}_{fuel}$ | number of fuel pebbles in the core |
| $N^{d}_{fuel}$ | number of fresh fuel pebbles required (1/d) |
| $N^{fuel}_{z,n}$ | number of fuel spheres in component z in node n |
| $N^{G}_{t}$ | mass of target nuclides in graphite dust (kg) |
| $N^{M}_{t}$ | mass of target nuclides in metal dust (kg) |
| $n$ | node |
| $n_f$ | number of control volume faces |
| $n'$ | target, activation, and fission product particles |
| $P$ | linear mass production rate (kg/d) |
| $P_{comp,n,p}$ | total dust production rate in the n$^{th}$ component for particle size “p” (kg/m.a) |
| $P_{fhs,n}$ | dust mass produced in node “n” of FHS (kg) |
| $P_{He}$ | helium pressure (MPa) |
| $P_n$ | surface dust production in node “n” (kg/d) |
| $P_{rel}$ | relative power to full power |
| $\dot{P}_{c,n}$ | production rate from the component node |
| $P^{C}_{n}$ | particle production rate into circulating helium in node “n” (kg/m.d) |
| $P^{D}_{n}$ | particle production rate on the deposited layer in node “n” (kg/m.d) |
| $P^{G}_{comp,n,p}$ | graphite dust production rate in the n$^{th}$ component for particle size “p” (kg/m.d) |
| $P^{G}_{FHS,n,p}$ | graphite dust particle “p” production rate in node “n” of FHS (kg/d) |
| $P^{G}_{z,n,p}$ | graphite dust particle “p” production rate at height “z”, node “n” (kg/m.d) |

| Symbol | Definition |
|---|---|
| $P^{M}_{comp,n,p}$ | metal dust particle “p” production rate in component node “n” (kg/m.d) |
| $P^{M}_{FHS,n,p}$ | metal dust particle “p” production rate in node “n” of FHS (kg/d) |
| $p$ | Dust particle size |
| $p_i$ | decay precursors for isotope “i" |
| $p_n$ | number of passes in operating regime |
| $Q^{p}_{mat}$ | activation energy for particle “p” on material “mat” (kJ/mol) |
| $R_i$ | gamma decay rate (kg/s) |
| $R_{FHS}$ | fractional removal rate from FHS (1/d) |
| $R_j$ | removal terms from the component node ($m^3$/d) |
| $R_N$ | Reynolds number |
| $R^{C}_{comp,n,k}$ | fractional removal rate of FP k from coolant (He) in component comp, in node n (1/d) |
| $R^{G}_{comp,n,k}$ | fractional removal rate of FP k from graphite dust in component comp, in node n (1/d) |
| $r_c$ | rotor radius (m) |
| $S$ | deposition coefficient |
| $S_{bm}$ | surface area of the component node base material ($m^2$) |
| $S_{dust}$ | surface area of deposited dust in component node ($m^2$) |
| $S_i$ | individual gain terms from all the processes discussed in Sections F.4 through F.8 (fraction) |
| $S_n$ | circulating particle deposition rate in node “n” ($m^3$/m.d) |
| $S_{pk}$ | source (kg/$m^3$. d) in “k” phase |
| $S^{G}_{t,n'}$ | deposition rate of nuclide in graphite dust (kg/d) |
| $S^{M}_{t,n'}$ | deposition rate of nuclide in metallic dust (kg/d) |
| $T_{He}$ | helium temperature (K) |
| $t$ | target isotope |
| $t_p$ | time per fuel pass in FHS (s) |

| Symbol | Definition |
|---|---|
| $t'$ | target, activation, and fission product particles |
| $t''$ | refers to the volumes feeding into volume $n'$ |
| $u_k$ | gas velocity (m/s) |
| $V_n$ | volume of node "n" ($m^3$) |
| $\dot{V}_n$ | fluid volume flow rate in node "n" ($m^3$/d) |
| $\dot{V}_{t'}$ | target isotope t' volumetric flow rate ($m^3$/d) |
| $V^C_{comp,n}$ | dust particle volume in coolant (He) in component comp, in node n ($m^3$) |
| $V^G_{comp,n}$ | dust particle volume in graphite in component comp, in node n for FP k ($m^3$) |
| $V^R_z$ | relative volume of core channel "z" ($m^3$) |
| $v_c$ | circulator rotor velocity (m/s) |
| $v_{g,n}$ | fluid flow velocity in node "n" (m/s) |
| $\alpha_k$ | volume fraction of the $k^{th}$ phase |
| $\alpha_{Henry}$ | Henry's sorption partition coefficient |
| $\alpha_{Freundlich}$ | Freundlich's sorption partition coefficient |
| $\alpha_{S,k}$ | partition coefficient of fission products between graphite and coolant for FP k (dimensionless) |
| $\beta_{ij}$ | branching ratio of isotope "i" from reaction "j" |
| $\beta_t$ | delayed neutron fraction |
| $\Gamma_{lk}$ | mass exchange between phases "l" and "k" |
| $\delta^F_n$ | fractional fuel movement (fraction of fuel) in node "n" (1/m.d) |
| $\delta^G_t$ | solid target isotope plateout onto graphite dust (kg/d) |
| $\delta^G_{t'}$ | plateout rate of isotope "t" onto graphite dust (kg/d) |
| $\theta_H$ | hydraulic angle (radians) |
| $\theta^n_d$ | component deposition angle in node "n" (degrees) |
| $\lambda_i$ | decay constant of nuclide "i" (1/s) |
| $\lambda_j$ | decay constant of precursor "j" (1/s) |
| $\lambda_t$ | decay constant of target isotope "t" (1/s) |

| Symbol | Definition |
|---|---|
| $\boldsymbol{\lambda_p}$ | decay constant of precursor "p" (1/s) |
| $\boldsymbol{\Pi_{c,n}}$ | circulating particle densities or deposited mass in each node. (kg/m$^3$) or (kg) |
| $\boldsymbol{\rho_G}$ | density of graphite dust (kg/m$^3$) |
| $\boldsymbol{\rho_g}$ | fluid density (kg/m$^3$) |
| $\boldsymbol{\rho_k}$ | density of precursor isotope "k" (kg/m$^3$) |
| $\boldsymbol{\rho_{n'}}$ | fluid density in node *n* (kg/m$^3$) |
| $\boldsymbol{\rho_p}$ | particle density (kg/m$^3$) |
| $\boldsymbol{\rho^C_{comp,n,k}}$ | FP density in coolant (He) component comp, in node n for FP k (mole/m$^3$) |
| $\boldsymbol{\rho^G_{comp,n,k}}$ | FP density in graphite in component comp, in node n for FP k (mMole/kg) |
| $\boldsymbol{\sigma_m}$ | precursor isotope one-group neutron capture cross section (cm$^2$) |
| $\boldsymbol{\sigma_n}$ | microscopic cross section in node "n" (b) |
| $\boldsymbol{\sigma_t}$ | target isotope one-group neutron capture cross section (cm$^2$) |
| $\boldsymbol{\phi}$ | 1-group neutron flux (neutrons/cm$^2$-s) |
| $\boldsymbol{\Phi}$ | scaling coefficient [user input] |
| $\phi_n$ | 1-group neutron flux in node "n" (neutrons/cm$^2$-s) |
| $\omega_t^G$ | graphite sorption rate for target isotopes (kg/d) |
| $\boldsymbol{\omega^G_{t'}}$ | sorption rate of isotope "t" from graphite dust (kg/d) |
| $\nabla$ | divergence operator |

## F.1 Introduction

As discussed in Section 3.2, the functional containment system is a collection of five radionuclide (RN) release barriers, designed to limit RN release from the core to the environment to very low levels during normal operation and a broad spectrum of DBAs, References 1 and 2. These barriers, together with the main phenomena and processes involved in radionuclide production, retention, transport, and release for a pebble bed reactor are depicted in Figure 3 of this Topical Report.

The Helium Pressure Boundary model (HPBM) calculates the mass balance of radionuclides and dust in the helium pressure boundary (HPB) using dust production and radionuclide release rates as well as their time-dependent transport, activation, plateout, and re-entrainment through all HPB components. The model also calculates releases into the RB in the event of a leak in the HPB.

## F.2 Theory and Methodology

The HPBM is an integrated effects model based on principles similar to those described in the Dust and Activity Migration and Distribution (DAMD) code [F-1].

The model calculates the plated-out particle mass and circulating particle concentration in each component of the pebble bed HTR. As described in Section F.2.1, each component in the HPB is divided into several nodes. The DUSTM model provides the dust generation rates in the core, FHS and RCS to the HPBM model. Fission product release rates calculated by the GASM and/or SOLM model(s) are also required inputs.

Graphite and metallic dust are generated due to friction forces between the fuel pebbles and other components. The helium coolant carries the entrained particles from the surface of the fuel pebbles and components in the gas stream to different components in the HPB. The processes and phenomena considered are modelled in each component's node and include:

- Sources
- Deposition
- Re-entrainment
- Transport
- Activation
- Depletion
- Radioactive decay
- Sorption into the graphite dust

[[

]]$^{P}$ The processes and phenomena together with the computational domain are shown in Figure F-1 through Figure F-3.

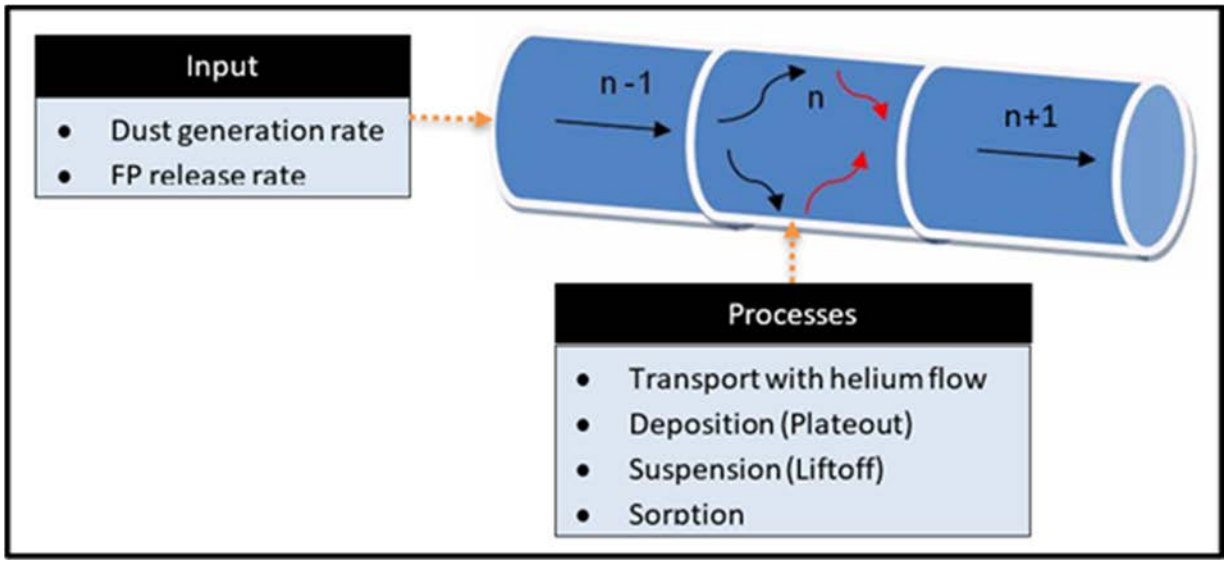


***Figure F-1: Production, Transport, and Mass Balance***

[[

]]$^{P}$

***Figure F-2: Processes and Phenomena***

[[

]]$^{P}$

***Figure F-3: Migration Models***

Governing equations for the rate of change of the plated-out particle mass and circulating particle concentration consist of loss, gain, and source terms. The foundation of these equations is conservation of mass theory for multi-phase flow systems based on first principles. The governing equations contain the rate of deposition and re-entrainment coefficients expressed as correlations. These correlations contain calibrated parameters as noted in Figure F-3. The calibration is performed with AVR operating experience and other experimental data as described in Section F.2.5.

### F.2.1 Computational Domain

Each HPBM component such as the core, hot leg and circulators is modelled in 1D and divided into nodes. Required component properties are listed in Table F-1 and numerical calculations performed on a 1D computational domain shown in Figure F-4.

***Table F-1: HPBM Component Input Parameters***

[[

]]$^{P}$

***Figure F-4: Computational Domain for Components in the HPBM***

## F.2.2 Modelling Approach

This subsection provides an overview of the HPBM modelling approach and assumptions with specific focus on the modelling of radionuclide and dust behavior within the HPB. Detailed descriptions are presented in the following sub-sections.

The main drivers of radionuclide production within the HPB of a typical pebble-bed HTR are:

- Graphite and metallic dust is produced in the core, FHS and RCS due to the movement of fuel pebbles and control rods during operations. The DUSTM model calculates the dust production that results from mechanical wear such as pebble-to-pebble and pebble-to-reflector interactions in the core, pebble-to-pipe interactions in the fuel handling system (FHS), and control rod-to-reflector interactions in the reactivity control system (RCS). These production rates are passed to the HPBM model where the dust is transported by means of the helium heat transfer fluid into the HPB components where the effects of dust on source terms are quantified.

- Radionuclide release rates from fuel pebbles, mostly from heavy metal contamination on the side reflector and fuel-element matrix, and failure probability of the TRISO-coated particles.
- Activation of the circulating nuclides in the core, including fission products released from the fuel pebbles and impurities in the helium.

The main drivers of radionuclide distribution within the typical pebble-bed HTR HPB are:

- Transport of nuclides as atomic species within the helium and the deposition of these radionuclides on metallic surfaces and already deposited dust.
- Migration of dust in the helium due to deposition and liftoff of nuclides attached to the dust.
- Migration of dust adhering to the fuel pebbles circulated through the core and fuel handling system.

Many physical factors are involved in the deposition and liftoff of dust ranging from helium flow distribution, gravitational forces, surface roughness of materials, thermophoresis, pipe vibrations, and particle charges in addition to chemical interactions. The plateout of atomic species is driven by complex absorption and desorption mechanisms. Engineered SSCs that reduce the dust and helium impurity concentrations include dust filters and the helium purification system. Helium gas leakage from the pressure boundary also influence the radionuclide transport and distribution.

[[

]]$^{P}$

### F.2.3 Underlying Theory

The migration of dust and atomic species in a helium gas flow system is considered combined with nuclear production and removal processes as applicable. Transport of particles on the surfaces of fuel pebbles and graphite is also accounted. Mass transfer between particles circulating in the helium gas, graphite dust and component surfaces is simulated. The entrainment and deposition of particles is dependent on the forces acting on the particles as a function of time; assumptions are required due to the complexity of these forces. In a pebble bed HTGR, particles are subjected to many different time dependent forces such as gravity, Coulomb, Van der Waals, hydraulic, vibration, friction, and acoustical forces as well as thermopheresis effects, etc. [[

]]$^{P}$

The following physical phenomena are considered, either as input parameters or otherwise by direct or indirect calculation by the model:

- Migration of particles, which includes transport, liftoff and deposition, throughout the system via the helium as heat transport fluid
- Migration of particles attached to moving fuel pebbles during online fuel handling activities
- Plant thermodynamics (reactor inputs obtained from the THM model)
- Nuclear reactions such as activation and depletion of target isotopes and radioactive decay
- Core neutronics (in terms of flux distribution) and cross-sections
- Production of graphite dust particles due to abrasion of fuel pebbles (obtained from the DUSTM model),
- Production of metallic dust particles on the surface of metallic components
- Addition of external particle sources into a component's node
- Leakage or removal of particles from a component's node
- Leakage of fission products from fuel pebbles into helium gas (obtained from the GASM and/or SOLM models)
- Activation of constituents and impurities in the graphite reflectors and matrix graphite of pebbles
- Activation of constituents and impurities of metallic dust particles
- Activation of constituents and impurities in the helium gas
- Radioactive decay
- Forces acting on particles
- Liftoff rate of particles from a wetted surface
- Deposition rate of particles onto a helium-wetted surface or dust layer
- Sorption of fission product atoms between the helium gas and graphite surfaces
- Accumulation of particles on helium-wetted surfaces
- Metallic and solid fission product plateout on component surfaces

The principles of the migration behavior of particles in an HTGR according to this methodology are depicted in Figures F-1 and F-5.

In Figure F-1, the particle's plateout and liftoff described in Section F.4 is depicted. Gas flowing from $V_{n-1}$ into $V_n$, carries a concentration $C_{n-1}$, of the particle under consideration. In volume $V_n$, some of the particles are deposited on the surface of $V_n$ at a rate of $S_n$ and some are lifted off from the surface at a rate of $L_n$. These gain and loss terms are shown in Equations F-4.1 and F-4.2 respectively. Equations F-4.1 and F-4.2 include another gain term, $P_n$, representing the dust particle production. Dust particle production is assumed to be on the surface layer, from where it can then be re-entrained into the carrier gas by means of the liftoff term, $L_n$. [[

]]$^{P}$

For atomic radionuclide transport, the complete physical phenomena are depicted and described in Figure F-5. Metallic fission products can be found in the following regions of the HPB:

- In the helium as the elemental radionuclides
- On the graphite dust layer (deposited or adsorbed)
- On the plant component surfaces (deposited)
- On the circulating graphite dust (deposited and adsorbed)

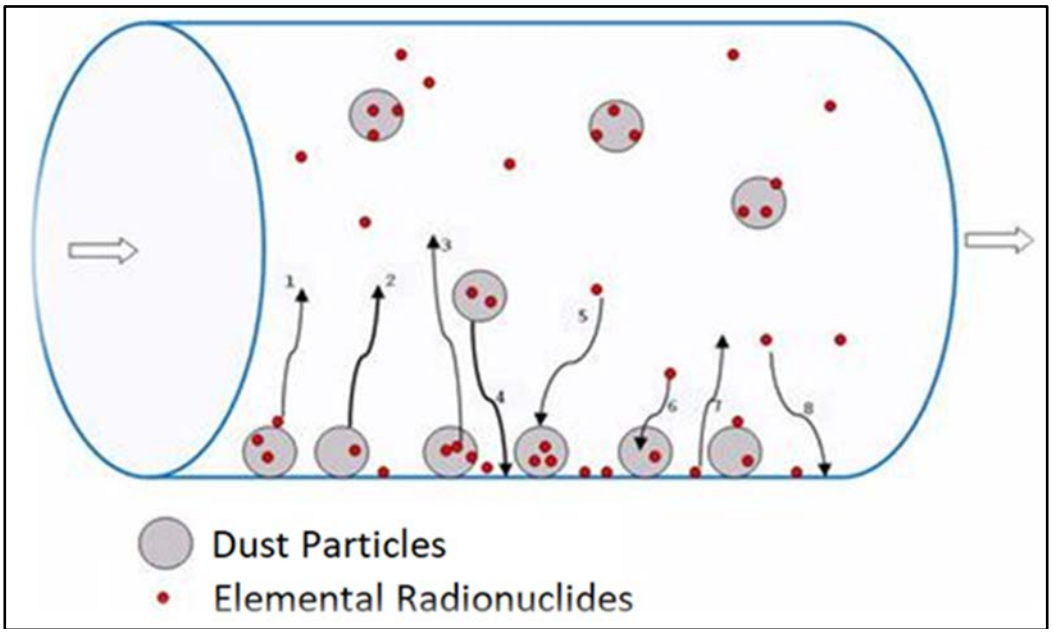


**(1)** Liftoff of elemental radionuclide from plated-out dust **(2)** Liftoff of plated-out dust from component surface **(3)** Sorption of elemental radionuclide from plated-out dust into helium **(4)** Plateout of entrained dust onto component surface **(5)** Plateout of entrained elemental radionuclide onto plated-out dust **(6)** Sorption of entrained elemental radionuclide into plated-out dust **(7)** Liftoff of elemental radionuclide from component surface **(8)** Plateout of elemental radionuclide onto component surface

***Figure F-5: Atomic Fission Product Transport and Mass Transfer Mechanisms***

In this methodology, particle migration by means of the helium gas is assumed to depend on the particle size, i.e., the migration behavior of smaller particles may differ from those of larger particles. Therefore, multiple particle size distributions for graphite and metallic dust are considered, see Table F-2.

In a pebble bed reactor, pebbles move continuously from the top of the core towards the bottom. This movement of pebbles is one of the main contributors of dust production in the reactor. The discrete dust particles will form a layer on the fuel pebble surfaces. Some of these particles may adhere to the pebble during the movement of the pebble through the core or the FHS. A fraction of the particles will therefore migrate on the fuel surfaces and eventually become retained in the Spent Fuel Tank (SFT).

Graphite and metallic dust particle production on the surface of fuel pebbles and reactor components such as graphite reflectors can be entrained into the helium heat transfer fluid. Dust particles are modelled with a [[ ]]$^{P}$ distribution of [[ ]]$^{P}$ bin sizes normalized to the total dust production from the DUSTM model. [[

]]$^{P}$

***Table F-2: HPBM Dust Particle Distribution***

[[

]]$^{P}$

## F.2.4 Methodology

The inter-related processes and phenomena described in Section F.2.3 are integrated into a methodology used for the estimation of the respective source terms in the Xe-100 HPB. Each plant component can be sub-divided into one-dimensional nodes (control volumes) connected in series or in parallel.

The following are the most important process information and data used in building a plant model using the HPBM model methodology:

- Helium mass flow rate, temperature, and pressure distributions
- Component surface temperature
- Volume, surface area and hydraulic diameter of each control volume
- Helium impurities and component materials
- Neutron flux and power distribution
- Nuclear data such as microscopic cross-sections, fission yields and decay constants
- Fuel management scheme (fresh fuel per Effective Full Power Days (EFPD), number of fuel passes)
- Operating history (proposed or historic)
- Graphite and metallic dust production rates
- Fission product release rates from fuel pebbles

Much of the required information is obtained from the suite of integrated models addressed in this LTR. Each node is modelled with a set of coupled differential equations describing the mass conservation and transfer phenomena under the prevailing node conditions. Neighboring nodes are coupled through helium flow and in the case of the core, FHS and SFT through the movement of fuel pebbles. An integrated plant system model is created and the time dependent mass distribution of particles throughout the system determined by means of a numerical solver. For radioactive particles, the activity levels are determined from the particle's mass distribution.

## F.2.5 Calibration of the HPBM Model Using AVR Data

To calibrate the HPBM transport models described in Section F.2.3, publicly available data [F-2] from the [[ ]]$^{P}$ AVR plant were used. [[

]]$^{P}$

## F.3 Methodology Assumptions and Simplifications

The HPBM methodology assumptions, grouped into processes and phenomena, are listed below.

### F.3.1 Plant Geometry

- A one-dimensional geometry is considered for all components with a helium-wetted surface area.
- A coarse linear nodalization is employed [[
  ]]$^{P}$
- The core is described by five parallel flow channels ignoring cross flow.

### F.3.2 Transport

- [[

]]$^{P}$

### F.3.3 Mass Transfer

- [[

]]$^{P}$

### F.3.4 Forces Acting on Particles

- [[

]]$^{P}$

### F.3.5 Particles

- All particle shapes are assumed to be spherical.
- [[

]]$^{P}$

- Atomic particle size is calculated for all atoms.

### F.3.6 Thermodynamics

- Power densities, profiles, fuel temperatures and neutron flux profiles are inputs from the THM model.
- [[

]]$^{P}$

- Since this is a 1D model, no He cross-flow effects are accounted for.
- The mass flow rate for each plant component for an operating period is determined based on reactor outlet temperature (ROT) and core power. ROT and core power are assumed to be fixed for the duration of the operating period if steady state operation is assumed.
- Core transients can be simulated if the core power and power distribution versus time are known. Decay heat transients can be calculated with inputs from THM model.
- [[

- 

]]$^{P}$

### F.3.7 Reactor Physics

- A one-group neutron flux distribution is employed. [[
]]$^{P}$
- One-group neutron cross-sections are used. [[

]]$^{P}$

### F.3.8 Numerical Solver

- A Modified Gauss Backward Iterative Implicit method is used to solve the transport and mass transfer equations.

### F.3.9 Fission Product Release Rates

Fission product release rates are generated from a chain of calculations based on neutronics, fuel performance, thermodynamics, and isotope release models THM, FPM, GASM, and SOLM. This calculation chain is performed at various stages of reactor operation to reflect the time dependencies of fission product release rates introduced by different fuel compositions in the core, core temperature distributions, the inventory build-up and delays in release caused by fission product retention in fuel pebble layers and matrix material. [[

]]$^{P}$

### F.3.10 Plateout Fraction

- Metallic fission product plateout is assumed to take place proportional to the bare component surface area available. The balance of the metallic fission products are deposited on dust and follow the dust migration and mass transfer behavior. As dust is accumulated on the surface the exposed bare surface area is reduced. Once a component surface area is fully covered by a mono-layer of dust or more, no further plateout on the bare material in that location is assumed possible. [[

]]$^{P}$

### F.3.11 Dust Production

- Graphite dust production rate in the core and in the FHS is obtained from the DUSTM model.
- [[

]]$^{P}$

### F.3.12 Dust Filters

- In calculations where dust filters are present, a filter efficiency is defined where all particles with a diameter larger than that of the capture size will be fully removed from the helium [[ ]]$^{P}$ Smaller particles will experience the normal liftoff and deposition behavior relevant to the dust filter inputs.

## F.4 Production and Transport

The production and transport of species (radionuclides and dust particles) by means of the helium heat transport fluid is modelled by a set of coupled first order linear differential equations [[

]]$^{P}$

**Deposition:** Equation F-4.1 describes the rate of change of the deposited particle mass per unit length of a node in the component. [[

]]P

**Circulation:** Equation F-4.2 describes the rate of change of the circulating particle mass per unit length of a node in the component. [[

]]$^{P}$

## F.5 Forces Acting on a Particle

In the HPBM model, the liftoff or re-entrainment, and the deposition behavior are dependent on the forces acting on the particle. The liftoff and deposition rates are directly proportional to the resultant force acting on the particle. In a pebble bed HTGR plant, different forces can be present at any given time such as gravity, Coulomb, Van der Waals, hydraulic, vibration, acoustical and thermophoresis forces/effects. If all the forces acting on a particle were known at all times, it would be possible to establish its transport behavior, but in reality, the magnitude of most these forces as a function of time, plant/component condition and location are unknown or include large uncertainties.

Well known forces such as gravity can be explicitly included in the deposition and adhesive force equations. Forces of unknown magnitude are lumped together, either as a deposition force or a liftoff force. A simplified modelling approach is used in HPBM for both deposition and liftoff forces.

### F.5.1 Adhesive Force

Based on observations and experience [F-1], it is reasonable to expect that a particle deposited onto a surface will experience some degree of adhesion to the surface. The adhesion may be the result of surface and/or particle roughness, electrostatic forces, or chemical bounding and thus depend on the particle's and surface's properties. [[

]]$^{P}$

### F.5.2 Deposition Force

Under certain conditions, circulating particles can settle on component surfaces. One such condition is the bonding force between the particle and the surface. Generally, gases do not have such a bonding force and will not settle on the surface of the components. Other particles such as the condensable radionuclides and dust particles do experience bonding forces and will settle if there is a deposition

force (from entrained phase to deposited phase) present. This section discusses the deposition forces considered in HPBM. These forces are added together to create a total deposition force on a particle in each of the plant component's nodes.

### F.5.2.1 Gravity Deposition Force

The gravity deposition force of the particle onto a component surface depends on the angle of the component node. In HPBM, a vertical component node will experience a zero-gravity deposition force. [[

]]$^{P}$

### F.5.2.2 Hydraulic Deposition Force

The hydraulic deposition force is related to the force that a particle will experience due to fluid flow. The assumption is that larger particles will be subjected to a larger force than smaller particles. [[

]]$^{P}$

### F.5.2.3 Total Deposition Force

The total deposition force is the sum of the gravity, hydraulic, and lumped deposition forces. The lumped deposition force contains all the deposition forces that cannot be explicitly modelled. [[

]]$^{P}$

## F.5.3 Liftoff Force

In HPBM, it is assumed that a particle can only be removed from a component surface once the liftoff (shear) force on the particle exceeds the total adhesion force between the particle and the surface. This section describes the liftoff forces included in the model.

[[

]]$^{P}$

### F.5.3.1 Transient Force

A deposited particle can experience a transient force from gas acceleration between two adjacent nodes. [[

]]$^{P}$

### F.5.3.2 Hydraulic Lift Force

A particle will experience a hydraulic liftoff force from the fluid flow. It is assumed that larger particles are subject to a larger force than smaller particles. [[

]]$^{P}$

### F.5.3.3 Centrifugal Lift Force

A centrifugal force is included in the circulator components where the circulator rotor speed is used to calculate the force on particles attached to the rotors. [[

### F.5.3.4 Total Liftoff Force

The total liftoff force, Equation (F-5.7) acting on a particle is the sum of all the individual liftoff forces and is used to determine the liftoff rate of the deposited particles from the component surface:

[[

]]$^{P}$

## F.6 Dust Production, Mass Transfer and Migration Theory

At a given time, any particle in the HPB is either attached to a helium-wetted surface or entrained in the cooling gas. Transport of particles attached to the surface of fuel pebbles is accounted as those particles can be transported with the pebbles. Atomic particles can be attached to graphite dust particles and thus migrate with the graphite dust particles. The behavior of all particle types at any point in time is dependent on the forces acting on these particles, and the net force on a particle determines its state of motion.

### F.6.1 Dust Migration and Deposition

The derivation of the equations for concentration of circulating dust and its deposited mass is provided in this section. The computational domain consists of helium gas, entrained particles, and deposited particles. The behavior of the circulating and deposited dust is described by conservation of mass for multi-phase flow. For each volume, $\alpha_k$ is the volume fraction of the $k^{\text{th}}$ phase and $N$ the total number of phases. Thus, $\sum_{=1}^{N} \alpha_k = 1$. The mass conservation for the k-th phase is therefore:

$$\frac{\partial \alpha_k \rho_k}{\partial t} + \nabla \cdot \alpha_k \rho_k \mathbf{u}_k = \sum_{l=1, l \neq k}^{N} \Gamma_{lk} + S_{p_k} \qquad \text{(F-6.1)}$$

Where:

$\alpha_k =$ volume fraction of the $k^{\text{th}}$ phase,

$\rho_k =$ density (kg/m$^3$),

$\mathbf{u}_k =$ gas velocity (m/s),

$S_{pk} =$ source (kg/m$^3$.d),

$\Gamma_{lk} =$ mass exchange between phases "$l$" and "$k$",

$\nabla =$ div operator,

$k =$ phase number [=1 for helium gas, =2 for circulating dust, =3 for deposited dust], and

$N =$ total number of phases [=3].

The shared volume consists of three phases therefore, $N = 3$. Equation (F-6.1) then reduces to:

$$\begin{aligned} k=1: &\quad \frac{\partial \alpha_1 \rho_1}{\partial t} + \nabla \cdot \alpha_1 \rho_1 \mathbf{u}_1 = \Gamma_{12} + \Gamma_{13} + S_{p_1} \\ k=2: &\quad \frac{\partial \alpha_2 \rho_2}{\partial t} + \nabla \cdot \alpha_2 \rho_2 \mathbf{u}_2 = \Gamma_{21} + \Gamma_{23} + S_{p_2} \\ k=3: &\quad \frac{\partial \alpha_3 \rho_3}{\partial t} + \nabla \cdot \alpha_3 \rho_3 \mathbf{u}_3 = \Gamma_{31} + \Gamma_{32} + S_{p_3} \end{aligned} \qquad \text{(F-6.2)}$$

[[

]]$^{P}$

The volumetric flow rate is calculated as follows:

$$\dot{V}_n = \frac{\dot{M}^K_{comp}}{\rho_n}, \quad K = 1...N \tag{F-6.40}$$

From the above equation, the velocity of the gas is determined as:

$$\mathbf{u}_n = \frac{\dot{V}_n}{A_n} \tag{F-6.41}$$

Where:

$A_n$ = flow area (m$^2$).

[[

]]$^{P}$

## F.6.2 Transport of Particles on Pebble Surface

In a pebble bed reactor, online refueling transports fuel pebbles continuously from the top of the core towards the bottom. This movement of pebbles is one of the main sources of dust production in the reactor. The loose dust particles will form a layer on the fuel pebble surfaces. Some of the particles on the fuel surface may adhere to the pebble during movement through the core or the FHS. A fraction of the particles will adhere to the fuel pebble surface and end up in the Spent Fuel Tank (SFT). The HPBM calculation of particles retained on the fuel surfaces is described by equations representing the fraction of particles removed from a control volume by means of the pebble movement.

### F.6.2.1 Particle Transport from Core to FHS

**Dust Removal from the Core**: [[

]]P

**Dust Fraction from Core to FHS**: [[

]]P

### F.6.2.2 Particle Transport from FHS to the Core

In HPBM, particles on the surface of fuel pebbles entering and in the FHS volume are subjected to the following behavior:

- A fraction can remain on the surface and will be returned to the core.
- A fraction can be removed into the FHS volume.
- Dust can be generated in the FHS volume by pebble movement through the FHS lines where:
    - A fraction of the dust produced will attach to the fuel line surface.
    - A fraction may remain on the fuel pebble.
    - A fraction may entrain into the gas volume of the fueling line.

- Particles in the FHS volume can be transported into the core (or a dust filter loop if present) as part of the carrier gas during the time the FHS is in use.

**FHS Dust Deposition Factor:** As the fuel pebble moves through the FHS line to be reloaded at the top of the core, a fraction of dust on its surface will be deposited on the fuel line surface as it contacts the sides of the line. [[

]]$^{P}$

**FHS Flow Time Fraction:** It is assumed that the carrier gas flow through the FHS would not be continuous but only be activated when a fuel pebble is transported from the bottom to the top. [[

]]$^{P}$

**Dust Fraction from FHS to Core:** [[

]]$^{P}$

Dust generated in the FHS from pebble movements can experience one of three processes, namely:

a. Dust mass (kg) generated and retained on the fuel pebble during its transit in the FHS is given by Equation (F-6.50): [[

]]$^{P}$

b. Dust mass (kg) generated and released directly into the FHS carrier gas during pebble transit in the FHS is given by Equation (F-6.51): [[

]]$^{P}$

c. Dust mass (kg) generated and deposited on the FHS fueling line surface during its transit in the FHS is given by Equation (F-6.52): [[

]]$^{P}$

## F.7 Fission and Activation Product Production, Mass Transfer and Migration Theory

### F.7.1 Fission Product Migration Equations

The transport models for target and activation isotopes are given. Four more phases are included, namely, the entrained and deposited isotopes for both *target* and *activation* isotopes.

The conservation of mass for helium gas ($k = 1$) given in Equation (F-6.5) is rewritten to include the mass transfer terms $\Gamma_{14}$ and $\Gamma_{15}$:

$$\frac{\partial \alpha_1 \rho_1}{\partial t} + \nabla \cdot \alpha_1 \rho_1 \mathbf{u}_1 = \Gamma_{12} + \Gamma_{13} + \Gamma_{14} + \Gamma_{15} + S_{p_1} \tag{F-7.1}$$

The mass transfer terms $\Gamma_{12} = \Gamma_{13} = \Gamma_{14} = \Gamma_{15} = 0$ because no mass transfer occurs from phase one to phases two, three, four and five. Equation F-7.1 then reduces to Equation (F-6.5). For $k = 4$ (entrained target isotopes) and $k = 5$ (deposited target isotopes) the general form of the conservation of mass is:

$$\frac{\partial \alpha_4 \rho_4}{\partial t} + \nabla \cdot \alpha_4 \rho_4 \mathbf{u}_4 = \Gamma_{41} + \Gamma_{42} + \Gamma_{43} + \Gamma_{45} + S_{p_4} \tag{F-7.2}$$

$$\frac{\partial \alpha_5 \rho_5}{\partial t} + \nabla \cdot \alpha_5 \rho_5 \mathbf{u}_5 = \Gamma_{51} + \Gamma_{52} + \Gamma_{53} + \Gamma_{54} + S_{p_5} \tag{F-7.3}$$

[[

]]$^{P}$

**Equations F-7.24 and F.7.25 not used**

### F.7.2 Activation of Constituents and Impurities

The HPBM model can use a one-group neutron flux in any of the axial nodes of any plant component included in the model. Any isotope having a non-zero one-group microscopic absorption cross-section present in a component node with a non-zero one-group neutron flux can be activated. The presence of isotopes can be modelled as free flowing atomic (or molecular) particles, impurities or constituents of graphite or metallic dust particles carried in the helium gas. Isotopes in graphite and metallic dust deposited on the wetted surfaces of components and plated-out atomic particles are also accounted for activation. Impurities in the helium gas are also considered. The one-group neutron flux and microscopic cross-section data is obtained from VSOP, MCNP and Oak Ridge Isotope Generation (ORIGEN) calculations.

The code uses the modified Gauss backward iterative implicit method for solving the isotope inventories in each component node. Activation gains and losses through neutron capture reactions and gamma decay are therefore treated as either a loss or a gain term as applicable. Standard nuclear physics equations are used for activation and decay.

**Activation Isotope Production Rate:**

$$A_i = N_i \sigma_i \phi \quad \text{(F-7.26)}$$

Where:

$A_i =$ production rate (kg/s), and

$N_t =$ target isotope mass (kg).

**Activation Isotope Gamma Decay Rate:**

$$R_i = -\lambda_i N_i \quad \text{(F-7.27)}$$

Where:

$R_i =$ gamma decay rate (kg/s),

$N_i =$ activation isotope mass (kg), and

$\lambda_i =$ activation isotope decay constant ($s^{-1}$).

### F.7.2.1 Neutron Activation Chains

The transport of metallic fission or activation products of radiologically significant nuclides generated in the reactor are analysed. Key radionuclides are selected based on the combination of their fission yield, their transport and release properties and the radiological hazard level. The radiologically most relevant radioisotopes monitored during DBA simulation testing include [[

]]$^{P}$ Additional nuclides may be considered depending on the expected fuel conditions.

The release and transport behaviour of the radionuclides are strongly dependent on the fuel temperature. A diffusion transport model is applied in the SOLM model to calculate the radionuclide distribution in the TRISO-coated particles and fuel pebbles, and the release rates from the fuel surfaces into the helium heat transfer fluid. The GASM model calculates the gaseous fission product release from the fuel elements into the helium gas under steady state conditions, using Richards or Roellig models, Appendix D. Both the GASM and SOLM models integrate with data such as fuel temperature, burnup and fluence levels from the THM model and failed particle fractions from the FPM model. The resulting release rates are used in the HPBM model to develop the radionuclide behaviour calculations in the HPB. [[

]]$^{P}$

***Table F-3: Activation Chains***

[[

]]P

### F.7.2.2 Neutron Activation of Graphite Dust

To determine the initial target isotope mass in graphite dust, the level (mg/kg) of the target isotope in the fuel matrix is specified. All new fuel added to the core will start with the specified impurity level of the target isotope. The target isotope contained in dust will depend on the migration history of the dust and will migrate according to one of the following mechanisms:

- In the bulk of the fuel pebble (i.e., not as dust)
- As dust attached to the surface of the fuel pebble
- As dust deposited on the component wetted surfaces
- As circulating dust

[[

]]$^{P}$

### F.7.2.3 Neutron Activation of Metallic Dust

Activation of metallic dust impurities is treated similarly to graphite dust activation, except that new pebbles loaded do not play a role as a source for metallic dust impurities as for graphite dust. [[

]]$^{P}$

## F.7.3 Radioactive Decay

Equation (F-7.39) is the general expression for the radioactive decay rate where $p_i$ denotes the decay precursors for isotope i. For all radioactive isotopes considered in the HPBM model, the decay is treated in the numerical solution of the isotope concentration as a simple removal term, $\lambda_i$, in the Backward Explicit-Implicit Iterative Method in the denominator while the decay precursors are included as gain terms.

$$\frac{dN_i}{dt} = -\lambda_i N_i + \sum_{p_i=1}^{P} \lambda_{p_i} N_{p_i} \quad \text{(F-7.39)}$$

Where:

$p_i$ = decay precursors for isotope I,

$N_{p_i}$= atomic density of precursor $p_i$ (atoms/m$^3$), and

$\lambda_p$= decay constant for precursor $p_i$ (1/s).

### F.7.4 Sorption of Atoms on Graphite Dust

The sorption of fission products is modelled in accordance with the theory described [[ ]][P]. It is based on the ideal gas law where an isotherm is defined to describe the ratio of fission product concentration in the helium gas to the concentration in the graphite surface layer, namely,

[[

]]$^{P}$

The transition of fission products between the gaseous and graphite volumes can be considered instantaneous, i.e., the concentration levels are always in equilibrium. In the HPBM methodology the flow between the gas volume and the graphite material is considered in the typical source and loss approach adopted in the solver methodology. Isotopes flowing from the graphite dust to the helium gas are considered as a source for the fission product in the helium and as a loss for fission product in the graphite dust and vice versa in the case of fission product flow in the opposite direction. [[

]]$^{P}$

## F.8 Production of Dust Particles

### F.8.1 Graphite Dust Production in the Core

Graphite dust is produced in an online fueled pebble bed reactor from abrasion between fuel pebbles and between pebbles and core structures. A linear graphite dust production rate is provided by the DUSTM model. Graphite dust production in the core for a dust particle size with *P* bins over time $\Delta t$ is calculated as:

[[

]]$^{P}$

### F.8.2 Graphite Dust Production in the FHS

Graphite dust is also produced from abrasion between fuel pebbles and pebbles against the FHS structures. The graphite dust production per fuel pebble per pass is an input from the DUSTM model into the HPBM model. HPBM converts this input to a linear graphite dust production rate in the FHS. The dust production rate is used to calculate the graphite dust production particles remaining on the surface of the FHS structures in a spectrum of P bins over time $\Delta t$ as follows:

[[

]]$^{P}$

### F.8.3 Metal Dust Production in Metallic Components

Metal dust may be produced through various physical and chemical mechanisms such as friction, erosion, corrosion, carburization, etc. The metal dust production rate is an input from the DUSTM model into the HPBM model for the different metal component surfaces in the plant. The input is a linear metal dust production rate in each metal component. This metal dust production rate is then used to calculate the metal dust production for a dust particle spectrum with P bins in the component over time $\Delta t$ as follows: [[

]]$^{P}$

### F.8.4 Metal Dust Production in the FHS

Metal dust is also produced from abrasion between fuel pebbles and pebbles against the FHS structures. The current model provides for a FHS metal dust fraction [[

]]$^{P}$ The metal dust production per fuel pebble, per pass, is then calculated from FPM model input and the FHS metal dust fraction assumed. The HPBM model converts this to a linear metal dust production rate in the FHS. This FHS linear metal dust production rate is then used to calculate the metal dust production for a dust particle spectrum with P bins remaining on the surface of the FHS structures over time $\Delta t$ as follows: [[

]]$^{P}$

## F.9 Numerical Methodology

### F.9.1 Backward Explicit Implicit Iterative Method

The HPBM model calculates the circulating particle densities and deposited mass in each node by means of a backward implicit-explicit method expressed in the following equation [F-8]: [[

]]P

## F.10 Cross References and References

| Document Title<br>Cross References: X-energy documents that may impact the content of this document.<br>References: X-energy or other documents that will not impact the content of this document | | Document No. | Rev./ Date of Issuance | Cross Reference/ Reference |
|---|---|---|---|---|
| **F-1** | "PBMR Radionuclide Source Term Analysis Validation Based on AVR Operating Experience," C.C. Stoker, et al., Nuclear Engineering and Design.Mechanistic Source Term Roadmap, Nuclear Engineering and Design | | October, 2009 | Reference |
| **F-2** | Fuel Performance and Fission Product Behavior in Gas Cooled Reactors | IAEA-TECDOC-978 | November, 1997 | Reference |
| **F-3** | AVR- Experimental High-Temperature Reactor: 21 Years of Successful Operation For A Future Energy Technology | ISBN 3-18401015-5 | 1990 | Reference |
| **F-4** | Reactor Core Design for High-Temperature Gas-Cooled Reactors Part 1: Calculation of the Material Properties of Helium | KTA 3102.1 | 1978 | Reference |
| **F-5** | Software Certificate: Flownex SE | 001671 | 4 | Cross Reference |
| **F-6** | "Validation of the Plate-out Model in the RADAX code used for Plate-out and Dust Activity Calculations at PBMR," L. Stassen, PHYSOR 2006 | | September, 2006 | Reference |
| **F-7** | [[<br>]]$^{P}$ | [[<br>]]$^{P}$ | January, 2021 | Reference |
| **F-8** | Explicit and Implicit Methods in Solving Differential Equations | 119 | 2010 | Reference |

# Appendix G. Core Corrosion Model

## G.1. Abbreviations/Acronyms

| Short Form | Phrase |
|---|---|
| AGR | Advanced Gas Reactor |
| DBA | Design Basis Event |
| DLOFC | Depressurized Loss of Forced Circulation |
| FDDM | Fuel Design Data Manual |
| FIMA | Fissions per Initial Metal Atom |
| FP | Fission Products |
| GA | General Atomics |
| HTGR | High Temperature Gas Reactor |
| HPB | Helium Pressure Boundary |
| IG | Isotropic (Nuclear Grade) Graphite |
| ISI | In-Service Inspection |
| LBE | Licensing Basis Event |
| LEU | Low Enriched Uranium |
| NBG | Nuclear Block Graphite |
| ORNL | Oak Ridge National Laboratory |
| RN | RadioNuclide |
| SiC | Silicon Carbide Layer |
| SRDC | Safety Related Design Condition |
| TRISO | TRiple coated ISOtropic Particle |
| UCO | Uranium-Carbon-Oxygen |
| VSOP | Very Superior Old Programs |

## Definitions

| Symbol | Definition |
|---|---|
| A | empirical constant |
| $a_1$ | empirical constant (1/Pa) |
| $a_2$ | empirical constant (1/Pa) |
| B | weight percent graphite oxidation |
| $b_\alpha$ | empirical constant (K) |
| A | frequency factor, constant |
| B | burn-off (depth of graphite reacted) (m) |
| $C_i$ | empirical constants |
| $C_{Ba}$ | concentration of barium (mg/g graphite) |
| $c_i$ | coefficients (empirically determined) |
| $C_{Sr}$ | concentration of strontium (mg/g graphite) |
| $d_\alpha$ | empirical constant (K) |
| $\frac{dm}{dt}$ | corrosion rate (kg/m$^2$-s) |
| $f(t)_h$ | fractional release of fission gases upon UCO hydrolysis |
| $f_B$ | burn-off dependent factor |
| $f_{p,0}$ | pressure-dependent factor (initial condition) |
| $f_{p,\infty}$ | pressure-dependent factor (final condition) |
| F | burnup (%FIMA) |
| $F_b$ | coefficient to account for the effects of oxidation |
| $F_c$ | coefficient to account for the effects of catalysts |
| $k_{o,i}$ | empirical constant (1/h) |
| $k_{ox,o}$ | empirical constant (1/h) |
| K | intrinsic reaction rate (kg/m$^2$-s) |
| $K_j^0$ | pre-exponential factor (empirical) |
| M | multiplier to account for burn-off and total pressure, steam corrosion model |
| N | empirical constant |
| P | total system pressure |
| $P_i$ | partial vapor pressure of gas i (Pa) |
| P | gas pressure (Pa) |
| Q | activation energy (J/mol) |
| $Q_j$ | activation energy for fission gas release (J/mol) |
| $Q_j/R$ | temperature coefficient (K) |
| $Q'_j/R$ | temperature coefficient (K) |

| Symbol | Definition |
|---|---|
| Q''/R | temperature coefficient (K) |
| R | reaction rate (g/g-hr) |
| R | gas constant (8.314 J/mol – K) |
| $R_h$ | graphite mass fraction reacting per unit time (1/s) |
| T | absolute temperature (K) |
| $T_g$ | gas temperature (K) |
| $T_{o,k}$ | empirical constant |
| T | time in seconds |
| $t_I'$ | empirical constant |
| $\alpha_c$ | fractional hydrolysis of $UC_2$ component |
| $\alpha_n$ | fractional hydrolysis of the TRISO UCO kernel |
| $\alpha_o$ | fractional hydrolysis of $UO_2$ component |
| $\alpha_{ox}(t)$ | fractional oxidation of exposed UCO kernels |
| $\delta_{g,x}$ | Kronecker delta; constant |
| Σ | standard deviation |
| Z | dummy variable of integration |
| X | twice the as-manufactured molar fraction of $UC_2$ in the UCO kernel |

## G.1. Introduction

As discussed in Section 3.2, the functional containment system is a collection of five radionuclide (RN) release barriers, designed to limit RN release from the core to the environment to very low levels during normal operation and a broad spectrum of DBAs, References 1 and 2. These barriers, together with the main phenomena and processes involved in radionuclide production, retention, transport, and release for a pebble bed reactor are depicted in Figure 3 of this Topical Report. The first three of these release barriers are within the reactor core and their effectiveness can be compromised by oxidation during water and air ingress events.

The Core Corrosion Model is used to simulate the mass transport and chemical reaction aspects of the core corrosion phenomena encountered during water or air ingress in the core of the Xe-100. The theory and mathematical models used in this model are addressed in this Appendix.

## G.2. Associated Physical Systems and Components

Oxidation events in HTGRs, including air- and moisture-ingress events, can potentially reduce the structural integrity of fuel elements and core components (e.g., the core support structure). If the core oxidation results in fuel failure, an increase in fission products release by hydrolysis of the failed fuel particles will occur. The corrosion model calculates corrosion rates of fuel and core materials using inputs such as temperature and oxidant partial pressure to predict the effects of water and air on the performance of the TRISO fuel particles. The gas mixtures considered are helium, trace H2O in the helium, H2O/helium mixtures, and air/helium mixtures. This model is integrated with the Helium Pressure Boundary (HPB) model.

## G.3. Core Corrosion Fundamentals

While the primary helium coolant of a modular HTGR is chemically inert, trace quantities of oxidants can be introduced into the primary circuit during normal operation and more significant quantities of water or air can be introduced into the reactor vessel during certain DBAs with a spectrum of consequences. Water and oxygen can react with the fuel elements and the structural graphite components potentially compromising the structural integrity of these components and, in the case of the fuel elements, result in enhanced FP release from the core.

### G.3.1 Heterogeneous Gas-Solid Reactions

The interactions of oxidants with the graphitic core materials are generally described as heterogeneous gas-solid reactions. Heterogeneous gas-solid reactions are characterized by three distinct reaction regimes as illustrated for oxygen reacting with graphite in Figure G-1 (Reaction Regimes for Gas-Solid Chemical Reactions, considered the current state-of-the-art in modelling the air oxidation of nuclear graphite).

As discussed in detail in [[ ]]$^{P}$ at higher temperatures the chemical reaction rate between oxygen and carbon is much higher than the rate of diffusion of oxygen into the interior of the porous graphite so that the oxidation takes place largely on the surface as shown in the left hand-side of the schematic. At much lower temperatures, the chemical reaction rate is much slower than the diffusion rate, thus the

oxygen penetrates throughout the graphite and the oxidation is essentially uniform as shown in the right hand-side of the schematic. At intermediate temperatures, the reaction and diffusion rates are comparable, and the oxygen penetrates into the interior to a degree, but the partial pressure is depleted along the diffusion path giving the decreasing profile in the center of the schematic.

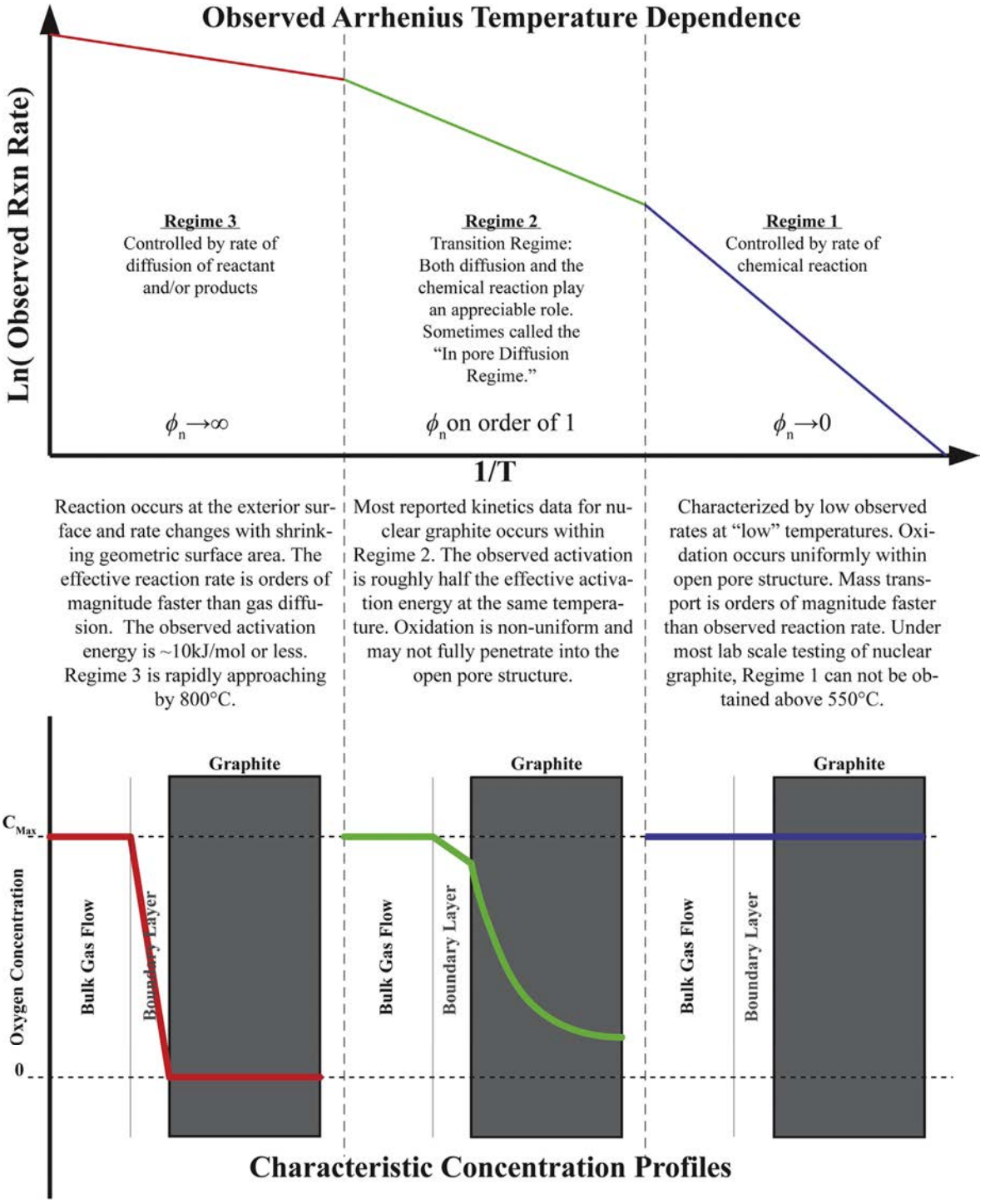


**While temperature is a substantial factor in determining the regime experimental data may fall within, other factors include sample size, geometry, gas flow rate, and microstructure.*

***The ideal Regimes 1 and 3 depicted in the characteristic concentration profiles can be thought of as the upper and lower bounds of the Thiele modulus. In reality all experimental data lies somewhere between these two extremes.*

**Figure G-1: Reaction Regimes for Gas-Solid Chemical Reactions**

As introduced above, the chronic ingress of trace quantities of oxidants into a modular HTGR core during normal operation and the ingress of larger quantities of oxidants during DBAs can impact the plant operability and safety.

Core corrosion has a potential effect on:

- Mechanical Properties of Core Structural Materials
- TRISO Fuel Particle Integrity
- Fission Product Release from the Core
- Reactivity Control
- Generation of Hazardous Gas Mixtures
- Corrosion Products on Structural Metals

The most common classical model to predict the reaction rates of gas-solid reactions is the Langmuir-Hinshelwood model, [[ ]]$^{P}$ which has been frequently used to model the reactions of water and oxygen with graphite. In the simplest version of this model, the gas-phase reactant must first adsorb on the surface of the solid reactant which is described by a Langmuir isotherm. The adsorbed gas now reacts with the solid to form a new surface species which subsequently desorbs from the surface into the gas phase. Another common model for gas-solid reactions is the Eley-Rideal model. With this model, the reaction occurs between a gas-phase reactant and the solid reactant to form a surface species which subsequently desorbs from the surface into the gas phase. Numerous other models (e.g., Mars-van-Krevelen model, etc.) and various modifications to the Langmuir-Hinshelwood model that add complexity have been proposed to better reproduce actual reaction data. Qualitatively, these models have the following basic functional form [[ ]]$^{P}$ :

$$\boldsymbol{Rate} = \frac{(\boldsymbol{Kinetic\ Factor})(\boldsymbol{Driving\ Force})}{\boldsymbol{Adsorption\ Term}} \quad \text{(G-1)}$$

In general, the (Kinetic Factor) and (Adsorption Term) terms are temperature dependent, [[ ]]$^{P}$ and the (Driving Force) term is a function of the gas-phase reactants [[ ]]$^{P}$

## G.4. Theory and Methodology

### G.4.1 Water Interactions with Graphitic Core Components

While the functional integrity of intact TRISO particles does not appear to be degraded by presence of water during normal operation or DBAs, the release of certain fission products stored in core materials during normal operation can be enhanced by the presence of water [[ ]]$^{P}$. In particular, numerous experiments have demonstrated that the release of fission gases from exposed UCO (and UO2) kernels is significantly enhanced during both irradiation and water-ingress DBAs (the effect on metal release from exposed kernel is assumed to be negligible).

### G.4.1.1 [[ ]]$^{P}$ Models for Water Interaction with H-451 Fuel Element Graphite

[[

]]$^{P}$

#### G.4.1.1.1 Validity Range

[[

]]$^{P}$

**Table G-1: Parameters for Equations (G-2) through (G-5)**

[[

]]$^{P}$

#### G.4.1.1.2 Assumptions

[[ ]]$^{P}$

#### G.4.1.1.3 Uncertainty

[[

]]$^{P}$

[11] G-4 model uses the term oxidation and hydrolysis interchangeably.

### G.4.1.2 Fission Gas Release from UCO Kernels during Water Ingress DBAs

During water ingress events, a transient hydrolysis model is required since the temperature, gas flow rates, and water concentrations are changing as a function of space and time. A model for the time-dependent fractional hydrolysis and fractional release of fission gases from an exposed LEU UCO kernel is derived in [| ]]$^{P}$

#### G.4.1.2.1 Fractional Hydrolysis of Exposed UCO Kernels

[[

]]$^{P}$

#### G.4.1.2.1.1 Range of Validity

[[

]]$^{P}$

### G.4.1.2.2 Fractional Gas Release upon Hydrolysis of UCO Kernels

[[

]]$^{P}$

### G.4.1.3 Steam Oxidation of the TRISO Particle Coatings

[[

]]$^{P}$

### G.4.1.4 TRISO Particle Integrity

Currently available data indicates that the functional integrity of an intact TRISO particle (i.e., the ability of the particle to retain fission products) is not compromised by the presence of trace amounts of water

during normal operation or high concentrations of water during large water ingress plus depressurization events [e.g., Safety Related Design Condition 6 (SRDC-6) in [[ ]]$^{P}$ at least up to 800 $^{o}$C and likely to much higher temperatures.

### G.4.1.5 [[ ]]$^{P}$ Model for Steam Corrosion of Matrix

[[

]]$^{P}$

#### G.4.1.5.1 Validity Range

[[

]]$^{P}$

### G.4.2 Air Interactions with Graphitic Core Components

The effects of air on UCO fuel kernels, TRISO particle coatings, fuel-sphere matrix, and core structural graphite and the potential release of stored fission products from these materials during oxidation is evaluated and modelled as necessary for DBAs. The experimental database and proposed predictive models for air oxidation of structural graphite, including NBG-18 graphite is extensive.

The potential for significant quantities of air to enter the primary coolant circuit during normal plant operation is extremely limited. A small quantity of air will be sorbed on fresh fuel elements. Air can also enter the primary circuit when depressurized for maintenance operations and in-service inspections (ISI). However, this limited quantity of air will be removed by the HPS during the subsequent rise-to-power and/or by reaction of the oxygen component with the massive quantities of carbonaceous materials in the active core and reflectors. Thus, the potential for significant quantities of air to interact with core materials is practically limited to various DBA scenarios wherein the primary pressure boundary is breached, and the primary circuit depressurized. Even under such scenarios, the quantity of air that can enter the primary circuit is limited by the lack of a large driving force once the pressure in the reactor vessel and reactor cavity have equalized. Given these circumstances, the investigations of the interactions of air with core materials have focused primarily on postulated DBA conditions.

### G.4.2.1 Fractional Oxidation of UCO Kernels

[[

]]P

### G.4.2.2 [[ ]]$^{P}$ Model for Air Oxidation of GKrS (“US A3-3”) Matrix

[[

]]

## G.5. Summary

The models and correlations used to simulate the corrosion of core components and the resulting increase in release of radionuclides from the core into the Helium Pressure Boundary (HPB) have been documented. A summary of these models is listed in Table G-5 and include oxidation and hydrolysis of core components such pebble matrix material, TRISO kernels and outer layers. The models describe conditions during normal operation, Depressurized Loss of Forced Circulation (DLOFC) DBAs as well as $H_2O$ ingress.

***Table G-5. Core Corrosion Models and Correlations Summary***

| Material | State | Atmosphere | Model | Section | Reference |
|---|---|---|---|---|---|
| **UCO kernel** | Normal | Trace $H_2O$ | [[ ]]$^P$ | G.4.2.1 | [[ ]]$^P$ |
| | DLOFC | Air/He | [[ ]]$^P$ | G.4.1.2 | [[ ]]$^P$ |
| **PyC coating** | $H_2O$ ingress | $H_2O$/He | [[ ]]$^P$ | G.4.1.3 | [[ ]]$^P$ |
| **"US A3-3" matrix (data for "US A3-27" matrix)** | Normal | Trace $H_2O$ | [[ ]]$^P$ I | G.4.1.5 | [[ ]]$^P$ |
| | DLOFC | Air/He | [[ ]]$^P$ | G.4.2.2 | [[ ]]$^P$ |

[[ ]]$^P$

## G.6 Cross References and References

| Document Title<br>Cross References: X-energy documents that may impact the content of this document.<br>References: X-energy or other documents that will not impact the content of this document | | Document No. | Rev./ Date of Issuance | Cross Reference/ Reference |
|---|---|---|---|---|
| G-1 | [[ ]]P | [[ ]]P | 13/ September 1995 | Reference |
| G-2 | J. Kane and e. al., "Understanding the reaction of nuclear graphite with molecular oxygen: Kinetics, transport, and structural evolution," *Journal of Nuclear Materials*. | | September 2017 | Reference |
| G-3 | J. Stempien, "AGR Irradiated Specimen Air/Moisture Heating Test Plan," , Idaho National Laborator. | PLN-5934 | 0/ December 2019 | Reference |
| G-4 | R. C. Martin, "Compilation of Fuel Performance and Fission Product Transport Models and Database for MHTGR Design." | ORNL/NPR-91/6 | October 1993 | Reference |
| G-5 | [[ ]]P | | September 2014 | Reference |
| G-6 | [[ ]]P | | April 2010 | Reference |
| G-7 | [[ ]]P | [[ ]]P | November 1981 | Reference |
| G-8 | [[ ]]P | | March 2014 | Reference |
| G-9 | [[ ]]P | [[ ]]P | November 2018 | Reference |
| G-10 | [[ ]]P | [[ ]]P | September 1995 | Reference |

## Appendix H. Xe-100 MST Models Relationship Chart

Figure H-1 depicts the relationship between the Xe-100 MST models described in this LTR.

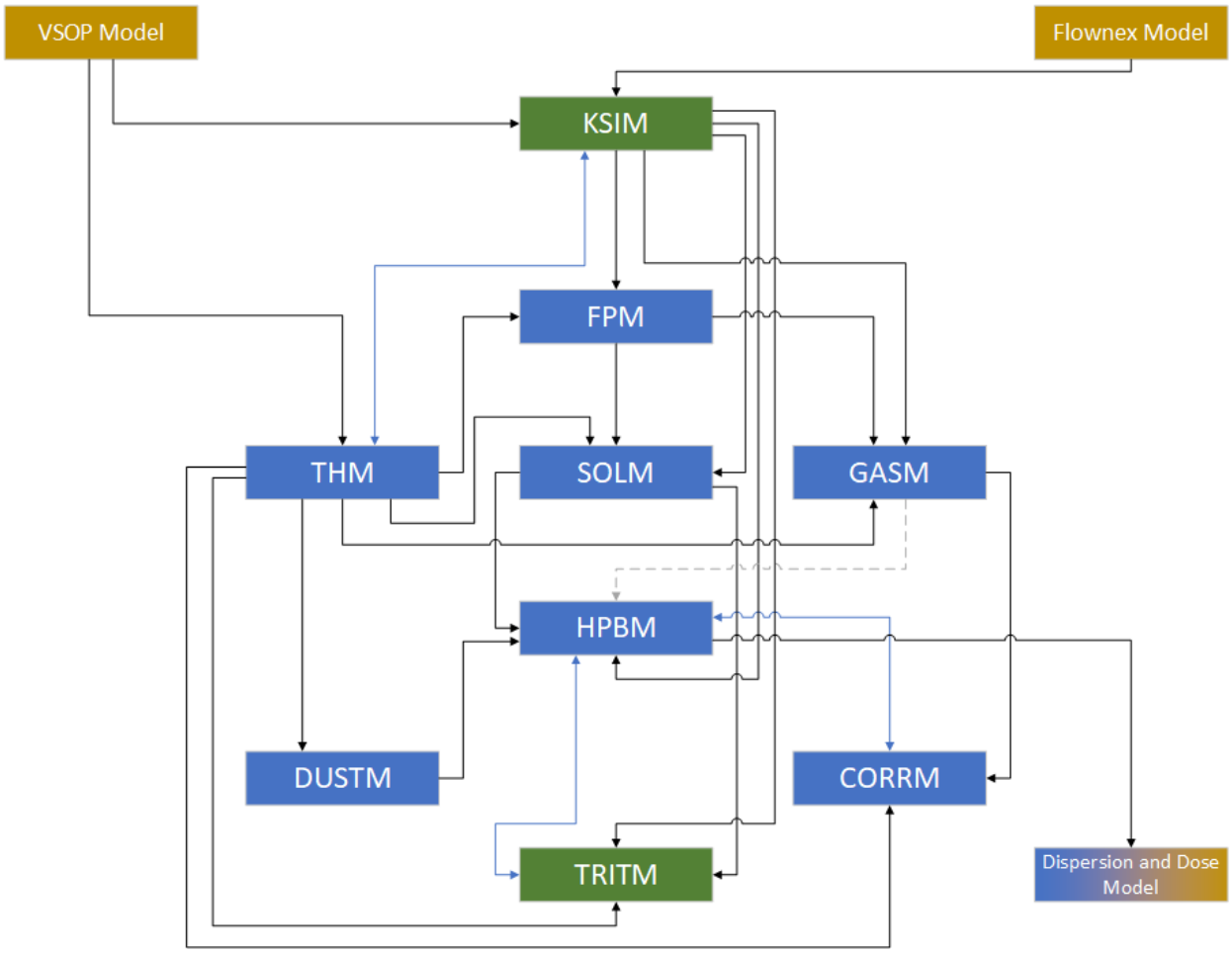


***Figure H-1: Xe-100 MST Models Relationship Chart***

- Gold box: Describe external models
- Blue box: Describe models described in detail with an Appendix in this LTR
- Green box: Describe models outlined in Section 5.1 only
- Gradient box, Dispersion/Dose box: Describe a model or external tool described in the LTR but documented elsewhere
- Black lines with arrow on one side: Denotes unidirectional data transfer from one model to another
- Blue lines with arrows on both sides: Denotes bi-directional data transfer between models
- Grey dashed lines: Denotes data transfer is optional depending on purpose

Note: The **GASM** model is also used to calibrate the effective gas diffusion coefficients used in the **SOLM** model.